

School of Electrical Engineering, Computing and
Mathematical Sciences

Mathematical Model and Cloud Computing of Road
Network Operations under Non-Recurrent Events.

Fahad Mesfer Aljuaydi

This thesis is presented for the Degree of
Doctor of Philosophy
of
Curtin University of Technology

December 2022

Declaration

To the best of my knowledge and belief this thesis contains no material previously published by any other person except where due acknowledgement has been made. This thesis contains no material which has been accepted for the award of any other degree or diploma in any university.

Ehab Mesfer Aliaydi

February 28, 2023

Acknowledgements

First and foremost, I wish to thank my parents for their enduring love and encouragement, without which I could not have attained where I am today.

I am grateful to my supervisor, A/prof. Benchawan Wiwatanapataphee and co-supervisor, Professor Yong Hong Wu for their advices, guidance and support. It is an honour to work with them.

Thank you, my wonderful wife, for the many sacrifices you have made and for always being there for me. I could not have finished this dissertation without you. Thank you, my son and daughter, for being patient with me when I could not give you all the attention you needed.

To my colleagues and administrators at Prince Sattam university. Thank you for being there. Finally, to the friends who have provided me with support in stressful times when things started to deviate from plan, thank you.

Abstract

Optimal traffic control under incident-driven congestion is crucial for road safety and maintaining network performance. Over the last decade, prediction and simulation of road traffic play important roles in road network operation. This dissertation focuses on development of a machine learning-based prediction model, a stochastic cell transmission model (CTM), and an optimisation model under non-recurrent events using big data of traffic flow, road incidents and rainfall. Numerical studies were performed to evaluate the proposed models. The results indicate that the prediction model can capture non-recurrent traffic congestion under road incidents and rainfall. The stochastic CTM with random demand arrivals and flow capacity is suitable for simulating traffic flow under lane closure. The traffic control optimisation model via variable speed limit with random demand arrivals and flow capacity is an effective tool for improving traffic flow under lane closure.

Contents

Declaration	ii
Acknowledgements	iii
Abstract	iv
1 Introduction	1
1.1 Background	1
1.2 Objectives	2
1.3 Outline of the thesis	3
2 Literature review	6
2.1 General Overview	6
2.2 Traffic Congestion	7
2.2.1 Recurrent Congestion	8
2.2.2 Non-recurrent Congestion	9
2.3 Traffic Prediction with Machine Learning	11
2.3.1 Time Series Prediction with Machine Learning	15
2.3.2 Model Evaluation	28
2.4 Traffic Modelling	29
2.4.1 Microscopic Modelling	33

2.4.1.1	Car Following Models	33
2.4.1.2	Intelligent driver models	35
2.4.1.3	Cellular-automata Models	38
2.4.2	Macroscopic Modelling	39
2.4.2.1	Classical LWR model	40
2.4.2.2	Modified LWR models	42
2.4.2.3	Cell Transmission Model (CTM)	48
2.4.3	Mesoscopic Modelling	51
2.5	Optimisation Models of Traffic Flow under Non-Recurrent events .	52
2.5.1	Traditional Optimisation Models	52
2.5.2	CTM-based Optimisation	57
2.5.3	Machine learning-based Optimisation	57
2.6	Concluding Remarks	58
3	Multivariate Prediction Models	60
3.1	General Overview	60
3.2	Study area	61
3.3	Data Analysis	62
3.3.1	Road incident data	62
3.3.2	Traffic data	65
3.3.3	Road incidents and rain effects	65
3.4	Multivariate learning models	67
3.4.1	Preparing data and pre-processing	68
3.4.2	Models' architecture	68
3.4.3	Baseline	70
3.4.4	Multilayer Perceptron (MLP)	70

3.4.5	Convolutional Neural Networks (CNN)	71
3.4.6	Long Short-term Memory (LSTM)	71
3.4.7	Convolutional Neural Networks -Long Short-term Memory (CNN-LSTM)	74
3.4.8	Autoencoder LSTM (AE-LSTM)	74
3.5	Results and discussion	75
3.6	Concluding remark	84
4	Simulation Models	86
4.1	General overview	86
4.2	Stochastic Cell Transmission Model	86
4.2.1	Traffic flow dynamics	87
4.2.2	Numerical studies	97
4.3	Stochastic Optimisation Model	105
4.3.1	Objective function and constraints	107
4.3.2	Numerical studies	108
4.4	Concluding Remarks	118
5	Conclusions and Further Work	119
5.1	Contributions	119
5.2	Future Research	121
	Appendix	122
	Bibliography	128

List of Figures

2.1	Traffic view on Jeddah road, Saudi Arabia.	8
2.2	Architecture of MLP network with two hidden layers of 4 neurons.	16
2.3	Structure of convolutional network	18
2.4	Structure of LSTM layer	21
2.5	Structure of AutoEncoder network	25
2.6	AE-LSTM network structure and AutoEncoder extracted features, and LSTM network used for the prediction of traffic flow (Wei et al., 2019)	26
2.7	Flow density relationship.	31
2.8	Model classification.	33
2.9	Relationship of density and flux.	40
3.1	Study region (red curve), Link9: between the Cranford Avenue on-ramp and the Canning Highway northbound off-ramp (Aljuaydi et al., 2022).	62
3.2	Frequency of road incidents on the study region.	63
3.3	Locations in latitude and longitude coordinates of traffic incidents and incident duration on the study region.	63
3.4	Box plot showing distribution and skewness of traffic variables associated with road incidents on the study region.	64

3.5	Fundamental diagrams showing relationship of traffic variables: (a) speed (km/hr) and volume (veh/min); (b) flow rate (veh/min) and density (veh/km); (c) speed (km/hr) and density (veh/km).	65
3.6	Relationships of traffic variables under road incidents and rainfall effects: (a) road incident; (b) rainfall between medium and heavy level.	66
3.7	Effect of rain on traffic speed from 1 August to 1 November 2018.	66
3.8	Box plot of traffic variables with and without road incident and rain.	67
3.9	Machine learning workflow.	67
3.10	Average traffic profiles of flow rate, speed and density during the study period.	69
3.11	MLP architecture.	70
3.12	Squared error loss, $L_2 = (\mathbf{y} - \hat{\mathbf{y}})^2$, for the training and the validation datasets in the MLP model.	71
3.13	CNN architecture.	72
3.14	Squared error loss, $L_2 = (\mathbf{y} - \hat{\mathbf{y}})^2$, for the training and the validation datasets in the CNN model.	72
3.15	LSTM architecture.	73
3.16	Squared error loss, $L_2 = (\mathbf{y} - \hat{\mathbf{y}})^2$, for the training and the validation datasets in the LSTM model.	73
3.17	1-D CNN LSTM architecture.	74
3.18	Squared error loss, $L_2 = (\mathbf{y} - \hat{\mathbf{y}})^2$, for the training and the validation datasets in the 1-D CNN LSTM model.	75
3.19	AE-LSTM architecture.	76
3.20	Squared error loss, $L_2 = (\mathbf{y} - \hat{\mathbf{y}})^2$, for the training and the validation datasets in the AE-LSTM model.	76

3.21	Observed traffic flow rate (top), speed (middle) and density (bottom) with road crashes and rainfall during the prediction period (4 September 2018).	77
3.22	Baseline predictions of traffic flow rate (veh/min), speed (km/hr) and density (veh/km) under a road incident (★) and rain.	78
3.23	Long-term traffic prediction of the flow rate (veh/min), speed (km/hr) and density (veh/km) obtained from the best multivariate ML model based on the MLP network.	79
3.24	Long-term traffic prediction of the flow rate (veh/min), speed (km/hr) and density (veh/km) obtained from the best multivariate ML model based on the CNN network.	79
3.25	Long-term traffic prediction of the flow rate (veh/min), speed (km/hr) and density (veh/km) obtained from the best multivariate ML model based on the LSTM network.	80
3.26	Long-term traffic prediction of the flow rate (veh/min), speed (km/hr) and density (veh/km) obtained from the best multivariate ML model based on the CNN-LSTM network.	80
3.27	Long-term traffic prediction of the flow rate (veh/min), speed (km/hr) and density (veh/km) obtained from the best multivariate ML model based on the AE-LSTM network.	81
3.28	Short-term predictions under a road incident on 4 September 2018 between 10:25 and 10:55 obtained from five prediction models based on various ML networks: the MLP, the CNN, the LSTM, the 1D CNN-LSTM and the Autoencoder LSTM networks.	82
3.29	Short-term predictions under the rain on 4 September 2018 between 20:10 and 20:40 obtained from five prediction models based on various ML networks: the MLP, the CNN, the LSTM, the 1D CNN-LSTM and the Autoencoder LSTM networks.	83

4.1	Merging zone	87
4.2	Diverging zone	88
4.3	Relationship of traffic variables.	90
4.4	CTM road network.	97
4.5	Road network with 3 on-ramps and 2 off-ramps.	98
4.6	Incoming and outgoing flows on 4 September 2018.	99
4.7	Queue size (veh) at the beginning and three on-ramps, including H558 (Leach WB on-ramp), H554 (Leach EB on-ramp) and H553 (Cranford AVE on-ramp) obtained from the CTM and the SCTM.	101
4.8	Surface and heatmap plots of flow rate (veh/h) and density (veh/km) obtained from the CTM.	102
4.9	Surface and heatmap plots of flow rate (veh/h) and density (veh/km) obtained from the SCTM	103
4.10	Queue size (veh) at the beginning and three on-ramps, including H558 (Leach WB on-ramp), H554 (Leach EB on-ramp) and H553 (Cranford AVE on-ramp) obtained from the CTM and SCTM with lane closure from 6:00 am to 10:00 am.	104
4.11	Surface and heatmap plots of flow rate (veh/h) and density (veh/km) obtained from the CTM with lane closure from 6:00 am to 10:00 am	105
4.12	Surface and heatmap plots of flow rate (veh/h) and density (veh/km) obtained from the SCTM with lane closure from 6:00 am to 10:00 am.	106
4.13	Queue size (veh) at the beginning and three on-ramps, including H558 (Leach WB on-ramp), H554 (Leach EB on-ramp) and H553 (Cranford AVE on-ramp) obtained from the optimisation model.	112
4.14	Surface and heatmap plots of flow rate (veh/h) and density (veh/km) obtained from the optimisation Model.	113

4.15	Variable speed limit (km/h) obtained from the optimisation model.	114
4.16	Queue size (veh) at the beginning and three on-ramps, including H558 (Leach WB on-ramp), H554 (Leach EB on-ramp) and H553 (Cranford AVE on-ramp) obtained from the optimisation model with lane closure.	115
4.17	Surface and heatmap plots of flow rate (veh/h) and density (veh/km) obtained from the optimisation Model with lane closure . .	116
4.18	Variable speed limit (km/h) obtained from the optimisation model with lane closure.	117

Chapter 1

Introduction

1.1 Background

The transport of people and goods is crucial for the community's economic and social development. To make this possible, significant investment is made in road networks. However, the majority of transport options are currently facing increased congestion, which may occur during recurrent and non-recurrent events in most urban locations. Recurring congestion happens primarily during peak hours while nonrecurring congestion occurs due to accidents, inclement weather, natural catastrophes, emergency evacuation, construction, and extensive sporting and cultural events. Aggravate congestion reduces the capacity of a road and may cause major delays on motorways, which affects the economies of many countries. There are various negative impacts of traffic congestion which may contribute to traffic collisions resulting in disability, cessation, and property damage to everyone involved. Traffic congestion also reduces regional economic health and contributes to air pollution. Thus, traffic management to reduce traffic congestion on motorways is a challenging problem.

In assessing the functioning of freeways, congestion from irregular sources is a big concern. In metropolitan regions with daily severe and frequent repeated congestion, the adverse effects of occurrences are much more apparent. To ef-

fectively reduce this negative impact, many incident management programs have been introduced in recent years to track and handle issues. Corridor reliability analysis can be facilitated by accurate and effective estimation of incident-induced delay. It can help with locating bottlenecks. Benefits may also result from applying corresponding measures, such as variable speed limits and ramp metering, from improving traffic flow and safety. Over the last decade, road network management services, namely Intelligent Traffic System (ITS), have been developed to keep the road network accessible for safe usage by road users. It comprises various approaches such as emergency response, weather-related services, planned interventions, automatic enforcement, traffic incident detection and management, and traveller information. It provides drivers with reliable, timely information on unforeseen or anticipated incidents. Depending on ambient traffic, the road layout, the incident's seriousness, lane obstructions, etc., the incident-induced delay might vary significantly in different contexts.

Several control strategies for traffic congestion have been proposed. However, two control strategies based on Ramp Metering (RM) and Variable Speed Limit (VSL) have been intensively studied to manage the on-ramp and mainline input flows, respectively. The ideal solution would be an implementable algorithm that dynamically identifies the event-induced delay at the individual incident level for modelling and performance evaluation. Recently, extensive research has focused on improving road network operation under non-recurrent events by developing and integrating simulation modelling and computing technologies in spatial and temporal analysis.

1.2 Objectives

This dissertation focuses on developing mathematical models for predicting, simulating and controlling traffic dynamics under non-recurrent events using traffic flow data (flow rate, density and speed), road incident data and rainfall data.

The primary goal of this study is to:

1. develop multivariate prediction model based on machine learning approaches for predicting traffic variables (traffic flow rate, density and speed) under non-recurrent events;
2. develop a simulation model with uncertain parameters to describe the physical processes of traffic on the regular freeway and lane-closure freeway using a stochastic cell transmission model (SCTM);
3. develop an optimal integrated VSL & RM control model based on the SCTM optimisation model for minimising total travel time;
4. investigate the impact of non-recurrent events on traffic dynamics with and without any traffic controls.

1.3 Outline of the thesis

This thesis is organised into five chapters. The five chapter titles are: (1) Introduction, (2) Literature review, (3) Multivariate Prediction Models, (4) Stochastic Simulation Model and Optimal Traffic Control Model and (5) Conclusions and Further Work.

Chapter 2, the literature review, presents various models that have been developed to predict, simulate and control freeway/highway traffic under various scenarios. A comprehensive literature of machine learning (ML) models to forecast traffic flow through time series analysis was reviewed. Various machine learning models, including the multilayer perceptron (MLP), the convolutional neural network (CNN), the long short-term memory (LSTM) network, and the combination of the CNN and LSTM networks (1D-CNN LSTM) and the combination of an autoencoder and the LSTM networks (AE-LSTM), were described in detail. Also, the traffic flows based on microscopic and macroscopic scale-type models were summarised. The microscopic models explain individual vehicle behaviour. Three popular microscopic models are the Car-Following model, the

Intelligent Driver model (IDM) and the Cellular-Automata model.

Since traffic involves flow rate, concentration (density) and speed, traffic flow may be described in terms of fluid behaviour based on some assumptions of conservation and the one-to-one relationship between flow and density or between density and speed. There are two main types of the model, namely, the one-equation and the two-equation models. The first one-equation model is the classical LWR model developed by Lighthill, Whitham and Richard in 1956. Another is the cell transmission model (CTM) developed by Daganzo in 1994, which has been widely used and modified. The two-equation models consist of the conservation equation and the equation of speed-density (or flow-density) relation in which traffic variables (flow, density and speed) are solved at any time and any road segment of the road network. As a typical model on a micro or macro scale cannot capture traffic phenomena, many attempts have been made to couple the microscopic and macroscopic models for predicting the complex traffic phenomena due to congestion. Lastly, optimisation models based on the CTM and the ML were presented. Traffic flow control on a freeway at on-ramp and off-ramp merged regions was summarised. Finally, applications of the traffic flow models for ramp metering and traffic lane changing conditions studies were described.

Chapter 3 demonstrates traffic prediction under non-recurrent events using machine learning (ML) networks. Various ML architectures based on multilayer perceptron (MLP), long-short term memory model (LSTM), convolution neural network (CNN), one-dimensional convolution neural network long-short term memory model (1-D CNN LSTM) and Autoencoder long-short term memory (AE-LSTM) networks were designed. The data used in this study includes information on 1-minute traffic variables, 15-minutes road incidents and rainfall between 1 January 2018 and 1 November 2018. The timestamp approach is utilised to generate study data with five columns (classes), including the flow rate, density, speed, incidents and rainfall. The input data with five features are split into two sets, 70% for the train set and 30% for the test set. For the best-

fitted model, two standard metrics, Root Mean Square Error (RMSE) and Mean Absolute Error (MAE), were used to assess the performance of the prediction models.

Chapter 4 on a numerical simulation model examines the traffic dynamics on a freeway with various on-ramp and off-ramp roads using the modified cell transmission model with uncertain parameters, namely the stochastic cell transmission model (SCTM). Two model parameters (on-ramp flow rates and the flow capacity) are random variables. A practical example of a freeway under two road conditions was utilised to validate the efficiency of the simulation model. A stochastic optimisation model has been proposed. Its control objective is to minimise total travel time in the road network and queue lengths at the main road entry, all on-ramp entries. Its constraint is traffic flow along a multilane roadway described by the SCTM. Using one-minute road data to determine the four-second demand/supply of the road network, two practical examples of freeway traffic were carried out to evaluate the performance of the proposed model.

Summarising conclusions and research contributions and suggestions for future research directions are given in Chapter 5.

Chapter 2

Literature review

2.1 General Overview

Throughout human history, transportation has played a vital role in our society, particularly in aiding economic development. Economic expansion has prompted a surge in demand in the transportation sector during the previous several decades. Ground transportation has long been one of the most advanced modes of people and commodities moving. However, the number of automobiles on the road has significantly increased. Various environmental consequences, such as increased energy usage, faster climate change, transportation safety, traffic congestion, difficulties etc., are some of the repercussions of this transportation growth.

Among all of these disadvantages, traffic congestion is the most visible and commonly experienced. For the reasons stated above, numerous freeway traffic models have been presented in order to map and analyze the dynamics that result in traffic flow. Studies have also looked into the environmental issues that come with traffic.

2.2 Traffic Congestion

Traffic congestion has been a major subject of research. Many studies have been carried out to determine the origin and remedy of traffic congestion. Congestion on the transportation network has become one of the most inconvenient aspects of modern life. The creation of congestion as a phase transition driven by the nonlinear impact in dynamical equations of motion was studied, and features of traffic congestion as well as the stability of the congestion structure were investigated (Bando et al., 1995).

Traffic congestion has increased everywhere in the cities with population growth and is worse than it has ever been (Arnott & Small, 1994). There are two forms of traffic congestion, including recurrent congestion (RC) produced by daily traffic patterns and non-recurrent congestion (NRC) brought on by unexpected incidents such as breakdowns, accidents, and so on (Anbaroglu et al., 2014; Skabardonis et al., 2003; McGroarty, 2010).

Globally, traffic congestion has been a continuous issue in cities. Working from home (WFH) can theoretically alleviate commuting-related congestion. WFH arrangements have been promoted or mandated to limit coronavirus transmission during the COVID-19 pandemic. It has been observed that traffic congestion has decreased in several locations under these circumstances. Nevertheless, there hasn't been much research done on how traffic patterns alter within a city. Throughout multiple waves of the epidemic, Loo & Huang (2022) concentrated on the congestion index (CI) in Hong Kong during peak hours, when commuting-related congestion is frequently the greatest. We have a limited grasp of individual exposures to traffic congestion during different types of journeys because the majority of the existing research on this topic focuses on commuting trips. Using taxi Global Positioning System (GPS) trajectory and Point of Interest (POI) information, Kan et al. (2022) assessed individual exposures to traffic congestion during various types of travel in Wuhan, China. They first used the allure of the POIs to infer personal travel objectives from GPS trajectories and Bayesian criteria. Par-



Figure 2.1: Traffic view on Jeddah road, Saudi Arabia.

ticular road congestion exposures related to various journey types were evaluated. Additionally, they calculated the exposures to excessive traffic-related emissions linked to different types of journeys because of traffic congestion. Individual traffic congestion exposures are more strongly correlated with the space-time rhythm of traffic flows than they are with the sorts of journeys or activities taken. The findings indicate that focusing solely on commutes would understate individual contact with traffic congestion and increased emissions caused by traffic. They provide insight into how each individual is impacted by activity-related traffic congestion at various times and locations.

2.2.1 Recurrent Congestion

Recurring congestion occurs at the same time every day on weekdays during peak hours (Stopher, 2004). Figure 2.1 presents recurrent traffic congestion on Jeddah road, Saudi Arabia. Due to the high demand for mobility, recurring congestion will cause a network to face delays.

There are many sources of recurring congestion. For example, an excess of people attempting to travel from one location to another during the same period may be the primary source. Daily, traffic congestion occurs around schools during

peak morning and evening hours between 6 am and 9 am, then again between 4 pm and 7 pm because of parents' dropping off and picking up their children. A bottleneck is also a primary source of recurring congestion (McGroarty, 2010). A bottleneck at which the flow capacity is unexpectedly reduced is created when a five-lane highway is suddenly dropped to four lanes because the right or left lane is forced to exit.

One of the most important aspects of traffic management for reducing delays and related costs is congestion identification. Thanks to the growing popularity of GPS-based navigation, promising speed data are now available. In Des Moines, Iowa Zarindast et al. (2022) made extensive use of historical probe data from the year 2016. To separate the speed signal and identify temporal congestion, they used Bayesian change point detection. The identified congestion occurrences were then divided into recurring and non-recurring categories. They recommended a robust statistical, big-data-driven expert system as well as a big-data-mining method as a result of their findings for recognising both recurrent and nonrecurring bottlenecks.

2.2.2 Non-recurrent Congestion

Non-recurrent congestion having more irrational transportation sources is unusual congestion caused by unforeseen or unpredictable circumstances such as work zones, inclement weather, and traffic incidents (Hallenbeck et al., 2003; Stopher, 2004). As non-recurrent congestion does not occur regularly, it is difficult to predict and address. This form of traffic congestion decreases the overall transportation system's capacity and reliability. Road users are usually aware of recurrent congestion since it occurs regularly, but they do not expect to encounter non-recurrent congestion. The primary reasons for non-recurrent congestion include traffic incidents, vehicle breakdowns, temporary construction zones, severe weather conditions, and special events (Sajjadi, 2013).

- **Traffic incidents:** Events that cause a road's traffic flow to be disrupted

usually involve road incidents such as vehicle crashes or breakdowns. When a car incident occurs ahead, or a vehicle breakdown occurs, drivers tend to slow down. As a result, reducing vehicle speed below the free flow speed affects the road's operation. Video footage captured by digital cameras mounted on moving cars is a crucial source of information for various dangerous traffic situations, such as collisions or near-collisions. This knowledge is freely accessible, and numerous methods for reconstructing traffic accidents using automobile video have already been proven. A fresh alternative method for recreating traffic events from automobile film was presented by Kolla et al. (2022). The method relies on the fusion of geometric objects, video evidence processing from a passing car camera, and kinetic vehicle trajectory modelling inside a 3D laser scanner point cloud. The method permits statistically gathering thorough technical information about a traffic event from video footage by correctly reconstructing general vehicle movements within the proper temporal domain. As a result, a moving monocular camera recorded actual vehicle motion and projected it using physics-based projection in three dimensions. During experimental test runs, the approach was shown to be accurate in terms of vehicle speed, distance travelled, acceleration/deceleration, and directional aspects (yaw rate, yaw angle). Then, the tactic was applied to mimic real-world traffic scenarios.

- **Construction zones:** Temporary pavement in work zones may cause one or more traffic lanes to close and reduce flow capacity as the right, or left shoulder width may be reduced.
- **Weather conditions:** Weather (e.g. rain, storms, winds, etc.) is one environmental risk factor. Severe weather commonly contributes to several hazards within the transportation sector, such as reduced visibility and road traction. Wet roads are a significant contributor to road fatalities and crashes.

- **Special events.** Sports events (national and long public holidays, school vocation, religious festivals, and other festivals cause traffic problems) commonly cause traffic jams within the local area.

Traffic congestion causes many problems within the local area. This problem includes delays, accidents, air pollution and health risks.

Any non-recurring incidents that have a substantial impact on roadway operations, such as traffic crashes, roadway repair and reconstruction projects, disabled cars, special non-emergency events, such as concerts, ball games, or any other event which can disrupt normal traffic flow, reduction of road capacity, and so on, are referred to as traffic incidents (Qi et al., 2018). Especially in developing countries, where traffic flows with many motorbikes, urban road traffic is particularly complicated, with unpredictability, dynamic, and uncertainty characteristics (Can et al., 2020). Non-recurring congestion is caused by incidents, for example, around a quarter of total congestion in the United States (Javid & Javid, 2018).

2.3 Traffic Prediction with Machine Learning

According to some studies (Zhang et al., 2008), traffic engineers, planners, and individuals benefit from understanding traffic conditions ahead of time. Uncertainty in traffic conditions leads to greater travel time unpredictability, which has a negative impact on traveller route choice, as well as other drawbacks such as increased safety hazards, traffic congestion, delays, and pollution. Since the introduction of Intelligent Transportation Systems (ITS) infrastructure, such as variable message signs and speed cameras, traffic flow prediction has gained importance among metropolitan planning agencies all over the world. Traffic flow prediction is useful for advanced traveller information systems (ATIS), traffic control towers, intelligent public transportation, and commercial vehicle operations. The weather can have a big impact on people's everyday decisions and actions.

In order to advance technology, specialists integrate weather-related data into traffic operations. Traffic flow is one element of a transportation system that is affected by weather variations; this can reduce the effectiveness of the road network Tsapakis et al. (2013). For the planning and execution of smart cities, intelligent transportation systems (ITS) must be developed. According to Koesdwiady, building more roads won't significantly improve the issues of severe traffic congestion, fuel consumption, extended travel times, and safety Koesdwiady et al. (2016). Since it is crucial for planning preemptive measures to lessen traffic congestion, anticipating traffic flow ought to be one of the primary ITS goals. Forecasting traffic flow under non-free flow conditions is still a challenging problem since traffic information (such as flow, speed, density, travel duration, etc.) is always highly nonlinear and non stationary and is influenced by many factors depending on the kind of traffic (e.g., peak hours, weather, incidents, etc.).

The forecasting approach uses traffic data obtained from loop detectors, cameras, radars, and other sources as inputs. Data might be obtained retrospectively or in real-time. Data from social media, Bluetooth, and others have been used in traffic forecasts. As a result, the data-driven cum analytical technique was used to forecast traffic conditions (Zhang et al., 2011a; Chen & Zhang, 2014). Most current models are concerned with future traffic conditions in terms of some explanatory variables, which define the model's realism and accuracy. As a result, there is a need to investigate analytical methodologies that use deep modelling architecture to bring in a large amount of data.

Due to their ability to adjust parameters without requiring prior knowledge, machine learning models offer interesting alternatives for traffic prediction in non-recurrent circumstances, but this has not been well-studied. In order to address this gap, Chikaraishi et al. (2020) investigated the applicability of various machine learning models during a transportation network failure, focusing on the model's capacity to forecast traffic conditions and the interpretability of the results.

Deep learning, an extension of the machine learning paradigm, has found

many applications in research and practice in recent years (Bengio, 2009). Image processing, motion detection, and language processing are some of the more common applications (Hinton & Salakhutdinov, 2006; Collobert & Weston, 2008; Goodfellow et al., 2013; Huval et al., 2013; Shin et al., 2012). Deep learning employs a complex, multilayered architecture to identify characteristics or features in data, allowing for a comprehensive relationship between features and the variable of interest. Given the complexity of traffic flow, the deep learning technique may be a good fit for understanding and forecasting it by utilising hybrid data obtained from multiple sources.

The deep learning method can project a posterior distribution of traffic flow, which may be used for short-term forecasts to influence traffic management operations, such as maximising vehicle throughput, minimising trip time, and so on, by finding hidden characteristics in traffic data. Deep learning algorithms are constantly being refined by researchers to increase their accuracy for real-world challenges. The primary component of traffic management operations and ITS systems has remained traffic flow prediction. Thus, traffic flow prediction modelling and its applications in efficient traffic operations with control measures have extensive literature.

The spatial and temporal evolution of traffic in a road network can be described. The following is a symbolic representation of traffic flow conditions: Consider X_i^t to be the traffic flow observed on a road network link I at instant time t . Traffic flow data is available for several time intervals, i.e. $t \in [1, T]$, where T is the most recent time interval for which data is available. Traffic flow prediction models attempt to predict traffic flow for time intervals more significant than T (i.e. $T + \Delta$) for which no data is available.

Statistical and machine learning models dominate the enormous literature on traffic flow prediction models. When dealing with short-term traffic forecasting, the models can be classified as parametric or non-parametric (Li et al., 2015a). The Autoregressive Integrated Moving Average (ARIMA) model is a widely used

parametric forecasting method. ARIMA models were utilised in some traffic engineering studies to produce improved forecasts for changeable traffic flow circumstances. Hamed et al. (1995) created the first application of the ARIMA model to predict future traffic flow.

Non-parametric models, in contrast to parametric techniques such as ARIMA, can account for variability and non-linearity in traffic flow (Zhang et al., 2011b). Chang et al. (2012), for example, developed a dynamic multivariate prediction technique based on the k-nearest neighbour (k-NN) algorithm. Castro-Neto et al. (2009) employed one of the machine learning (ML) techniques, online support vector regression, for flow prediction. The Artificial Neural Network (ANN), another ML-based non-parametric approach with a flexible structure, has been widely utilised in applications to simulate traffic flow (Hu et al., 2010). The fundamental idea behind ANN is that of a brain that utilises numerous neurons to process information instantaneously and process the information at the same time from all neurons (Fitch, 1944). Existing research has shown that social media data can be utilised to forecast traffic parameters (Ni et al., 2014; Abidin et al., 2015). Ni et al. (2014) constructed a model for predicting short-term traffic using Twitter data to anticipate inbound traffic flow ahead of sporting events. A method was tested using four models: support vector regression, k-nearest neighbour (k-NN), neural network, and ARIMA. Abidin et al. (2015) applied a Kalman-filter model and used Twitter data for predicting a bus arrival time.

The results of many, if not all, of the most recent research that examined the effects of employing non-traffic input datasets for forecasting urban traffic parameters showed that more precise forecasts were made (Essien et al., 2019a,b; Jia et al., 2017). A deep bidirectional Long Short-Term Memory (LSTM) model, for instance, was provided and trained using rainfall and temperature data as well as traffic flow parameters Essien et al. (2019a). The results of the study ((Jia et al., 2017)) demonstrated an improvement in predicting accuracy when compared to the baseline, which is only traffic datasets. Similar results were

noted in tests that used input data other than traffic.

This is because data-driven traffic parameter prediction frequently applies predictive analytical techniques to observations of historical data in order to identify trends that may be used to predict observations of the future. This has proven to be useful because urban traffic statistics are seasonal, recurrent/cyclical. Examples include peaks during the morning and evening rush hours, which can be precisely predicted and so anticipated. As a result, if a model can recognise and understand these tendencies from historical data, it will be "skilful" at forecasting future traffic aspects.

Even the most precise prediction models would struggle to account for unforeseen or irregular events, such as occurrences or incidents that cannot be predicted using historical data (Essien et al., 2019b). Non-recurring or stochastic events/incidents include things like accidents, lane closures, sporting events, and public gatherings. It is crucial to build strong predictive models since such events may be unanticipated, uncommon, or unexpected, making it possible to predict traffic accurately in these circumstances.

For traffic flow prediction, researchers have combined the ANN with various data mining approaches such as the k-NN (Lin et al., 2013) and the Bayesian networks (Zheng et al., 2006).

2.3.1 Time Series Prediction with Machine Learning

Various machine learning techniques have been applied to time-series prediction. These include Multilayer Perceptron (MLP), Convolutional Neural Networks (CNN), Long short-term memory (LSTM), One-dimensional CNN LSTM and Autoencoder LSTM network.

- **Multilayer Perceptron**

The data moves forward in this network as the preceding layer receives the inputs from the previous layer and feeds the output to the nodes of the subsequent layer. As seen in Figure 2.2 the neurons in the same layer are

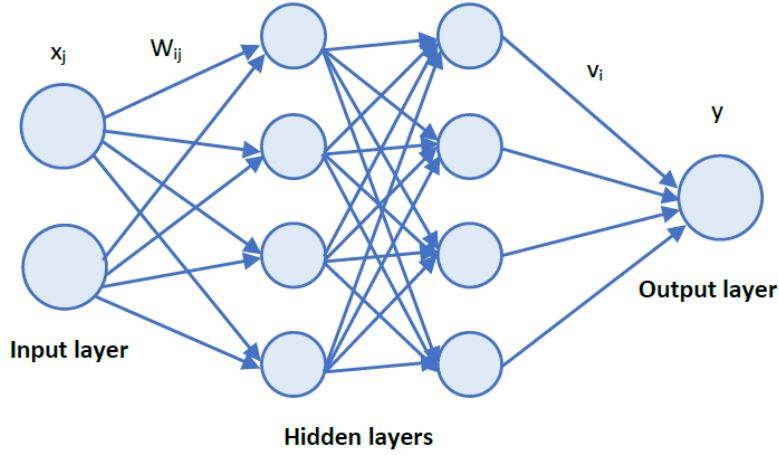


Figure 2.2: Architecture of MLP network with two hidden layers of 4 neurons.

interconnected. If more than one input is provided, the net input can be expressed in matrix form. Assume $X = (x_1, x_2, \dots, x_i, \dots, x_n)$ that represents the inputs provided for n features of the input layer and $W = w_{ij}$ is the network's weight matrix. As a result, the weight matrix for a connected hidden layer with m neurons is given in equation (2.1)

$$W = \begin{bmatrix} w_{11} & w_{12} & \dots & w_{1n} \\ w_{21} & w_{22} & \dots & w_{2n} \\ \vdots & \vdots & \dots & \vdots \\ w_{m1} & w_{m2} & \dots & w_{mn} \end{bmatrix} \quad (2.1)$$

the algorithm that generates results via backpropagation and supervised learning. These neural networks can learn non-linear functions and may include one or more hidden layers. The model is trained in three steps:

1. Forward Pass: Pass the input, multiply with weights and add bias b at every layer. $v_{in} = \sigma(b + \sum x_i w_i)$, where σ is a non-linear activation function.
2. Calculate Error/Loss: $E_j = \bar{y}_j - y_j$, Total error= $E = \frac{1}{2} \sum E_j^2$

3. Backward Pass: Then back propagate the loss, i.e. this process leads from output layer and performs until input layer is reached. It updates the weights of the model by using gradient $\Delta w_{ji} = -\alpha \frac{\partial E}{\partial v_j} y_i$

where y_i is the output of the previous neuron, v_j input of the j layer, and α is a constant.

An MLP is a simple and straight feed-forward ANN with input layers, hidden layers, and output layers. The number of hidden layers that can be employed in the procedure is known as the depth of ANN. A specific number of linked neurons, each with a variable weight, make up each buried/hidden layer. These weights are changed to establish information-based input-output relationships. A supervised machine learning method known as backwards propagation perceptions (Rosenblatt, 1962; Rumelhart et al., 1985) is used to learn the weights. MLP only contains forward connections between two neurons when compared to other deep learning architectures like the feedback loop. By adding more hidden layers, a better prediction or better resolution of information can be characterised. In reality, a deep learning algorithm is an MLP with multiple hidden layers.

MLPs have a high degree of robustness and prediction capability in the event of intricate, nonlinear, and scarcely foreseeable scenarios, according to earlier studies (Ishak et al. (2003); Lam et al. (2005)) employed dual-loop vehicle detectors to collect data. The data set included the average speed, vehicle volume, and rainfall to build a journey time prediction model in non-recurrent congestion.

In order to predict traffic flow, the MLP network was tested with traffic flow data that included meteorological information. Koesdwiady et al. (2016) showed that the MLP network performed better than statistical models, such as the ARIMA model, and had a single hidden layer with 90 neurons. Since there are fewer parameters in MLPNs and ARIMA methods than in

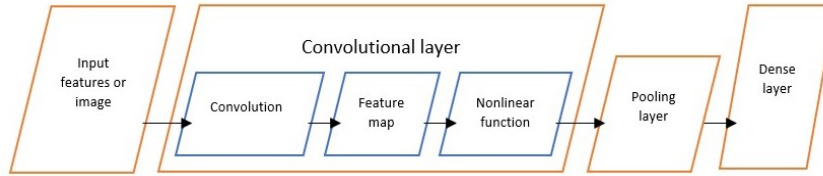


Figure 2.3: Structure of convolutional network (Kumar & Kumar, 2022).

deep architectures, training takes less time and space. This problem can be viewed as one of deep architecture’s drawbacks. The MLP network is used in Peng et al. (2018) to forecast traffic flow, utilising data on traffic flow and rainfall. The MAPE values of the MLP Network are 15.12% when applied to the traffic flow data and 14.95% when rainfall data is included along with the traffic flow data, which represent higher prediction accuracy than other models such as seasonal ARIMA and exponential smoothing. Its structure has two layers of neurons 40 and 30 for each step ahead forecast. For traffic prediction during special events, the MLP network is built with three hidden layers totalling 400 neurons in Ren et al. (2022), and the forecast accuracy topped that of various statistical models. The BNNN model, a sort of MLP network, was used to forecast traffic based on rainfall data, however it did not outperform other deep learning models in terms of prediction accuracy.

- **Convolutional Neural Network**

The convolutional network is a special kind of deep neural network that is intended for feature extraction. Two convolutional layers, a pooling layer, and a convolutional network were used. The convolutional network’s structural layout is shown in Figure 2.3.

The convolution layer uses convolution rather than scalar multiplication to extract information from the incoming data. Its training technique, referred to Goodfellow et al. (2016), includes three features: sparse connection, parameter sharing, and equivalent representations. Very few features from the last layer are input to each neuron and filtered in the next levels. The

$$y_m^n = \sigma \left(\sum_{s=1}^{m_{n-1}} y_s^{n-1} w_{sm}^n + b_m^n \right), \quad m \leq s, s = 1, 2, 3, \dots, N \quad (2.2)$$

$$y_m^{n+1} = \sigma \left(\sum_{s=1}^{m_n} y_s^n w_{sm}^{n+1} + b_m^{n+1} \right), \quad m \leq s, s = 1, 2, 3, \dots, N \quad (2.3)$$

network's output is improved via the pooling function. The value extracted from the convolutional layer at a particular position is altered in order to represent the summaries of the neighbouring outputs. The pooling layer of the network (with $L2$ -norm, max-pooling, or average pooling as the function) decreases complexity while accelerating convergence. The pooling layer is mathematically represented by Equation (2.2), while the convolutional layer is represented by (2.3). This tactic was taken from Ranjan et al. (2020).

where y_m^n is the convolutional layer with m^{th} feature map and y_s^{n-1} is the pooling layer with s^{th} feature map, y_m^{n+1} is the pooling layer with m^{th} feature map and y_s^n is the convolutional layer with s^{th} feature map, w is the weight matrix, b is the bias vector, N is the number of filter and σ is the element-wise non-linear activation function.

A feedforward neural network is a convolutional neural network (CNN). A Typical, deep-learning structure that harvests data features while reducing model complexity, it looks like a grid. Due to its effective local feature extraction capability, CNN is commonly used in traffic flow prediction to accurately evaluate the spatial correlation between traffic flow data (Ma et al., 2017).

Zhang et al. (2019) short proposed a short-term traffic flow prediction model built on CNN using traffic flow data to identify temporal and spatial features and a selection strategy to pick the optimum input data. The effectiveness of the model was then verified by comparing the results to actual traffic data.

An et al. (2019) used a novel fuzzy-based CNN traffic flow prediction model to identify the characteristics of traffic accidents. They asserted that their model outperformed others. Similar to how Liu et al. (2018) short discovered their model was effective at forecasting traffic flow, they used a CNN-attention model to estimate traffic speed. It was also useful to estimate how various models predict the traffic flow temporal and spatial variables, and they will affect traffic flow by visually representing the weights generated by the attention model. Peng et al. (2020) predicted the urban traffic passenger flow using a spatial-temporal incidence by utilising a dynamic graph recurrent CNN. According to their experiments, their model network had better prediction capabilities than conventional techniques.

It is critical to forecast weather conditions in order to conjecture traffic flow in beach areas because the wealth of the beaches depends on variables like temperature, wind, solar radiation, and others. These climatic data are therefore also inputs into the model. Braz et al. (2022) used the CNN, LSTM, and autoregressive LSTM models to calculate traffic flow. The results demonstrate that it is possible to anticipate traffic flow with a respectable margin of error within one-hour time intervals. The forecasts produced using the CNN model had the lowest prediction error values and used the least amount of forecasting time.

To enhance the accuracy of the predictions made for the entire city in Zhou et al. (2021), the CNN model has been employed to predict traffic flow under the temporal transportation flow data with information on weather conditions and some significant events.

- **Long Short-term Memory (LSTM)** The MLP network and recurrent network are both LSTM network extensions. It was developed to address the recurrent network issue. The buried layer in the recurrent network is altered by the LSTMN. The cell state is kept in the memory module, also referred to as the LSTM layer. The information flow in the memory module

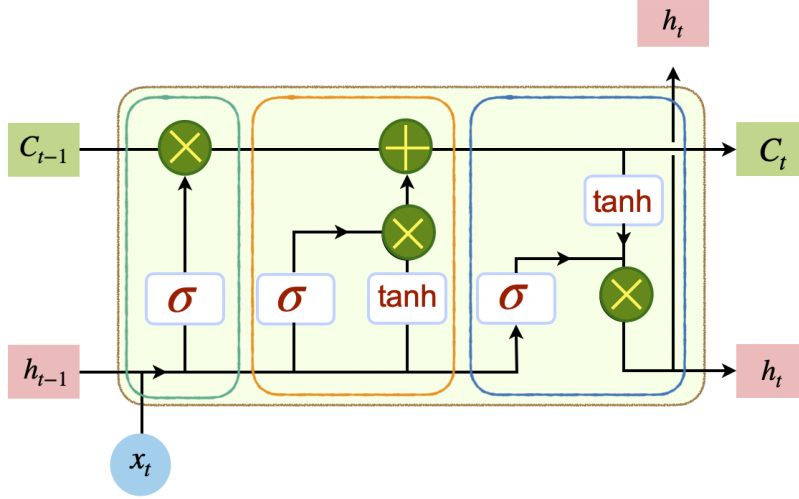


Figure 2.4: Structure of LSTM layer
(Kumar & Kumar, 2022).

is controlled by multiplicative gates at the input (i_t) and output (o_t). Due to the addition of cell state and extra paired regulating gates, LSTMN can solve the vanishing error problem in traditional recurrent networks. To prevent the inner cell values from rising when a continuous time series that hasn't already been fragmented is used, a multiplicative forget gate was added to the memory module. The Figure 2.4 presents the basic structure of the LSTMN model. This work adheres to the LSTMN mathematical approach suggested by (Ma et al., 2015). The network processes the input sequence $x = (x_1, x_2, \dots, x_N)$ by iterating from $n = 1$ to N in the way of equation (2.4) to (2.7) (Kumar & Kumar, 2022):

$$i_t = \sigma(u_i x_t + v_i h_{t-1} + w_i c_{t-1} + b_i) \quad (2.4)$$

$$f_t = \sigma(u_f x_t + v_f h_{t-1} + w_f c_{t-1} + b_f) \quad (2.5)$$

$$g_t = \tanh(u_g x_t + v_g h_{t-1} + b_g) \quad (2.6)$$

$$o_t = \sigma(u_o x_t + v_o h_{t-1} + w_o c_t + b_o) \quad (2.7)$$

The weight matrices of input, recurrent connections, and cell state are rep-

resented, respectively, by w 's, u 's and v 's, while the bias vectors are b 's. The Logistic and Hyperbolic tangent (or Tansig) activation functions, which have been employed for gate activation and cell activation, respectively, are denoted by the symbols σ and \tanh . Equation (2.8) and (2.9) (Kumar & Kumar, 2022) provide information about these gates as well as the current concealed state and internal cell state (or output) (or output). Before the training phase, the biases and weights were initialised. Once the parameters were learned through backpropagation, the loss that occurred during this process was subsequently optimised using the gradient boost approach.

$$c_t = f_t \odot c_{t-1} + i_t \odot g_t \tag{2.8}$$

$$h_t = o_t \odot \tanh(c_t) \tag{2.9}$$

Recurrent Neural Network (RNN) issues owing to gradient disappearance may arise (Sameen & Pradhan, 2017). Applying LSTM (Hochreiter & Schmidhuber, 1997), a deep learning structure, to the field of traffic flow prediction can solve this issue. Ma et al. (2015) discovered that the LSTM network had a prediction accuracy that was higher than that of most statistical techniques for capturing the time correlation and nonlinearity of traffic.

A model for the forecasting of traffic built on LSTM was shown to be able to identify the correlation for the time and space for the traffic systems by Zhao et al. (2017b). Zhao et al. (2019) Traffic validated the suggested LSTM model and discovered that the model can outperform the support vector regression prediction strategy in terms of prediction performance.

Tian et al. (2018) employed an LSTM model to estimate traffic parameters and a multiscale smoothing method to restore missing values in data on traffic flow. Their numerical experiment showed that the LSTM model

beats other methods in terms of prediction performance.

In addition to these studies, a time series prediction model using LSTMs based on the attention mechanism was created by Wang et al. (2020). According to Zhang Zhang & Kabuka (2018), the architecture with two hidden layers of 500 neurons performed better than recurrent architectures with two hidden layers of 50 neurons, GRU-based architectures with two hidden layers of 50 neurons, or three hidden layers of 500 neurons, as well as other statistical models and machine learning models.

Many, if not all, of the most recent studies that looked at the effects of using non-traffic input datasets for predicting urban traffic parameters have produced more accurate predictions (Essien et al., 2019a,b; Jia et al., 2017). In Essien et al. (2019a), a deep bidirectional Long Short-Term Memory (bi-LSTM) model, for example, was given, which was trained using rainfall and temperature data as well as traffic flow factors. When compared to baseline (i.e. traffic-only) datasets, the study’s findings revealed an improvement in predictive accuracy. In experiments that incorporated non-traffic input data, similar findings were observed (Jia et al., 2017).

- **One-dimensional CNN long short-term memory network**

The ConvLSTM network is built by combining the CNN and LSTM layers. It simultaneously captures both the temporal and spatial components of the flow. The variable dimensions of the ConvLSTM network are different from those of the LSTM network, but it is possible to train it to be comparable to equation (2.4) to (2.9). Cell states and hidden states are designated by C 's and H 's, respectively, whereas input tensors are represented by the symbol X . Keep in mind that input, forget, and output are represented by the letters \mathcal{I}_t , \mathcal{F}_t , and \mathcal{O}_t respectively. The ConvLSTM network is expressed

by equations (2.10) and (2.14) (Kumar & Kumar, 2022):

$$\mathcal{I}_t = \sigma_a(U_i \oplus X_t + V_i \oplus H_{t-1} + W_i \oplus C_{t-1} + b_i) \quad (2.10)$$

$$\mathcal{F}_t = \sigma_a(U_f \oplus X_t + V_f \oplus H_{t-1} + W_f \oplus C_{t-1} + b_f) \quad (2.11)$$

$$C_t = \mathcal{F}_t \odot C_{t-1} + \mathcal{I}_t \odot \tanh(U_c \oplus X_t + V_c \oplus H_{t-1} + b_c) \quad (2.12)$$

$$\mathcal{O}_t = \sigma_a(U_o \oplus X_t + V_o \oplus H_{t-1} + W_o \oplus C_t + b_o) \quad (2.13)$$

$$H_t = \mathcal{O}_t \odot \tanh(C_t) \quad (2.14)$$

where \oplus represents the convolutional operator; U 's, V 's, and W 's are the weight tensors; b 's are the bias tensors.

Researchers are actively looking into the pairing of two machine learning models, particularly those that are helpful for deep learning, to more accurately predict traffic flow. One study Li et al. (2020) used a one-dimensional CNN long short-term memory network to evaluate real-time movement-based traffic volume prediction at signalised junctions (1-D CNN LSTM). To better understand temporal linkages and assess the spatial aspects of traffic volume, they used CNN and LSTM in their model. ConvLSTM network is employed in the study cited in Du et al. (2018) to forecast traffic flow in the event of congestion or accidents (at the trough or peak time periods). The root mean squared error (RMSE) for the ConvLSTM network is 9.75, higher than CNN's RMSE of 9.34 and lower than the RMSE for the LSTM network of 11.14. According to Ren et al. (2022), the SRCN model is a type of ConvLSTM network that has been used for traffic prediction during special events and has a reasonable forecast accuracy.

- **Autoencoder LSTM**

Archetypal, features or dimensions are extracted using an autoencoder. In this case, the encoder's output acts as the decoder's input. In accordance with the character sequence T , the decoder duplicates the original data.

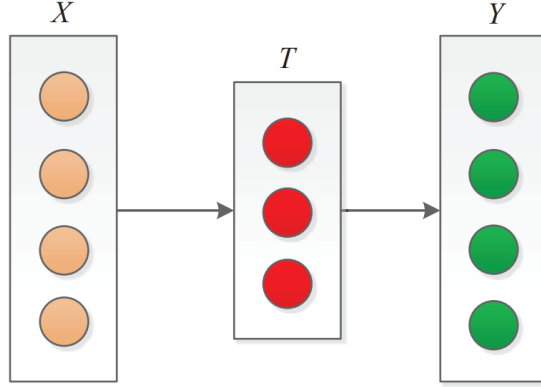


Figure 2.5: Structure of AutoEncoder network
(Wei et al., 2019).

Decoding is carried out to ensure that the qualities that were derived are accurate. After the AutoEncoder has finished training, we simply utilise the encoder to extract features from the original data in order to enhance the internal structure of the data. The Autoencoder’s operation is described as follows and is represented in Figure 2.5.

$$t_i = \sigma(w_t x_i + b_t) \quad (2.15)$$

$$y_i = \sigma(w_y t_i + b_y) \quad (2.16)$$

when σ is the activation function, w 's and b 's are the weights and biases, respectively. The error is decreased throughout the training phase using equation (2.17)

$$E(X, Y) = \frac{1}{2} \sum_{i=1}^n \|x_i - y_i\|^2 \quad (2.17)$$

when the difference between Y and X is sufficiently small or the coding procedure produces a legitimate result, it is thought that T represents the features extrapolated from the original data.

The urban traffic network is impacted by the volume of traffic on the current and surrounding roads. Any changes to the upstream and downstream traffic levels, as well as the historical traffic flow statistics for the current

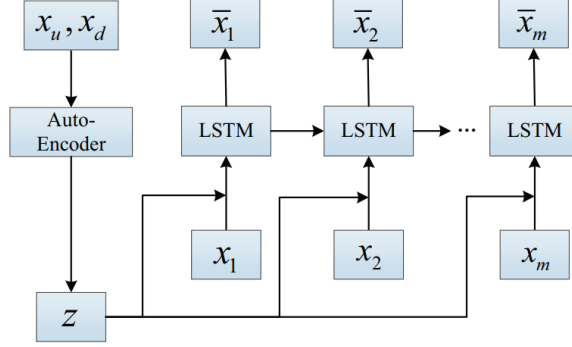


Figure 2.6: AE-LSTM network structure and AutoEncoder extracted features, and LSTM network used for the prediction of traffic flow (Wei et al., 2019)

site, must be reported. We employ AutoEncoder to extract features for this model from the data on upstream and downstream traffic flow. To improve the accuracy of the traffic flow estimate for the current location, the prediction network is then updated with the new features. Figure 2.6 depicts the structural layout of the AE-LSTM network. The essential AE-LSTM model formulas are provided by equation (2.18)-(2.25) (Wei et al., 2019; Kumar & Kumar, 2022).

$$z_i = \sigma(w_z(x_{ui} + x_{di}) + b_z) \quad (2.18)$$

$$y_i = \sigma(w_y z_{ui} + b_y) \quad (2.19)$$

$$i_t = \sigma(u_i x_t + r_i z_t + v_i h_{t-1} + w_i c_{t-1} + b_i) \quad (2.20)$$

$$f_t = \sigma(u_f x_t + r_f z_t + v_f h_{t-1} + w_f c_{t-1} + b_f) \quad (2.21)$$

$$g_t = \tanh(u_g x_t + r_g z_t + v_g h_{t-1} + b_g) \quad (2.22)$$

$$o_t = \sigma(u_o x_t + r_o z_t + v_o h_{t-1} + w_o c_t + b_o) \quad (2.23)$$

$$c_t = f_t \odot c_{t-1} + i_t \odot g_t \quad (2.24)$$

$$h_t = o_t \odot \tanh(c_t) \quad (2.25)$$

The characteristic sequence is defined as $Z_t = \{z_1, z_2, \dots, z_k\}$, where $X_u =$

$\{x_{u1}, x_{u2}, \dots, x_{um}\}$ and $X_d = \{x_{d1}, x_{d2}, \dots, x_{dm}\}$ are the inputs of the AutoEncoder in terms of the upstream and downstream traffic flow. While the other parameters are comparable to those of the LSTM network, r 's represents the weight matrices of Z . In Wei et al. (2019), you may get more details regarding the AE-LSTM network.

The autoencoder LSTM (AE-LSTM) model combines the autoencoder with LSTM. The autoencoder network extracts features, and the LSTM network predicts data. For traffic prediction, the autoencoder is used to extract features of traffic data, while LSTM is for predicting traffic flow (Wei et al., 2019). The autoencoder is used to extract features from traffic data for traffic prediction, whereas LSTM is used to predict traffic flow. The LSTM-LSTM model, used in Nigam & Srivastava (2023) to forecast traffic flow utilising both traffic and weather data, is an illustration of an AE-LSTM network. The prediction outcome of the LSTM-LSTM network is compared with that of the ConvLSTM, CNN, LSTM, and MLP networks in Nigam & Srivastava (2023) for the time periods of 5, 15, and 60 minutes. The LSTM-LSTM confirms that this network is superior to the others. For forecasting traffic, the AE-LSTM network TBSM has been proposed in (Ren et al., 2022). Compared to the MAE values of 5.01 for the MLP network and 4.92 for ConvLSTM, the MAE value of TBSM is 2.48, which is lower. Wang et al. (2021) uses a specific type of AE-LSTM network called 1DCNN-LSTM-Attention to predict traffic flow, and its performance was better than that of other AE-LSTM networks when the weather element was taken into consideration. The AE-LSTM network, which combines AutoEncoder and LSTM, was introduced in (Wei et al., 2019), to forecast traffic flow. The AE-LSTM recommended method employs upstream and downstream data in addition to the time elements to capture the spatial properties of traffic flow. In trials, the AE-LSTM model outperformed CNN in terms of performance.

2.3.2 Model Evaluation

The prediction model's performance may be evaluated using the following performance metrics (Miglani & Kumar, 2019; Jiang, 2022; Do et al., 2020).

Let y_i be the observed values and \hat{y}_i be the predicted values and n be total observations, we have

Root Mean Squared Error (RMSE)

$$\text{RMSE} = \sqrt{\frac{1}{n} \sum_{i=1}^n (y_i - \hat{y}_i)^2} \quad (2.26)$$

Mean Absolute Error (MAE)

$$\text{MAE} = \frac{1}{n} \sum_{i=1}^n |y_i - \hat{y}_i| \quad (2.27)$$

- Mean Square Error (MSE)

$$\text{MSE} = \frac{1}{n} \sum_{i=1}^n (y_i - \hat{y}_i)^2 \quad (2.28)$$

Mean Relative Error (MRE)

$$\text{MRE} = \frac{1}{n} \sum_{i=1}^n \frac{|y_i - \hat{y}_i|}{\hat{y}_i} \quad (2.29)$$

Absolute Percentage Error (APE)

$$\text{APE} = \frac{\hat{y} - y_i}{y_t} \quad (2.30)$$

Variance Absolute Percentage Error (VAPE)

$$\text{VAPE} = \text{var}\left(\frac{y - \hat{y}}{\hat{y}}\right) * 100 \quad (2.31)$$

Normalised Root Mean Squared Error (NRMSE)

$$\text{NRMSE} = \frac{\sqrt{\frac{1}{n} \sum_{i=1}^n (y_i - \hat{y}_i)^2}}{\max(\hat{y}_i) - \min(\hat{y}_i)} \quad (2.32)$$

Root Mean Squared Error Proportional (RMSEP)

$$\text{NRMSE} = \frac{\sqrt{\frac{1}{n} \sum_{i=1}^n (y_i - \hat{y}_i)^2}}{\sum_{i=1}^n \hat{y}_i}. \quad (2.33)$$

Lower RMSE enhances a model's performance. An RMSE of 0 represents a perfect match. The lower values of MAE provide super performance, and it gives a sense of accuracy which can be achieved by comparing the actual values to the predicted values.

It is necessary to combine several metrics to evaluate the performance of the proposed model (Miglani & Kumar, 2019).

2.4 Traffic Modelling

The traffic flow models have been used to investigate the effects on long-term planning as well as to analyze short-term predictions on traffic movement behaviour. Other applications of traffic flow models include infrastructure design and adjustment, network management to determine the need for intersections, and assessment of what causes congestion to spread throughout the network. Several developments have been carried out in the literature for on-ramp and off-ramp controls, variable speed limits, and rerouting systems.

In order to map and analyze the dynamics that result in traffic flow, several freeway traffic models have been proposed. Studies have also been conducted to investigate the environmental concerns associated with traffic. There are numerous types of traffic flow models. The main ones are determined by the variables and equations used to define the dynamics process. A common classification

scheme divides models into three types: continuous, discrete, and semi-discrete, based on how the elements describing a system change in their states. The two main models are deterministic and stochastic, based on the type of processes represented within the model.

When considering the degree of underlying traffic behavioural regulations, deterministic models are divided into five categories: microscopic, sub-microscopic, macroscopic, mesoscopic, and hybrid models.

Green shield introduced the first traffic flow model in 1935 (Greenshields et al., 1935b). Many traffic flow models based on the Green shield model have been proposed. Then, in the 1950s, microscopic and macroscopic models were introduced (Wardrop & Whitehead, 1952; Pipes, 1953; Moskowitz & Raff, 1954; Lighthill & Whitham, 1955a; Richards, 1956a; Beckmann et al., 1956; Chandler et al., 1958; Gazis et al., 1959). Later in the 1960s, mesoscopic models have been proposed (Edie, 1961; Gazis et al., 1961; Haight et al., 1963; Montroll & Potts, 1964; Drake & Schofer, 1966; Newell, 1993; Maerivoet & De Moor, 2005; Underwood, 2008).

Understanding the relationships between the distance between cars and their velocity is critical in traffic flow models. Greenfield examined these relationships for the first time in the 1930s, you can see (Greenshields et al., 1934, 1935a). Greenfield offered a number of relationships between these variables, ranging from linear to parabolic.

In 1934, the fundamental concept of traffic flow was introduced. The relationship between traffic density (vehicles/km) and traffic flow (vehicles/hour) was described as follows:

1. The density, k , rises as the number of vehicles increases, and equal zero when there is no vehicle on the road.
2. The displacement situation becomes impossible as more vehicles are added. This is referred to as jam density, k_{jam} or critical density, k_c . The vehicles will not move, $v = 0$, and the flow, q , will be zero at the jam density.

3. The density is typically represented by a parabolic curve, see Figure 2.7.

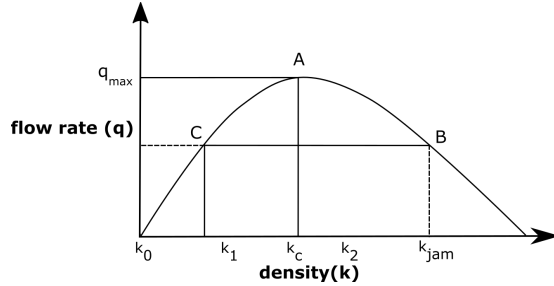


Figure 2.7: Flow density relationship.

Edie (1961) proposed the fundamental diagram with capacity drop. He described that the outflow is slightly lower when compared to the inflow just before breakdown, taking in a road section.

Treiterer and Myers came to the conclusion that hysteresis can explain a lot of the dispersed data (Treiterer & Myers, 1974). Kerner and Rehborn argued, in 1997, that other non-unique relationships between density and flow exist (Kerner & Rehborn, 1997). Newell (1993) presented the idea of hysteresis, which refers to the phenomenon where, in congested areas, the density-speed relationship is different from the relationship when cars decelerate.

Chanut & Buisson (2003) proposed a traffic flow model in which Hyperbolic conservation equations were used. Their model was designed to take into account the differing impacts of heavy and light vehicles in terms of length and space on speed and flow behaviours on European roads. However, these researchers emphasised that their model had limitations that still needed to be addressed, and recommended that further research be undertaken in this domain.

In efforts to better understand the nature of traffic flow, several models have been suggested at both macroscopic and microscopic levels in the past few decades. Various parts of these models have been used to develop a range of computerised traffic simulation software packages that have contributed to the development, analysis and visualisation of designs and control scenarios for use in determining the preferred systems for creating a safe environment. As a re-

sult, road traffic can now be observed in diagrams at the macroscopic level, and in the shape of vehicle trajectories at microscopic levels. Basic graphics that combine traffic flow, speed, and density can now be created to determine the trajectory of vehicles in a variety of circumstances (Ni, 2020). For example, Treiber et al. (2010) simulated driving movements with accelerations, deceleration and lane changes in reaction to traffic flow conditions. An empirical study was conducted by Reina and Ahn to examine lane flow distribution in 3-lane congested freeways (Reina & Ahn, 2019). Their findings identified that lane-specific traffic behaviours had significantly varying flow trends along with constant lane flow distribution, with four recurrent combinations identified across the 72 sites of their analysis. They found that although the varying lane flow distributions were not uniform, their probability increased when approaching freeway merges. Apart from experimental models such as these, a number of other mathematical models including microscopic, macroscopic and mesoscopic models (or coupled microscopic and macroscopic models), have been proposed. However, despite traffic flow modelling having been extensively examined, when comparing their results with ideal outcomes, some limitations in both traffic flow theory and simulation can be found. These include a lack of consistency between the models, a lack of flexibility in addressing driver diversity, and a lack of ability to provide predictions into the near future (Reina & Ahn, 2019). Microscopic models, in particular, are concerned with analysing the behaviour of individual vehicles, with a particular emphasis on the traffic dynamics of individual vehicles. Macroscopic models, on the other hand, depict vehicle interaction as a continuous function. Mesoscopic traffic flow models define the behaviour of separate vehicles by describing transportation elements in small groups. Cluster models, headway distribution models, and gas-kinetic models are examples of Mesoscopic models. In recent years, hybrid mesoscopic models have emerged, which combine microscopic and macroscopic models.

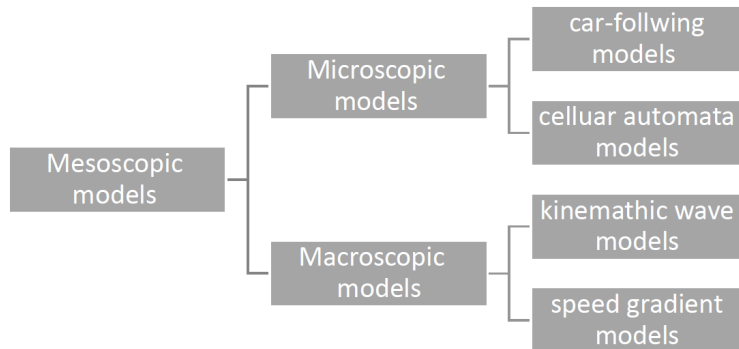


Figure 2.8: Model classification.

2.4.1 Microscopic Modelling

In microscopic models, vehicles are numbered to track their behaviour. For example, the n^{th} vehicle is followed by the $(n + 1)^{\text{th}}$ vehicle. The behaviour of each vehicle is then modelled based on the velocity, position, and acceleration of the leading vehicle.

The road is a series of cells that can be occupied by a single vehicle in Cellular Automata models.

Figure 2.8, displays an overview of microscopic models and the different model types making up the classification.

2.4.1.1 Car Following Models

Car-following and cellular automata models are the two most common types of microscopic models. Leading and following vehicle locations are continuous functions in car-following models, using ordinary differential equations, and are dependent on each vehicle's speed and distance between them.

In the literature, several models have been proposed to characterise the nature of car following. This entails describing how automobiles in continuous traffic react to one another. Pipe produced one of the first car-following models in 1953, emphasising that a linear increase in the minimum safe distance headway may

occur as speed increases (Pipes, 1953). The model's shortcoming was that when speeds were low, the resulting headway distance provided by the model was found to be less than the on-field observations.

The time gap between the leader and follower cars should not be smaller than the reaction time measured from the back of the leader car to the head of the follower car for the model to work properly. This means that the shortest time stimulating is equal to the reaction time multiplied by the time it takes the leader car to go a distance of its own length. As a result, the model distinguishes between the minimum distance that should be maintained at moderate and high speeds. The simplicity of the Lighthill, Whitham and Richards (LWR) model, together with the advancements in modelling that were occurring in statistical physics, sparked the development of various particle system models in the 1990s. As a result, Nagel & Schreckenberg (1992), introduced the cellular automata model, which represents a class of computationally efficient microscopic traffic models. The ideal velocity model was proposed by Bando et al. (1995, 1998), based on calculating the distance between the lead and follower vehicles. The model's fundamental concepts were developed using second-order differential equations, which were used to create the density pattern of a congested traffic flow. The model, on the other hand, lacked reaction times. It was shown, in Davis (2002), that reaction delays were crucial in determining the qualitative behaviour of the best velocity model via numerical simulations. He presented a methodology to account for the delays caused by the drivers.

Parameter identification in microscopic driving models is difficult, since reaction time and sensitivity to stimuli are not evident from typical traffic data. There is also a scarcity of statistical estimating procedures that are reliable. Many approaches have been developed in an attempt to address such issues.

Li et al. (2017) developed a car-following model based on the spring-mass system theory. The model takes advantage of the parallels between traffic flow acceleration behaviour and spring scaling properties and uses the perturbation

approach to obtain the stability condition for the proposed model's stability.

Wen and Karim, Shen & Shikh-Khalil (2017) implemented a microscopic traffic flow model in which each vehicle's behaviour is determined by the distance of the automobile in front of it in a monotone manner (follow-the-leader). Their research focuses on a travelling-wave profile that satisfies a delay differential equation. They established the existence, uniqueness, and local stability of the wave profile using very typical methods for (delay) differential equations. Their work establishes intriguing connections between current results for both continuous and discrete models of moving waves.

A while back, Hossain & Tanimoto (2022) suggested a knowledge traffic flow model that takes into account multiple preceding cars and the system time-delay impact to reproduce a more realistic flow field in the context of the widespread adoption of intelligent transportation systems with a wireless connection. The neutral stability criterion and linear stability theory were used to assess the model.

It demonstrates an improvement in the stability of a traffic flow field when compared to the traditional complete velocity difference model (optimal velocity model). For nonlinear analysis, the modified Korteweg-de Vries equation was developed and studied.

2.4.1.2 Intelligent driver models

The intelligent driver model (IDM), a special type of time-continuous car-following model, is an adaptive Cruise Control (ACC) allowing the vehicle to adjust its speed in response to the environment. There are various approaches applied to the IDM models, distinguished by the ease of use and accessibility of the parameters. For example, the simple approach equation (2.34) is applied when the actual vehicle deceleration is exceeded during emergency braking. In the case of safety studies, they ensure driver safety in a severe situation like an accident.

Moreover, emergency braking scenario is utilised to prevent a collision. In order to improve driver safety and give a realistic response in critical situations

like accidents, development of the IDM model is to create challenging addressing the stability requirement in relation to both acceleration and velocity.

In the IDM, longitudinal velocity, v_n , and safety time gap, s_n , of the n^{th} vehicle may be described by (Treiber & Helbing, 2002):

$$\frac{dv_n}{dt} = a_n \left(1 - \left(\frac{v_n}{v_n^0} \right)^4 - \left(\frac{s^*(v_n, \Delta v_n)}{s_n} \right)^2 \right), \quad (2.34)$$

where a_n is the maximum acceleration of the n^{th} vehicle v_n^0 are the velocity and the desired velocity of the n^{th} vehicle. The distance *gap* s_n defined by

$$s_n = \Delta x_n - l_{n+1}, \quad (2.35)$$

where l_{n+1} is n^{th} vehicle length and Δx_n denotes bumper to bumper distance *gap*.

The vehicle n 's desired minimum gap, s^* , in equation (2.34) is provided by

$$s^*(v_n, \Delta v_n) = s_n^0 + T_n v_n - \frac{v_n \Delta v_n}{2\sqrt{a_n b_n}} \quad (2.36)$$

where s_n^0 is the jam distance of the vehicle n , T_n is the safety time gap, and b_n is desired deceleration.

In traffic simulation models, IDM has also been used to assess VISSIM (Verkehr In Stdten - SIMulationsmodell: German for Traffic in Cities - Simulation Mode) and SUMO (Simulation of Urban Mobility). Treiber et al. (2000) investigated single-lane traffic in homogeneity using the IDM to compute and compare vehicle density and traffic flow with the empirical data of extended congested traffic to determine the varying percentages of cars and trucks. Analysis of the flow density and time series found in heterogeneous single-lane traffic revealed a typical inverse form, with differing gaps between the free and congested traffic data. The IDM model has been applied in a study designed to simulate longitudinal vehicle motion in a Multi-model Open-source Vehicular-traffic Simulator with a lane-changing strategy (Treiber & Helbing, 2002). In comparing the character-

istics of free and congested traffic, Treiber et al. determined the sensitivity of the IDM's parameter in relation to the platoon vehicle's traffic stability (Treiber et al., 2006). Kesting (2008) extended the IDM model to human drivers by modifying its parameters and adding noise to explore the impact of an IDM-equipped car on traffic flow and journey time in an open system with a bottleneck. Treiber & Kesting (2011) used the IDM to investigate convective instability in crowded traffic flow. Their study suggested that extended open systems, such as those occurring in traffic flow, are unstable when stationary perturbations accumulate and increase in a single direction, resulting in a departure from the system. Driver safety studies employing the IDM Model in other investigations of mixed traffic have been performed Derbel et al. (2012) examined the proportion and relative safety of IDM's automated vehicles in the event of accidents when the platoon leader abruptly brakes and comes to a complete stop following platoon stabilisation (catastrophic scenario). Their findings suggest that traffic is safer in terms of collision frequency when there are more IDM-equipped vehicles. The dwell time safety indicator was used to assess the safety of a mixed-traffic road in the absence of a collision. Driver safety increases in line with the percentage of automated vehicles fitted with IDM. Furthermore, driving safety increases as traffic congestion rises when 80 per cent or more of vehicles in circulation are equipped with IDM. However, although traffic density has no effect on driver safety, this may depend on the driver, safety indicator and automated vehicle model is chosen (Two Velocity Difference Model (TVDM) for manual and IDM as ACC for automated). Derbel et al. (2013) looked at how IDM can be tweaked to improve driver safety while still respecting the real-world capabilities of the vehicle. A new IDM version was constructed and evaluated using a microscopic traffic simulator in terms of string stabilisation, taking into account the last two adjustments and assuming that the driver should take into consideration the tail vehicle behaviour. They showed that although an increase of autonomous vehicles (AVs) in local traffic improves traffic stability, their car-following behaviours are not

entirely understood due to differences in their black-box controllers. Although IDM has been utilised in a range of studies, this model presents several flaws related to driver safety and respect for the true capabilities of a vehicle. Therefore, this model has been altered to include the addition of a positive term that is dependent on vehicle speed, deceleration capability, and an additional parameter of c_n , which is calculated based on a collision scenario. The optimal value of this parameter ensures that both traffic flow and the safety of the driver coincide. The model also includes a minor constant in the inter-distance term within the model. These two changes ensure that the model respects the vehicle's actual deceleration capabilities. In addition, a third change in the IDM model includes the human element, ($h_f = 1$ for stable platoon's acceleration and velocity), to allow the driver to consider the state of vehicles in front and behind him. Recent research has focused on the influence of the new IDM version on driver safety on mixed-traffic roads. Alhariqi et al. (2022) employed data from a real-world experimental trajectory to calibrate the IDM for mixed autonomous traffic. They added a standard deviation of velocity to the calibration goal function to account for stop-and-go traffic. This feature allows us to reproduce the traffic fluctuations observed in the experimental data in the goal function. They claimed that mixed independent traffic patterns may be modelled using their calibration and adaptive IDM approaches.

2.4.1.3 Cellular-automata Models

Cellular-automata concept was established by Von Neumann (1951) to examine biological systems. The concept of self-reproduction and theoretical machines known as kinematics were used to further Neumann's proposal. The model was advanced further by incorporating the concept of cellular spaces. The entire notion describes how cellular automation, also known as a grid of cells, works physically. Compared to other models, cellular automata have the following advantages:

- i) the model is essential, making it simple to program on a computer;
- ii) the model can represent complex traffic phenomena while also reflecting traffic flow properties;
- iii) roadways are separated into multiple portions, allowing for the simulation of changing vehicle circumstances;
- iv) models are dynamic models with finite discrete space and states;
- v) after local cell interactions are handled, the system can be scaled to any size without any further modelling challenges.

Due to the difficulties of traffic in nature, traffic simulation is one of the most effective ways to evaluate the effectiveness of traffic systems and to provide solutions to traffic problems. SUMO (Simulation of Urban Mobility) is an open-source microscopic multi-modal traffic simulator (Krajzewicz, 2010). It enables the user to model how a particular traffic demand behaves on a specific road network. Each vehicle is explicitly described, has its own route, and moves around the network independently. It is one of the solutions for high-precision transportation tasks. The simulation results of Can et al. (2020) show that the duration of the traffic event has a significant impact on travel time and mean speed. At the same time, it may result in greater traffic congestion.

2.4.2 Macroscopic Modelling

Macroscopic models describe the traffic flow as a continuum flow of fluids. To improve incident identification, researchers looked into estimation approaches that combined traffic states and event severity using a macroscopic traffic model. Dabiri & Kulcsár (2015) and Wang et al. (2016) showed how incident data may be incorporated into model-based traffic estimation methods by adjusting certain parameters (e.g. free flow speed and/or critical density) that represent the

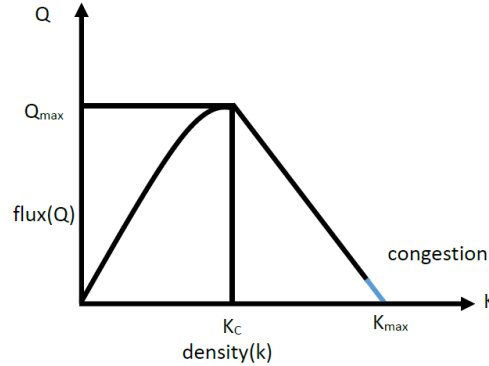


Figure 2.9: Relationship of density and flux.

incident impact. A macroscopic model uses substantially less memory and calculation time in the surrounding areas, producing less-detailed results (for instance, on a highway ring road around an urban area).

2.4.2.1 Classical LWR model

In 1955, a model based on fluid dynamics was introduced as the first macroscopic flow model, established a relationship between vehicle density and flux (Lighthill & Whitham, 1955a) as shown in Figure 2.9. One year later, Richards (1956a) proposed the LWR model (2.37) to describe the evolution of traffic density along a route in real-time. The road was depicted as a one-dimensional entity, without the realism of crossings and on-and-off ramps, but including traffic signals. The density of traffic at the location x at time t is denoted by $k(x, t)$. The LWR model, based on a basic conservation law for vehicle density, is

$$\frac{\partial k}{\partial t} + \frac{\partial}{\partial x}(q(k)) = 0, \quad (2.37)$$

where $q(k) = kv_e(k)$ denotes traffic flow rate (traffic volume) and $v_e(k)$ is an equilibrium (ideal) traffic velocity. The true meaning of such a formulation becomes clear when the density $k(x, t)$ is integrated over an interval $[a, b]$ on the highway. Then the rate of change of the total traffic volume in the interval $[a, b]$ is defined

by

$$\frac{d}{dt} \int_a^b k(x, t) dx = - \int_a^b (kv_e(k))_x dx = k(a, t)v_e(k(a, t)) - k(b, t)v_e(k(b, t)). \quad (2.38)$$

The difference between the traffic volume coming at point a per unit time and the traffic flow departing at point b per unit time is the right-hand-side term.

The velocity v_e in equation (2.38) must satisfy the following conditions:

1. $v_e(k_{min}) = v_f$ indicating a maximum speed at low traffic density,
2. $v_e(k_{jam}) = 0$, where k_{jam} indicates a maximum traffic density at which the speed comes to a halt;
3. $kv_e(k)$ is a concave function of k . Because such nonlinear conservation laws tend to have solutions with embedded shocks and rarefaction waves, this latter criterion is a bit technical, but it allows for a simplified explanation of the set of solutions to such a differential equation. To explain the long-term behaviour, consider that the number $kv_e(k)$, also known as the flux, is concave.

We can look at an example to better understand the phenomena. Suppose that

$$v_e(k) = 1 - k \text{ for } 0 \leq k \leq 1 = k_{jam},$$

the flux function

$$q(k) = kv_e(k) = k(1 - k).$$

For smooth traffic density, we can write the conservation law as

$$k_t + q'(k)k_x = 0, \quad (2.39)$$

where $q'(k) = 1 - 2k$. Since $q''(k) = -2$, $q(k)$ is concave on the interval $[0, 1]$. This form of the conservation law implies that along characteristics, i.e., curves $x(t)$ for which $\frac{dx}{dt} = q'(k)$ that $\frac{dk(x(t), t)}{dt} = 0$, and therefore that $k(x(t), t)$ is constant

along such characteristics. Therefore, $a = q'(k)$ is constant along such a character, and we see that $k(x_0 + at, t) = k(x_0, 0)$. The characteristics' method breaks down when different characteristics intersect at the positive time when shocks form, or when diverging initially nearby characteristics produce what are called rarefaction waves.

In 1955, Lighthill & Whitham (1955b) proposed the traffic flow model while taking into account the kinematic wave (KW) theory. Their theory held that a flow of water was equal to a flow of traffic, the speed of which is defined by the slope of the flow-density graph relative to the road. Bottlenecks and intersections were discussed in relation to traffic flow. Their design, on the other hand, has a significant flaw because it was created especially for long-distance cars. A year later, Richards (1956b) proposed the model, giving it the name Lighthill-Whitham-Richards (LWR) model. The foundation of this model is the partial differential equation that represents the evolution of traffic density along a road.

2.4.2.2 Modified LWR models

For lane-changing effect, various models, namely the kinematic wave theory (KW) model, have been developed based on either the Lighthill-Whitham-Richard (LWR) method (Lighthill & Whitham, 1955b; Richards, 1956b), or the speed gradient (SG) method (Jin, 2010a; Chang-Fu et al., 2007). In the kinetic wave (KW) model, the traffic flow is modelled in terms of kinematic waves in either of three quantities: flow q , speed v and density k . The model describes two basic forms of waves:

- 1) decelerating shock waves, which generally arise due to slow moving vehicles,
- 2) accelerating rarefaction waves, which generally occur when a congested regime of traffic enters a low traffic density area.

In a KW model, conservation of traffic is applied to obtain a partial derivative equation given in equation

$$\frac{\partial k}{\partial t} + \frac{\partial}{\partial x}(q) = 0, \quad (2.40)$$

In other words, KW models assume that flow q is expressed in terms of density k . Upon substituting this relationship in equation (2.40), one gets a simplified version which is shown in equations

$$\frac{\partial k}{\partial t} + \frac{\partial}{\partial x}(q(k)) = 0, \quad (2.41)$$

and

$$v = v(k) = \frac{q(k)}{k}. \quad (2.42)$$

Some important points from the KW model may be concluded as follows.

- As k approaches zero, q also approaches zero.
- Initially, more k leads to higher q which occurs until the maximum q value which is known as capacity of a road
- Beyond capacity, any further addition to k leads to lower q value.
- As k continues to increase, there comes a point when the q value approaches zero. This is known as jam density of a road.

Jiang et al. (2002), proposed an anisotropic model with the speed gradient term instead of the density gradient term in the dynamic equation. Another novel anisotropic continuum model was proposed by Gupta & Katiyar (2006, 2005), which was based on an improved car-following model. Tang et al. (2008b, 2014), developed higher order models which took into consideration the varying physical and traffic conditions on the roads along with the traffic interruption probability. Furthermore, Chen et al. (2013) included the impact of the gradient of the roads in the macroscopic model. The speed gradient model developed by Jiang et al. (2002) comprised the traditional continuity equation (shown earlier in equation (2.40) along with the dynamic equation shown in equation (2.43)

$$\frac{\partial v}{\partial t} + v \frac{\partial v}{\partial x} = \frac{v_e(k) - v}{T} + c_0 \frac{\partial v}{\partial x}, \quad (2.43)$$

where T is the relaxation time and c_0 is the speed at which the disturbance propagates. The first term on the right of equation (2.43), referred to as the relaxation term, represents the situation when a driver adjusts its speed to attain equilibrium speed. The second term represents that the driver reacts to the downstream (in-front) traffic conditions, which is also referred to as the anticipation term. Many researchers have proposed experimental models and mathematical models to describe the traffic flow on lane-changing roads with two lanes (Tang et al., 2008a; Jin, 2010b; Huang et al., 2006), three lanes (Hu et al., 2018; Chen & Fang, 2015) and multi-lanes (Delis et al., 2018; Laval & Daganzo, 2006; Shvetsov & Helbing, 1999). To understand the free-flow traffic on a freeway, analysis of real-time traffic data is essential. Many experimental frameworks have been proposed to investigate many traffic aspects such as traffic jams without bottleneck (Sugiyama et al., 2008), and instability of traffic flow (Jiang et al., 2018; Jin et al., 2019).

As the lane changes may be induced by on-ramp traffic and road conditions such as closures and other incidents. In an urban traffic region, a lane-changing vehicle is likely to generate a temporary movement bottleneck on its target lane while it increases the speed acceleration on that lane (Laval & Daganzo, 2004). For controlling vehicle traffics, understanding the effect of lane-changing activity on the traffic flow is important. Research in this area has received increasing attention to help civil engineers control freeway traffics.

A lane change manoeuvre is characterised by the transition of a vehicle from a lane to an adjoining lane (Mathew, 2014). These inter-lane movements create hindrances for other vehicles in the vicinity, which eventually has implications on the micro and macroscopic traffic flow (Al-Kaisy et al., 2005; Daganzo et al., 1999). While it is easy to model the intraplate movement of a vehicle (by taking into consideration the speed and spacing of the leading vehicle), lane change is

more complex as it involves multiple criteria (the available gap between the subject vehicle and leading vehicle in the adjoining lane for example) to determine a safe manoeuvre. Frequent lane changes lead to speed reduction and capacity drop, resulting in the formation of shock waves (Jin, 2010a; Sasoh & Ohara, 2002). Furthermore, these manoeuvres, which are usually concentrated around ramps, lead to the formation of traffic oscillations, eventually resulting in stop-go waves during congested traffic in a highway (Daganzo et al., 1999; Hoogendoorn & Bovy, 2001; Wall & Hounsell, 2020). These stop-go waves require more drivers' focus, leading to driver frustration and safety concerns. Thus, developing a lane change model that genuinely reflects real-world conditions is essential in traffic flow modelling. The real-world applications of lane change models are visible in two domains, namely: Adaptive Cruise Control (ACC) and simulations. The ACC, which is equipped with modern automobiles and facilitates driving assistance, can be further subdivided into collision avoidance and automation models. While the former aids the driver in undertaking safe lane change manoeuvres, the latter automatically controls the steering wheel to execute a safe lane change (Rahman et al., 2013).

Most of the lane change models, in general, comprise a two-stage decision process, namely: lane selection and execution. The desire to change lanes is generally triggered by two factors: 1) Compulsory or Mandatory Lane Changing (MLC) (i.e., approaching the end of the lane, avoiding an incident, etc.), and 2) Optional or Discretionary Lane Changing (DLC) (overtaking a slow, leading vehicle, etc.). The behavioural characteristics of drivers motivate them to undertake the lane selection process (Ramanujam, 2007). The execution of lane change is characterised by lane selection followed by applying gap acceptance models.

Toledo (2007) conducted an extensive review of the literature in lane change modelling and reported that the key shortcoming of a majority of the existing models was the inability to accurately model driver characteristics and preferences such as temporal correlations among driving decisions, short-term decision-

making, etc. A similar literature survey was conducted by Moridpour et al. (2010), to discuss the pros and cons of the several existing methods. The change method is classified into two categories, rigid mechanistic models and AI-based models. The shortcomings of the existing lane-change decision models are as follows.

Firstly, none of the developed methods models the decisions of the drivers of heavy vehicles. Secondly, a majority of the models focus mainly on the lane-change decision models and do not much on the execution component. Thirdly, the models were validated against macroscopic traffic information.

Similarly, Rahman et al. (2013) reviewed the state-of-the-art microscopic lane-change modelling used in simulations. The authors discussed how advancements in data collection techniques such as detailed vehicle trajectory information could potentially contribute to the development of newer models. Zheng (2014) reviewed the existing lane-change models with lane-change behaviours, including capturing the decision-making process of the driver and determining the impact of lane change on the nearby vehicles.

Tang et al. (2009) developed a macroscopic lane-change model for a two-lane road using the linear stability theory. Their model was found to affect the stable region and wave speeds emanating from the first and second-order models. The flow-density relationship was expressed as a function of the rate of a given flow, its difference with the expected flow and lane change.

Jin (2010a) implemented the KW model to study the impacts of two lane-changing traffic on overall traffic flow with bottleneck region. Jin (2013) modified the LWR model to determine lane change for different vehicle categories. The fundamental diagram for each vehicle category was obtained using the car following model having lane-change parameters along with road and traffic characteristics. The fundamental diagrams were calibrated and validated using the available data. Using entropy maximisation, the multicommodity LWR model was solved using the Riemann problem over a homogeneous lane-changing area.

The resulting flux function was obtained, relating to demand and supply. The flux function was then used to study the impact of lane change for a site experiencing lane reduction. It was suggested that the modified LWR model with lane-changing could be integrated into a mesoscopic framework for alleviating bottleneck formation due to frequent lane changes. Tang & Huang (2004) proposed an SG model to study traffic dynamics for two-lane freeways where the faster vehicles are allowed to travel on both lanes while the slower ones are on one lane only. Chuan & Di-Hua (2010) proposed a continuum model based on the SG approach. The initial conditions and boundary conditions for density and velocity fields were given. The equilibrium speed-density relationships for both lanes were presented. Many multi-lane changing models have been proposed to quantify the impacts of lane-changing manoeuvres on traffic flow. Chen & Fang (2015) proposed an SG traffic flow model for a three-lane highway taking into account lane changing. They claimed that their model could capture real traffic phenomena such as shock, rarefaction, stop-and-go waves and local clusters. Hu et al. (2018) proposed a lattice model based on the KW approach to study the characteristics of lane-changing traffic flow on a three-lane freeway. Delis et al. (2018) proposed a multi-lane SG model to simulate lane changes due to vehicle interaction on the three-lane motorway. The effects of adaptive cruise control or cooperatives were investigated. Zhang et al. (2018) studied the effect of off-ramps on lane changes and traffic performance across several traffic conditions using the Shanghai Naturalistic Driving Study (SH-NDS) data. The SH-NDS captures driver behaviour in a naturalistic environment over an extended period. A logistic regression was carried out to model driver choice towards the target lanes across three traffic conditions: free flow, medium flow and heavy flow. The results showed that the behaviour exhibited by the drivers using the off-ramp was a combination of route planning and preferring better driving conditions. In fact, under heavy flow, the latter behaviour became more prevalent. It was also found that the speed distribution was more dispersed for the scenario which involved

a vehicle moving from a slower lane to a faster lane, thus increasing the crash likelihood. The contribution of the study was to understand the driver behaviour around off-ramp locations and implement strategies aimed at an overall improvement in traffic performance and minimising traffic incidents. Similarly, Zhang et al. (2018) also studied driver lane-changing behaviour on three highways in China. With different lane changing patterns (lane change rate, choice of target lane, etc.) and the impact of ramps, high-speed lanes vehicle types were studied. The results show that lane change is an instantaneous decision which is triggered due to aggressive driving behaviour of drivers. These existing models give a basic understanding of the effect of lane changes on traffic flow. However, there are limitations to the model.

2.4.2.3 Cell Transmission Model (CTM)

To characterise the propagation process of congestion in road networks, Daganzo (1994) introduced a cellular transmission model based on traffic flow theory. In simulating metropolitan settings, this model presents a discrete road network form equivalent to the Godunov (1959) approach. Several CTM-based techniques for explaining the propagation characteristics of recurring and incident congestion have been developed using simple implementations (Long et al., 2011; Zhang & Gao, 2012; Tao et al., 2016).

However, although much research has been undertaken in the field of congestion propagation, many models have been impractical due to various mathematical assumptions and the oversimplified modelling of road networks in regular grids (Qi et al., 2013; Zhao et al., 2017a). Assuming that the equilibrium traffic velocity is solely determined by density is unrealistic, which is why so many efforts have been made to improve the models. Forward-looking drivers can maintain a lower front traffic density by accelerating (accelerating), and decelerating as traffic density increases in the forward direction.

As the velocity is the function of car position at time t ,

$$\frac{dv(t)}{dt} = \frac{dv(x(t), t)}{dt} = v_t + v_x \frac{dx}{dt} = v_t + vv_x. \quad (2.44)$$

The two-equations model of traffic flow, namely, the Payne (1971),

$$\begin{cases} k_t + (kv)_x = 0 \\ v_t + vv_x = \frac{v_e(k)-v}{\tau} - \frac{v(k)}{k\tau} (k)_x \end{cases} \quad (2.45)$$

where τ is relaxation time and v is anticipation coefficient (Payne, 1971)

The vehicle's acceleration is on the right side of the equation (2.45), which is then the models on the right side. The velocity is then driven to the equilibrium velocity by the first term on the right side of (2.45), where τ is a relaxation time. The second component is effectively a term of deceleration: when the forward-looking traffic density grows ($k, x > 0$), and when the forward-looking density decreases, the term of acceleration increases.

The vast majority of traffic flow models are isotopic. On the other hand, it was suggested, in Daganzo (1995), that vehicles travelling backwards have anisotropic behaviour. The anisotropic models have progressed quickly as a result of Daganzo's work. The most well-known model is arguable that in Aw & Rascle (2000). Instead of Payne's velocity equation (2.45), the velocity equation is

$$\frac{\partial}{\partial t} (v + p(k)) + v \frac{\partial}{\partial x} (v + p(k)) = 0 \quad (2.46)$$

with a pressure term $p(k) = k^c$ with some constant $c > 0$. In 2002, it was presented the so-called speed gradient model (Jiang et al., 2002). In equation (2.46), the speed gradient substitutes the density gradient in the motion equation, ensuring that the characteristic velocities do not exceed the macroscopic flow velocity. Backward travel is not a problem in the (2.46) model, as it is in other models.

For instance, consider the following Payne model (Payne, 1971).

$$\begin{cases} k_t + (kv)_x = 0 \\ v_t + vv_x = \frac{v_e(k)-v}{\tau} + c_0 v_x, \end{cases} \quad (2.47)$$

where the second term on the right side of (2.47) controls the driver acceleration and deceleration for stop-and-go waves, shock waves, and rarefaction waves. For the local cluster impact on highway flow dynamics, the following model has been proposed (Jiang et al., 2002):

$$\begin{cases} k_t + v_e(k)k_x + kv_x = 0 \\ v_x + vv_t = \frac{v_e(k)-v}{\tau} + k_1 v'_e(k) \frac{\xi}{\tau} k_x + k_2 \frac{\eta}{\tau} v_x, \end{cases} \quad (2.48)$$

where K_1 and K_2 are model parameters and $\xi = \xi(k, v)$ is for the anticipating driving behaviour and $\eta = \eta(k, v)$ is for the adaptive driving behaviour. Stability for the model (2.48) requires that,

$$kv'_e(k) + k_1 \frac{\xi}{\tau} + k_2 \frac{\eta}{\tau} \geq 0. \quad (2.49)$$

Recently, various studies have applied these concepts to more realistic traffic conditions. Soheili et al. (2013) simulated adaptive traffic flow density. Tang et al. (2015), proposed a macroscopical traffic flow model taking into account real-time traffic circumstances. Mollier et al. (2019), developed a two-dimensional macroscopic model for large-scale traffic networks. Khan & Gulliver (2018) presented a macroscopic traffic model to examine flow harmonisation. The macroscopic models were also used to analyze traffic flow on curving roadways with weather conditions (Khan et al., 2018; Xue & Dai, 2003). In Suwanno et al.'s work, a way for quantifying urban flood problems was proposed by applying the notion of a macroscopic fundamental diagram (MFD) to convey traffic circumstances in specified ranges. In order to develop a traffic model with vehicle-flow characteristics and evaluate the effectiveness of the transport system, MFD analysis was used to identify correlations between traffic flow-density and density-velocity.

The developed model improved the performance of the traffic flow on the road network under various flood conditions.

2.4.3 Mesoscopic Modelling

To bridge the gap between the microscopic models and the macroscopic models, mesoscopic traffic flow models were created. Vehicle flow is described by conventional mesoscopic models in aggregate terms. On the other hand, individual cars have a unique set of rules for acceptable behaviour. Members of the family include headway distribution models, cluster models, gas-kinetic models, and macroscopic models derived from these. Recently, a novel branch of the tree that combines microscopic and macroscopic models has appeared: hybrid mesoscopic models.

The mesoscopic traffic flow models have been proposed to ensure accuracy and computing efficiency (Li et al., 2015b). Various softwares such as DynaMIT (Ben-Akiva et al., 2002), DynaSMART-X (Mahmassani, 2001), PTV Visum-online (Ploss & Vortisch, 2006), and DynaTAIWAN (Hu et al., 2005), have been developed based on simulation-based dynamic traffic assignment techniques with mesoscopic traffic flow model as the core theoretical model. Traffic flows are calculated using temporal headway in headway distribution models. The time headways are independent random variables with the same distribution. The models depict the distribution of individual vehicle headway rather than directly tracing the vehicles (Li & Chen, 2017; Buckley, 1968; Branston, 1976).

Moreover, traffic flow is described as a flow of clusters of automobiles in cluster models. Each cluster contains numerous vehicles, and flow parameters such as velocity and headway are assumed to be uniform within each cluster. When passing opportunities are restricted, clusters might form, for example, as a buildup of vehicles behind a slow vehicle. Clusters can either grow or die. The cluster model is the most common and well-known (Mahnke et al., 2005). Gas-kinetic models have been developed to investigate the motion of many small particles

(atoms or molecules). When applied to traffic flow, the gas models can capture the dynamics of vehicle velocity distribution functions (Kessels, 2019).

To summarise, hybrid models have been created to mix modelling techniques from different branches. Most hybrid models, also known as multiscale models, combine a continuum model and a car-following model. In situations and places where it's necessary, like the city centre, they often employ a tiny model to get the level of detail and precision they need.

2.5 Optimisation Models of Traffic Flow under Non-Recurrent events

Severe traffic jams and dangerous situations can occur at any time and in any locations. Because of the uncertainty of occurrence, traffic modelling for optimal management under non-recurrent events is a major required. Civil engineers focus exclusively on applying adaptive methods in normal (recurrent) traffic conditions. Various control strategies have been applied to manage traffic under recurrent and non-recurrent events. However, the use of appropriate control strategies in the events of catastrophic catastrophes is still a difficult problem, especially when multi-lane roadways with various intersections are considered. Thus, many optimisation models have been proposed to obtain an optimal set of control strategies for traffic management.

2.5.1 Traditional Optimisation Models

One of the most effective and economical methods to reduce traffic is optimal traffic control on highway networks.

Over the past two decades, a vision of developing of Intelligent Transportation Systems (ITS) has led to numerous research works focusing on Ramp Metering as part of Advanced Traffic Management Systems (ATMs) on highways. Three primary mechanisms that have been used to regulate and manage the traffic

throughput on highways are ramp metering (RM), variable speed limit (VSL), and lane change controls.

It in Variable Speed Limits (VSL) and Ramp Metering (RM) are two of the most efficient types of control strategies (Papageorgiou & Kotsialos, 2002; Han, 2017). (Maciejowski, 2002) proposed model predictive control (MPC) using network operators to obtain the best control inputs for a road network based on its current condition across a given time horizon. The control inputs were then applied to the network (Hajiahmadi et al., 2015; Frejo & Camacho, 2011; Muralidharan & Horowitz, 2015).

1) Ramp Metering and Lane Change controls

A ramp meter is basically a traffic signal at the entry of a highway, via an on-ramp, to regulate the number of vehicles which intend to join the highway. The idea is to allow a vehicle to enter the highway once gaps are detected in the traffic stream on the highway (Arnold, 1998). The metering rate depends on the prevailing speed and volume on the highway. Ramp metering restricts bottleneck formation and delays on the highway by avoiding situations such as bunching of vehicles around the merge points, which leads to a reduction in the speed on the highway. Ramp meters in fact shift the location of delay and bottleneck towards the on-ramp, away from the highway, which facilitates a smooth flow of traffic. There are two types of ramp metering mechanisms:

- Pre-timed controller which allows a vehicle to enter in fixed time intervals;
- Available gaps on the highway and queue length on ramps before deciding the green time (Arnold, 1998).

A variety of ramp metering techniques and algorithms have been developed to date aimed at smoothing traffic flow on highways and making them more efficient. The choice of a given algorithm is governed by the geographic location of the highway, ramp and objectives of the traffic management authority. Papageorgiou & Kotsialos (2002) conducted an extensive review of the state-of-the-art

on-ramp metering and pointed out that futuristic highway networks should be autonomous in their operations to avoid bottleneck formation, delays, and safety issues. Li et al. (2018) presented an RM model based on CTM which was calibrated using traffic data collected on a section of the highway. Hou et al. (2008) presented an iterative approach as a way to control density using a macroscopic model comprising highway and ramp meters. The findings were that the iterative learning control method performed very well in improving the traffic conditions on the highway. Shaaban et al. (2016) conducted a review of the literature on the advances made in adaptive ramp metering. The studies taken into consideration were segregated into two categories: traditional and recent strategies. The traditional methods such as ALINEA, Bottleneck Algorithm, Zone Algorithm, METALINE, HELPER Algorithm, System-Wide Adaptive Ramp Metering (SWARM), Fuzzy Logic, Linear Programming, Dynamic Ramp Metering, Advanced Real-Time Metering System (ARMS), COMPASS and Linked Algorithm have been reviewed and discussed. Recently, a new ramp metering algorithm, Feedforward ALINEA (FF-ALINEA), for studying the bottleneck formation in the vicinity or at a distance from on-ramps was proposed by Frejo & De Schutter (2018). The results from simulations showed that FF-ALINEA was superior to other algorithms (ALINEA and Proportional Integral ALINEA (PI-ALINEA)) in maintaining the optimal traffic throughput in the system. Furthermore, FF-ALINEA was found to be more stable under different demand scenarios. In another recent study, Han et al. (2020) developed a hierarchical control method to allow for coordinated ramp metering on a highway (including ramps) network. The method uses a simplified aggregate traffic model which expresses total throughput as the total number of vehicles on the highway. This method was found to bring further reduction in traffic congestion and the resulting delays.

More recent works have focused on developing novel strategies for achieving advanced ramp metering. Tajdari et al. (2019)] introduced a novel method involving ramp metering and lane changes for a highway system that even comprised

connected and semi-autonomous vehicles. The inclusion of these vehicle types was based on the idea that a proportion of vehicles in the traffic stream followed certain instructions received, such as to change lanes, etc. It involved a Linear Quadratic Integral (LQI) regulator and an anti-windup scheme derived from a simple Linear Time-Invariant (LTI). The method led to a significant improvement in the throughput on the highway. The performance was tested using a first-order multi-lane macroscopic traffic flow model with capacity drops and led to a significant improvement in the throughput on the highway.

Vishnoi & Claudel (2021) proposed an LWR optimisation approach to handle the problem of VSL control on road networks. They also gave certain mathematical concepts that allow the optimisation problem's size and computational time to be reduced. The more recent approaches include Dual Heuristic Programming Control (DHPC), Heuristic Ramp-Metering Coordination (HERO), Additive Increase Multiplicative Decrease (AIMD) algorithm, Proportional Integral ALINEA (PI-ALINEA), ALINEA with Speed Discovery, Genetic Fuzzy Logic Control (GFLC), Zippered Control Strategy (ZCS) and Iterative Local Control (ILC).

2) Variable Speed Limit Control

The intelligent transportation system (ITS) solutions known as VSL systems enable for the modification of speed restriction requirements in response to shifting traffic, incidents, and/or weather conditions. Based on variations in traffic speed, volume detection, and road weather information systems, variable speed limit systems are utilised to establish the proper speeds for vehicles. The necessary modifications in speed limits are posted on overhead or roadside variable message signs (VMS). The following are the key advantages of VSL implementation:

1. Reducing the velocity disparities among cars in the same lane and/or next to it can increase safety. By synchronising driving habits and discouraging lane-changing, this decrease in speed variance lowers the risk of an accident.

2. Steering clear of traffic jams: When traffic is almost at capacity, any interruption in the flow could cause traffic congestion. A variable speed limit can help restore freeway capacity by decreasing traffic that would otherwise approach bottleneck regions and averting or delaying traffic flow disruptions Hegyi et al. (2005).

3. Increased throughput and environmental benefits: Because traffic congestion is linked to increased fuel consumption and emissions, VSL's capacity to improve traffic flow has environmental benefits Zegeye et al. (2009).

Wang et al. (2019) developed a hybrid model to study the nonlinear traffic dynamics and some other interesting properties around the ramp sections and the highway by using the finite difference method. The traffic dynamics were studied by capturing the change in the traffic flow parameters (density, flow and speed) under different traffic conditions. The robustness of this method was checked by testing linear and nonlinear dynamics for different traffic states. Wang et al. (2019) further included variable speed limit signs around the on-ramp locations to assess their effect on the throughput. A variety of coordinated and isolated scenarios were tested using micro-simulation to compare the control strategies. The sources of error were studied by disentangling the forecasting and simulation models. The results showed improvement in vehicle throughput, each under the coordinated and isolated cases, the extent of which varied depending on the prevailing demand.

3) Ramp Metering and Variable Speed Limit Controls

Under highway circumstances, an increase in traffic demand reduces the motorway's Level of Service (LOS). Increased inflow causes traffic disruptions or congestion in the on-ramp merging zones of the highway. Due to the merging of vehicles from the on-ramp into the mainline, the influx slows down the main traffic flow. Such occurrences are exclusive to peak demand during rush hours. A bottleneck is when the mainline traffic flow volume on a particular length of highway surpasses the designated throughput (capacity) and the traffic flow becomes

unstable. Vehicle contacts become more intense as a result of the mainline traffic flow being unsteady due to increased traffic demand. When traffic is moving unevenly, a single car or a small group of cars can slightly quicken or slow down the pace of neighbouring vehicles. On urban freeways, ramp metering and variable speed limits (VSL) are the two traffic control strategies most frequently employed (RM). VSL alters the dynamics of the traffic flow by controlling the speed of the major highway traffic flow. Through the use of Variable Message Signs (VMS), VSL is able to manage the increase in traffic on the controlled length in an indirect manner (Vrbanić et al., 2021). The VSL control system was created in order to increase operational capacity without adding additional lanes to the current traffic infrastructure on metropolitan highways. On the other hand, the RM used as a closed-loop or open-loop control system restricts the amount of vehicles using the controlled on-ramp to enter the highway. For instance, the ALINEA algorithm is a feedback control loop-based RM algorithm. For additional details, refer to Vrbanić et al. (2021).

2.5.2 CTM-based Optimisation

Gu et al. (2022) proposed a distribution resilient optimisation model using CTM approach for dealing with the ramp metering problem in the presence of unknown traffic demand flows. Their model requires only partial distributional knowledge of stochastic demand flows. To approximate the distribution robust change requirements, the proposed issue can be conservatively represented as a semi-definite programming (SDP) problem utilising the Worst-Case Conditional Value-at-Risk (WCVaR) constraints. They claimed that the distribution robust control strategy produced consistent results in a range of uncertain environments.

2.5.3 Machine learning-based Optimisation

Machine learning-based optimisation models have been developed to analyse recurrent and non-recurrent traffic behaviours for evaluating congestion levels. In

Singh and Mohan’s work (Singh & Mohan, 2018), a model including a stacked autoencoder was devised in an effort to determine road car accidents. Surveillance videos were thus adopted to produce pixel-intensity images, with cases examined in Hyderabad City, India. Wang et al. (2018) described the spatio-temporal impact of traffic incidents via a mathematical integer programming approach, resulting in 98 per cent of the total computing time. Zhang et al. (2016) adopted a dictionary-based comparison theory to observe traffic flow patterns across three geographical levels, namely detector, intersection, and sub-region. He et al. (2019) utilised low-frequency probe vehicle data (PVD) to detect traffic congestion, while Tian et al. (2019) adopted cooperative vehicle infrastructure systems (CVIS) and machine vision in order to automatically detect car accidents. They also developed an image database, CAD-CVIS, to improve the approach’s accuracy. In Pu et al. work (Pu et al., 2019), a framework was developed, named STLP-OD, to detect non-recurrent traffic outliers by determining propagation between roads. Machine learning techniques were also deployed. Cheu et al. (2003) used machine learning algorithms, namely support vector machine (SVM), in order to detect incidents on freeways in San Francisco. Dogru & Subasi (2018) on the other hand, used Random Forest models, combined with simulations to detect traffic incidents. Krupitzer et al. (2019) developed a Gradient Boosting Machine (GBM) algorithm framework to detect traffic issues with incident detection.

2.6 Concluding Remarks

A comprehensive literature of deep learning models to forecast traffic flow through time series analysis was reviewed. Three different deep learning models including MLP, CNN, LSTM, 1D-CNNLSTM and AE-LSTM, were described in detail. Also, the traffic flow based on microscopic and macroscopic scale-type models was summarised. Two main types of microscopic models include the car-following models and the Cellular-automata models. For the macroscopic models, there are two main parts, including the LWR model and the Cell Transmission Model.

The typical models cannot capture real traffic phenomena. Therefore, many attempts have been made to couple the microscopic and macroscopic models in order to predict the types of phenomena that are frequently observed with congestion, investigate the effects of disturbances such as a random interrupting the traffic flow, and also predict the clustering conditions that are frequently observed during times of high traffic density in real traffic systems. Moreover, the development of mesoscopic traffic flow models was summarised. They serve as a link between microscopic models that explain individual vehicle behaviour and macroscopic models that represent traffic flow as a continuous flow. Lastly, optimisation models based on CTM and machine learning were presented. Traffic flow on a freeway with on-ramp and off-ramp regions was summarised. Finally, applications of the traffic flow models for ramp metering and traffic lane changing conditions studies were described.

This is due to the fact that data-driven traffic parameter prediction commonly uses predictive analytical approaches on historical data observations to find patterns that can be utilised to anticipate future observations. Due to the seasonal, recurrent/cyclical nature of urban traffic statistics, this has turned out to be helpful. For instance, peaks during the morning and evening rush hours can be clearly predicted and thus anticipated. As a result, a model will be "skilful" at forecasting future traffic features if it can identify and comprehend these trends from prior data.

With unexpected or non-recurring events, such as occurrences or incidents that cannot be predicted based on prior data, even the most accurate prediction algorithms would struggle (Essien et al., 2019b). Non-recurring or stochastic events/incidents include things like accidents, lane closures, sporting events, and public gatherings. It is crucial to build strong predictive models since such events may be unanticipated, uncommon, or unexpected, making it possible to predict traffic accurately in these circumstances.

Chapter 3

Multivariate Prediction Models

3.1 General Overview

Determining future traffic flow conditions is a vital component in managing traffic operations. A variety of Intelligent Transport System (ITS) infrastructure methods such as variable message signs can anticipate future traffic conditions resulting from traffic incidents and bad weather. Traffic flow prediction is a widely researched field in transport engineering, with numerous statistical and machine learning techniques developed to determine future traffic conditions using existing data. Recently, there has been an interest in exploring the effectiveness of deep learning techniques in traffic flow prediction.

This chapter concerns multivariate machine learning-based prediction models of freeway traffic flow under non-recurrent events.^{1 2} Five model architectures are based on the multi-layer perceptron (MLP), convolutional neural network (CNN), long short-term memory (LSTM), CNN-LSTM and Autoencoder LSTM

¹Copyright permission: please see in Appendix A.

F. Aljuaydi, B. Wiwatanapataphee and Y. H. Wu, "Deep Learning-Based Prediction Models for Freeway Traffic Flow under Non-Recurrent Events," 2022 8th International Conference on Control, Decision and Information Technologies (CoDIT), 2022, pp. 815-820, doi: 10.1109/CoDIT55151.2022.9803892.

²Copyright permission: please see in Appendix A.

F. Aljuaydi, B. Wiwatanapataphee and Y. H. Wu, "Multivariate machine learning-based prediction models of freeway traffic flow under non-recurrent events, Alexandria engineering journal

(AE-LSTM) networks have been developed to predict traffic flow under a road crash and the rain. Using an input dataset with five features (the flow rate, the speed, and the density, road incident and rainfall) and two standard metrics (the Root Mean Square error and the Mean Absolute error), models' performances are evaluated. The models have been developed using series traffic data for Kwinana freeway.

The remaining chapter's sections are divided as follows. Section 3.2 presents the study area and available data set. Section 3.3 describes the study data analysis (road incident data and traffic flow data). It also describes the effect of road incidents on traffic flow. Section 3.4 studies predictions of freeway traffic flow under non-recurrent events using multivariate machine learning models including the multilayer perceptron network, Convolutional Neural Networks, Long Short-term Memory, the one-dimensional CNN long short-term memory network and the Autoencoder LSTM networks. Section 3.6 describe the conclusion remark.

3.2 Study area

The study area, the Kwinana Smart Freeway in Western Australia between the Cranford on-ramp and the Canning Highway off-ramp (link 9) with a total length of 2.13 kilometres as shown in Figure 3.1, is chosen because it has a distinguished record of the highest number of road accidents. For an effective multivariate ML model for long short-term traffic prediction, a dataset of traffic variables (the flow rate, the speed, and the density), road incidents and rainfall is used in this study. Traffic data including the flow rate (volume), the speed and the density from the Main Road Western Australia (WRWA) are available between 1 January and 25 November 2018. In the same period of available traffic data, road incidents and rainfall data are obtained from the Web Emergency Operations Centre (WebEOC) and the Bureau of Meteorology (BOM) WA, respectively.

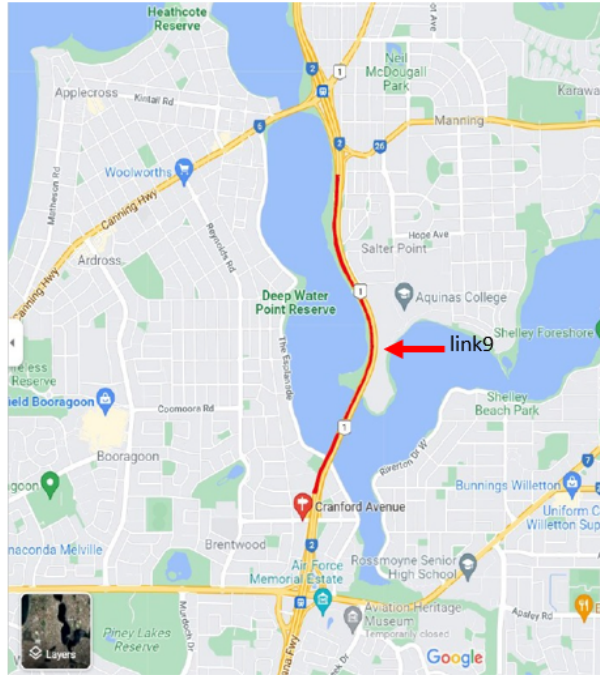


Figure 3.1: Study region (red curve), Link9: between the Cranford Avenue on-ramp and the Canning Highway northbound off-ramp (Aljuaydi et al., 2022).

3.3 Data Analysis

3.3.1 Road incident data

The data of road incidents affecting traffic capacity during the study period come from the following two sources, MAINROADs WA (MRWA) and Web emergency operation centre (WebEOC):

- MRWA: Weather flood/fog hazard; Heavy/moderate; stand still Jam; Major and minor accidents; Road closure
- WebEOC: Break down/tow away; Road crash; Debris/trees/lost loads; Vehicle fire; Animal/livestock; Pothole/road surface damage

Breakdown, road crashes, and road debris are common incident types in this link. Figure 3.2 shows the study region’s frequency of road traffic incidents. Locations in latitude and longitude coordinates of traffic incidents are shown in Figure 3.3, in which a bigger circle size indicates a longer incident duration.

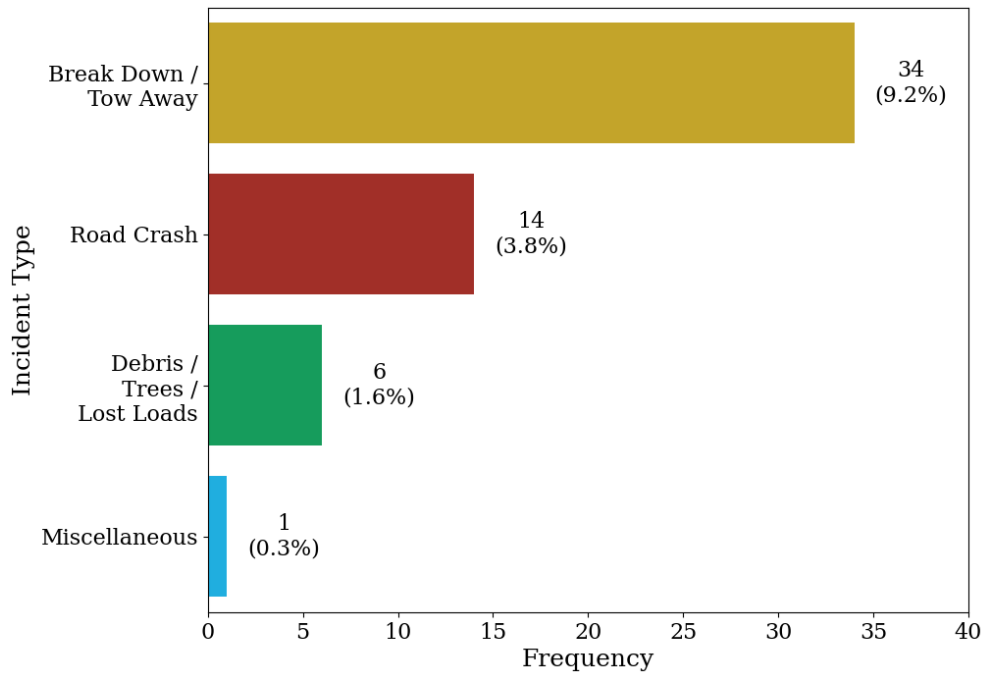


Figure 3.2: Frequency of road incidents on the study region.

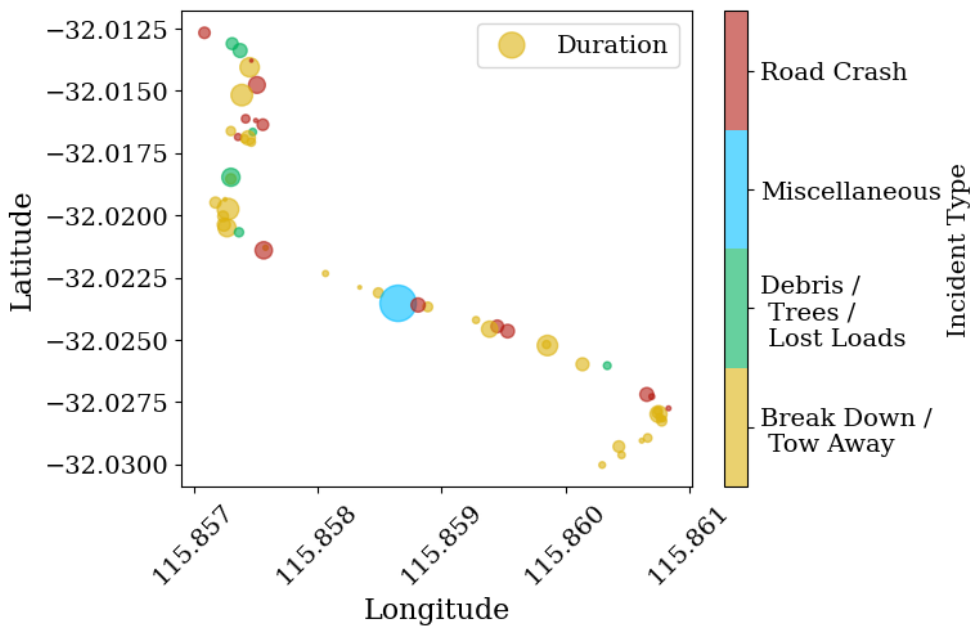


Figure 3.3: Locations in latitude and longitude coordinates of traffic incidents and incident duration on the study region.

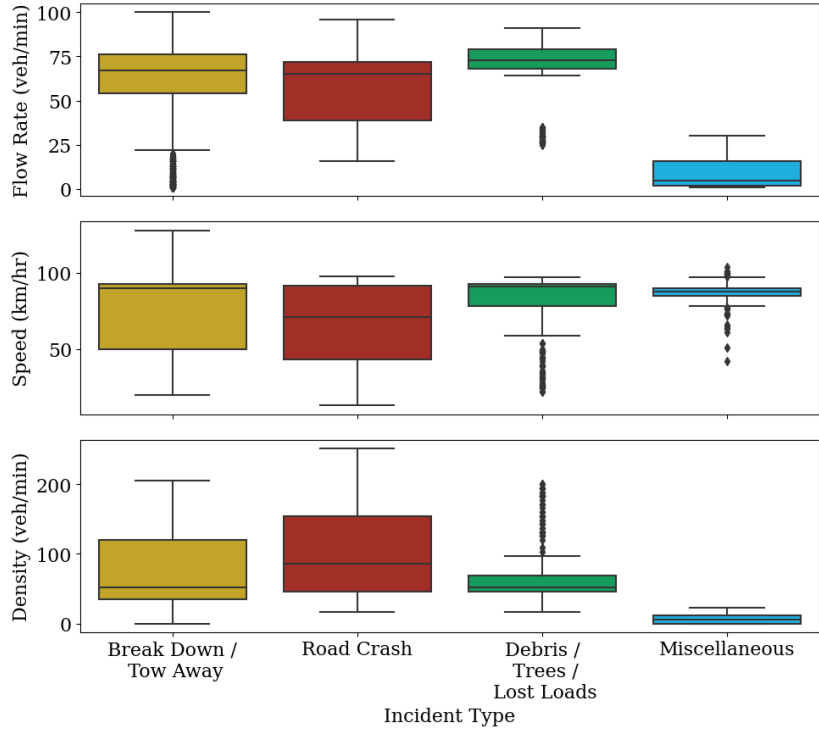


Figure 3.4: Box plot showing distribution and skewness of traffic variables associated with road incidents on the study region.

As shown in Figure 3.4, the box plot shows the distribution and skewness of traffic data associated with road incident types. It is noted that traffic capacity is associated with road crashes and breakdowns.

Road incident data is converted into Boolean data by considering the non-existence as zero and the existence of the incident as one. For rainfall message, rain rate intensity, is considered in three categories including the light rain with precipitation less than 0.1 inches per hour (*iph*), the moderate rain with precipitation between 0.1 and 2.5 *iph* and the heavy rain with rainfall greater than 2.5 *iph*. The input data is then obtained by matching the timestamp of the traffic data, the boolean incident data and the rainfall data. In this study, we have a 1-min input dataset with 429,120 observations and five features.

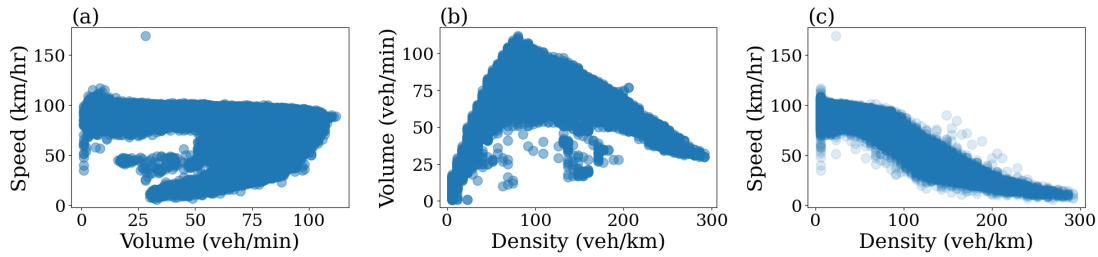


Figure 3.5: Fundamental diagrams showing relationship of traffic variables: (a) speed (km/hr) and volume (veh/min); (b) flow rate (veh/min) and density (veh/km); (c) speed (km/hr) and density (veh/km).

3.3.2 Traffic data

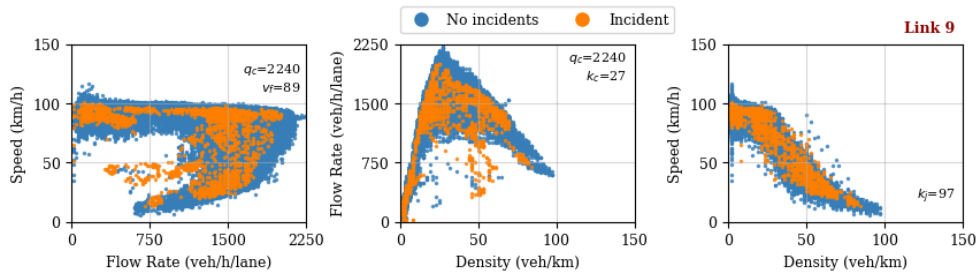
Traffic data of flow rate (volume), speed and density is provided by Main Roads Western Australia (MRWA) between 1 January and 25 October 2018. It is 1-min dataset with 429,120 observations and 3 features including traffic flow rate (veh/min), speed (km/hr) and density (veh/km).

Figure 3.5 shows fundamental traffic flow diagrams on the study road, i.e., the relationship of the speed and the flow rate, the relationship of the flow rate with the density, and the relationship of the speed, and the speed with the density, respectively.

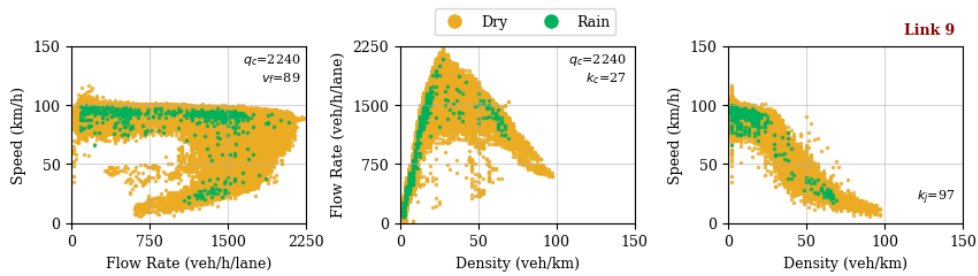
3.3.3 Road incidents and rain effects

Road incidents including crashes, vehicle breakdowns and debris commonly affect the flow of traffic. Figure 3.6 shows the relationships of traffic variables under road incidents and rainfall effects. It is noted that the road incidents have an impact on the traffic flow on the roadway. It may reduce 10 - 25% of traffic capacity. Figure 3.7 presents speed profile with rain's effect on Link 9 between 1 August and 1 November 2018. It indicates that speed will drop on the roadway when it rains, as a driver driving in the wet commonly reduces the speed to allow the car's tyres to grip to the road at all times.

Figure 3.8 presents a box plot showing traffic flow with and without the impact of the road incidents and the rain. It demonstrates that the road incidents have



(a) Road incident effect



(b) Rainfall effect

Figure 3.6: Relationships of traffic variables under road incidents and rainfall effects: (a) road incident; (b) rainfall between medium and heavy level.

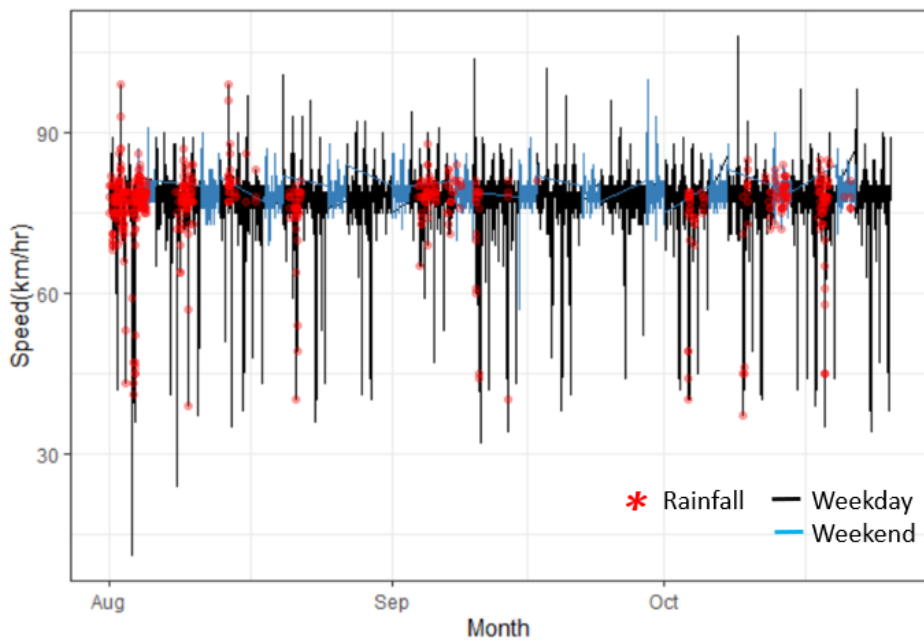


Figure 3.7: Effect of rain on traffic speed from 1 August to 1 November 2018.

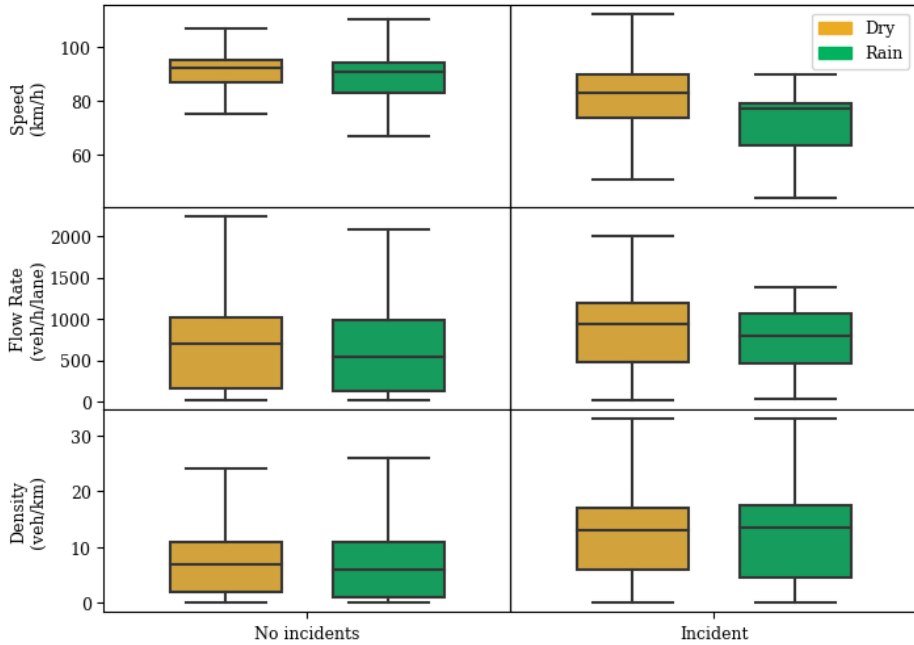


Figure 3.8: Box plot of traffic variables with and without road incident and rain.

a negative impact on the speed and the density of traffic, and the rain seems to magnify the effect of road incidents on the flow of traffic, indicating by the significant higher density and lower speed. When road incidents occur, the flow capacity decreases while the density increases.

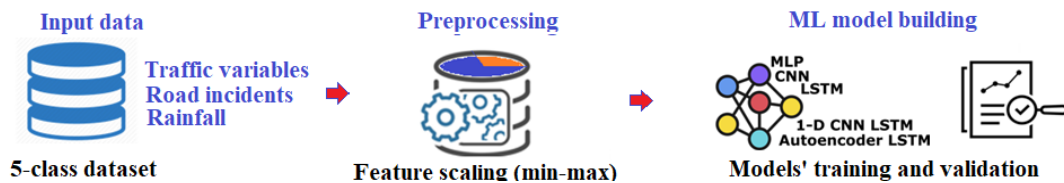


Figure 3.9: Machine learning workflow.

3.4 Multivariate learning models

This section concerns building model architectures of multivariate prediction models based on the MLP, CNN, LSTM, CNN-LSTM and Autoencoder LSTM networks to predict traffic flow rate, speed and density under non-recurrent events. As shown in Figure 3.9, the machine learning workflow comprises prepar-

ing the data, pre-processing, model training, and model testing.

3.4.1 Preparing data and pre-processing

Gathering, sorting and cleaning all datasets are needed for development of the predictive learning model as any discrepancies in the data will lead to the failure analysis of the predictive model. The input dataset with n observations and five features (classes) is in the form of

$$\mathbf{X} = (X_i^1, X_i^2, X_i^3, X_i^4, X_i^5)_{i=1}^n,$$

where traffic parameters X^1 , X^2 , X^3 denote respectively traffic volume, speed and density, X^4 is the boolean road incident data, and X^5 is the rainfall data.

The traffic parameters, road incident and rainfall data are homogenised by feature scaling. By implementing the min-max normalisation, x_i^c is transformed to ξ_i^c , provided ξ_i^c greater than zero and less than 1,

$$\xi_i^c = \frac{x_i^c - \min_c}{\max_c - \min_c}, \quad c = 1, \dots, 5, \quad (3.1)$$

where X^c is the values of the observed set of x_i^c , \max_c and \min_c represent the maximum and minimum values of X^c , respectively.

3.4.2 Models' architecture

Five ML models are used in our thesis. The following subsections explain them in more details. In this section, we describe the training configuration and evaluation metrics used in the performance evaluation.

The normalised input data with n observation and five features are split into the test set (30%) and the training set (70%). For each ML model, its optimal hyperparameters are found by grid searching, the Adam optimiser Kingma & Ba (2014) and an early stopping technique. The accuracy and efficiency of each trained model are assessed by two standard metrics, the Mean Absolute Error

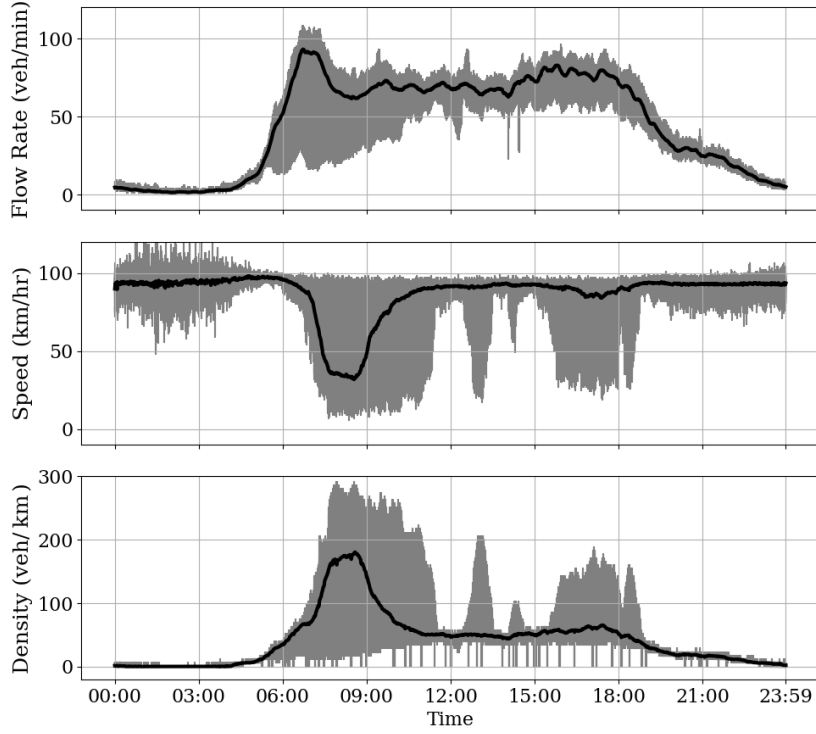


Figure 3.10: Average traffic profiles of flow rate, speed and density during the study period.

(MAE) and the Root Mean Squared Error (RMSE). These accuracies and efficiency give information about the goodness of the learning model. The deviation from the mean value estimated through the MAE and RMSE can be calculated using the following equations:

$$\text{MAE} = \frac{1}{n} \sum_{i=1}^n |y_i - \hat{y}_i|, \quad (3.2)$$

and

$$\text{RMSE} = \sqrt{\frac{1}{n} \sum_{i=1}^n (y_i - \hat{y}_i)^2}. \quad (3.3)$$

respectively. A lower value of the RMSE or the MAE signifies a better model fit, as the level of deviation is low.

3.4.3 Baseline

The benchmark performance of all other models utilised for any particular problem provides an insight into how accurately it works for that problem along with comparison as well. The used model should perform better than the benchmark (baseline) test case, in case it will under perform then there is a need to fix the utilised method/technique or replaced it with the suitable one. Our baseline model is the average traffic variables from the training set (Figure 3.10) to find the suitable model for the freeway traffic predictions under non-recurrent events.

3.4.4 Multilayer Perceptron (MLP)

Figure 3.11 shows the MLP model used in our study. The model consists of the input layer followed by a flatten layer. Then, three dense fully connected layers are used before the output layer. A ReLu activation function is used after every dense layer except the output layer.

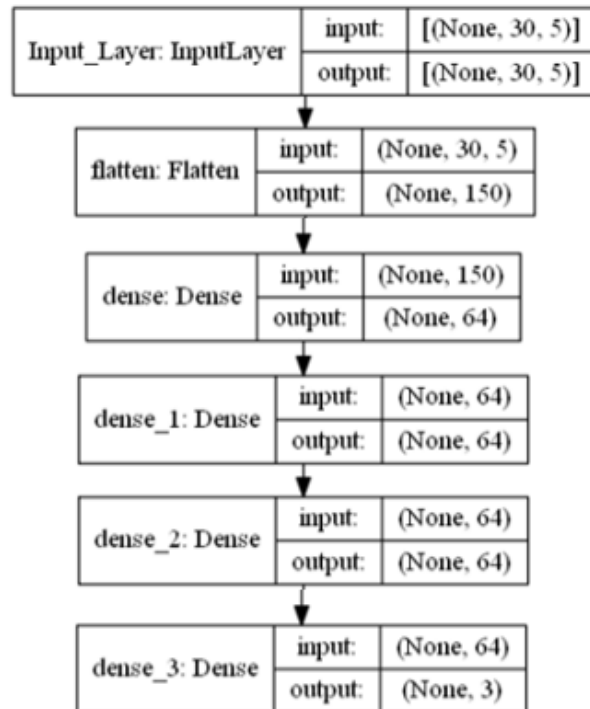


Figure 3.11: MLP architecture.

The models with a batch size of 30 are fit over 20 epochs, as shown in Figure 3.12.

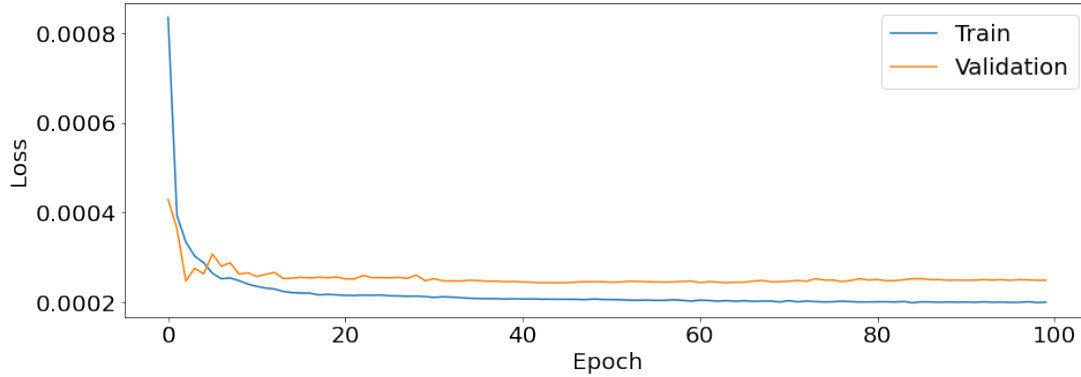


Figure 3.12: Squared error loss, $L_2 = (\mathbf{y} - \hat{\mathbf{y}})^2$, for the training and the validation datasets in the MLP model.

3.4.5 Convolutional Neural Networks (CNN)

Figure 3.13 shows the CNN model used in our study. The model consists of the input layer followed by three 1-D convolutional layer and a flatten layer. Then, one dense fully connected layer is used before the output layer. A ReLu activation function is used after every layer except the output layer.

The models with a batch size of 30 are fit over 20 epochs, as shown in Figure 3.14.

3.4.6 Long Short-term Memory (LSTM)

Figure 3.15 shows the LSTM model used in our study. The model consists of the input layer followed by three LSTM layers and the output layer. A ReLu activation function is used after every layer except the output layer.

The models with a batch size of 30 are fit over 20 epochs, as shown in Figure 3.16.

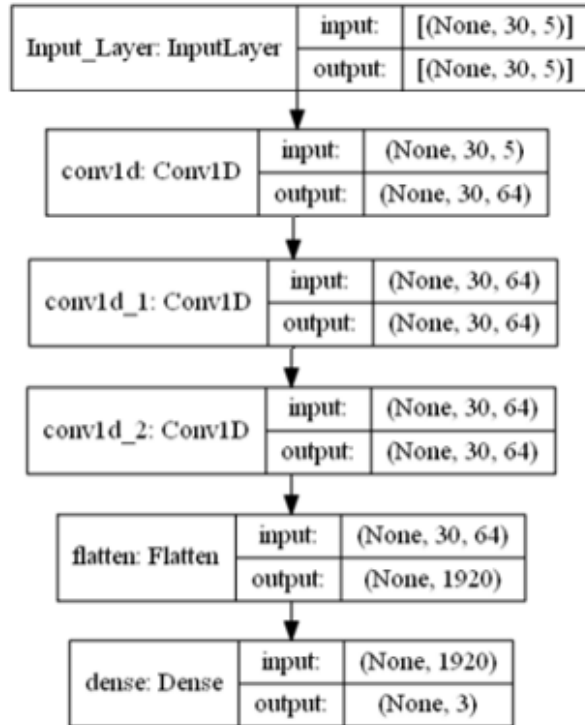


Figure 3.13: CNN architecture.

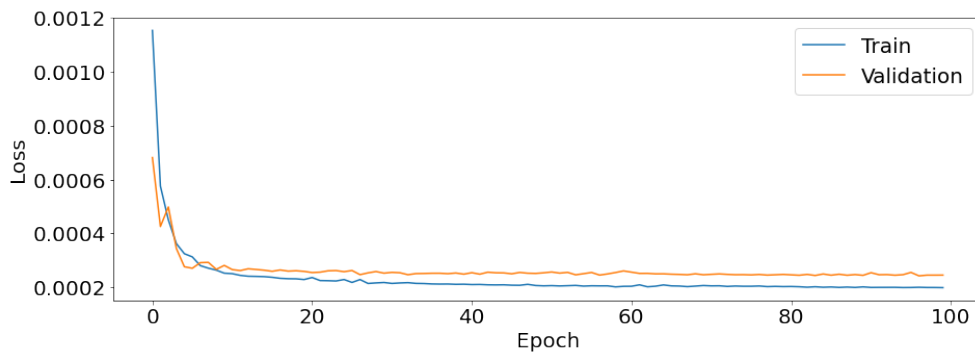


Figure 3.14: Squared error loss, $L_2 = (\mathbf{y} - \hat{\mathbf{y}})^2$, for the training and the validation datasets in the CNN model.

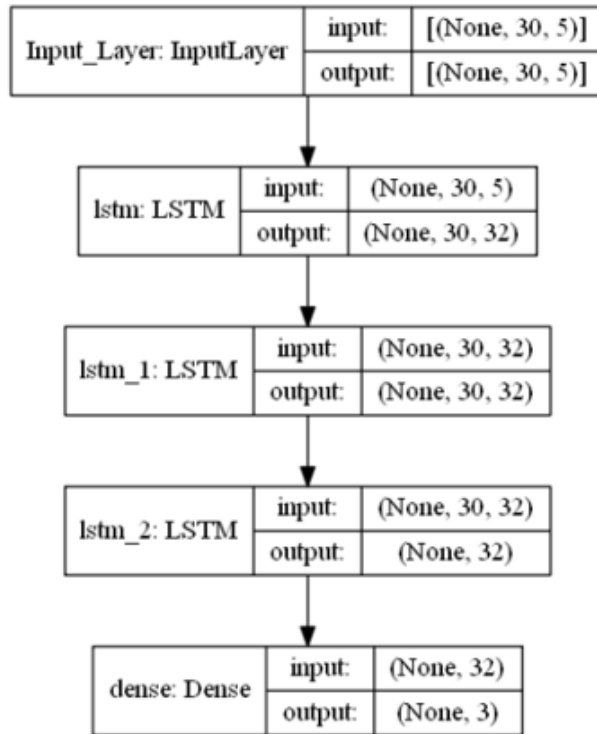


Figure 3.15: LSTM architecture.

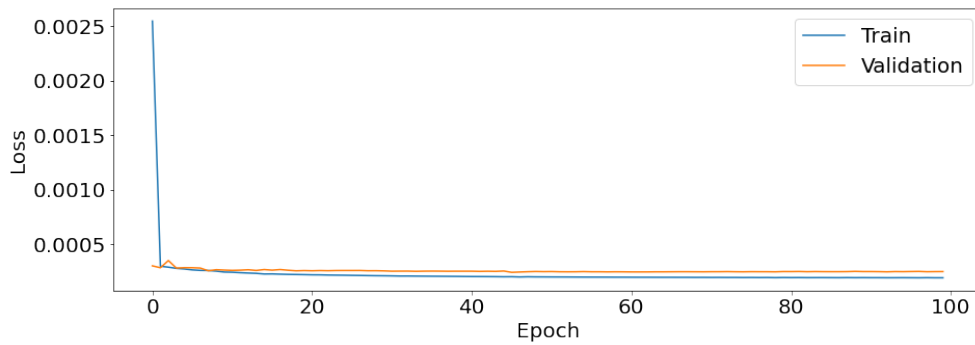


Figure 3.16: Squared error loss, $L_2 = (\mathbf{y} - \hat{\mathbf{y}})^2$, for the training and the validation datasets in the LSTM model.

3.4.7 Convolutional Neural Networks -Long Short-term Memory (CNN-LSTM)

Figure 3.17 shows the 1-D CNN LSTM model used in our study. The model consists of the input layer followed by a 1-D convolutional layer followed by two LSTM layers and the output layer. A ReLu activation function is used after every layer except the output layer.

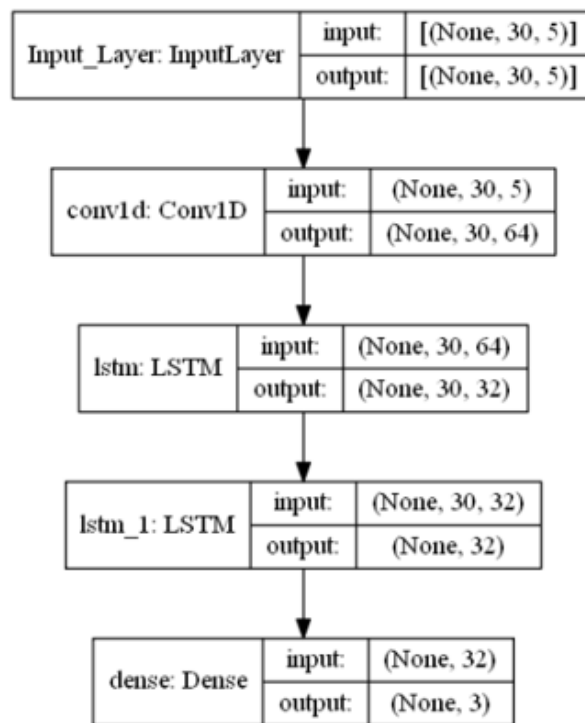


Figure 3.17: 1-D CNN LSTM architecture.

The models with a batch size of 30 are fit over 20 epochs, as shown in Figure 3.18.

3.4.8 Autoencoder LSTM (AE-LSTM)

Figure 3.19 shows the Autoencoder LSTM model used in our study. The model consists of the input layer followed by LSTM layer, Repeat Vector layer, Time Distributed layer and another LSTM layer. Finally, a flatten layer and the output

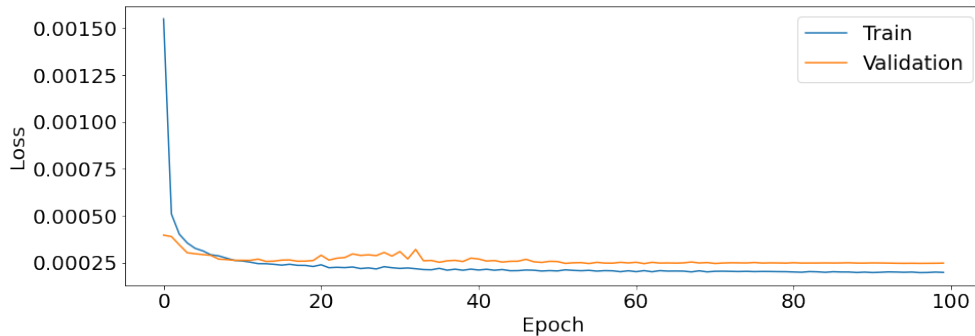


Figure 3.18: Squared error loss, $L_2 = (\mathbf{y} - \hat{\mathbf{y}})^2$, for the training and the validation datasets in the 1-D CNN LSTM model.

layer are added. A ReLu activation function is used after every LSTM layer.

The models with a batch size of 30 are fit over 20 epochs, as shown in Figure 3.20.

3.5 Results and discussion

Table 3.1 presents model validation using two standard metrics, the RMSEs and MAEs. A lower value of the MAE or the RMSE signifies a better model fit. The results indicate that all ML models give better prediction than the baseline model and the 1D CNN-LSTM model outperforms other ML models including the MLP, the CNN, the LSTM and the Autoencoder LSTM models. Comparing the RMSEs and the MAEs of other models, the 1D CNN-LSTM model gives the lowest values of the RMSEs and MAEs for all cases, i.e., RMSEs of 2.65, 4.63 and 6.70 and the MAEs of 3.75, 2.50 and 5.0 for the flow rate, speed and density predictions, respectively.

For long and short-term predictions of traffic flow under a road crash and the wet road with rain intensity between medium and high rate, the Link-9 observed traffic flow under non-recurrent events on 4 September 2018 is chosen in this study because there was a long-period road crash between 10:24 and 13:09 (black star with dark solid line) and three periods of heavy rain, i.e., 4:30-6:00, 14:00-14:30 and 19:00-21:30 (purple star with purple solid line) as shown in Figure 3.21.

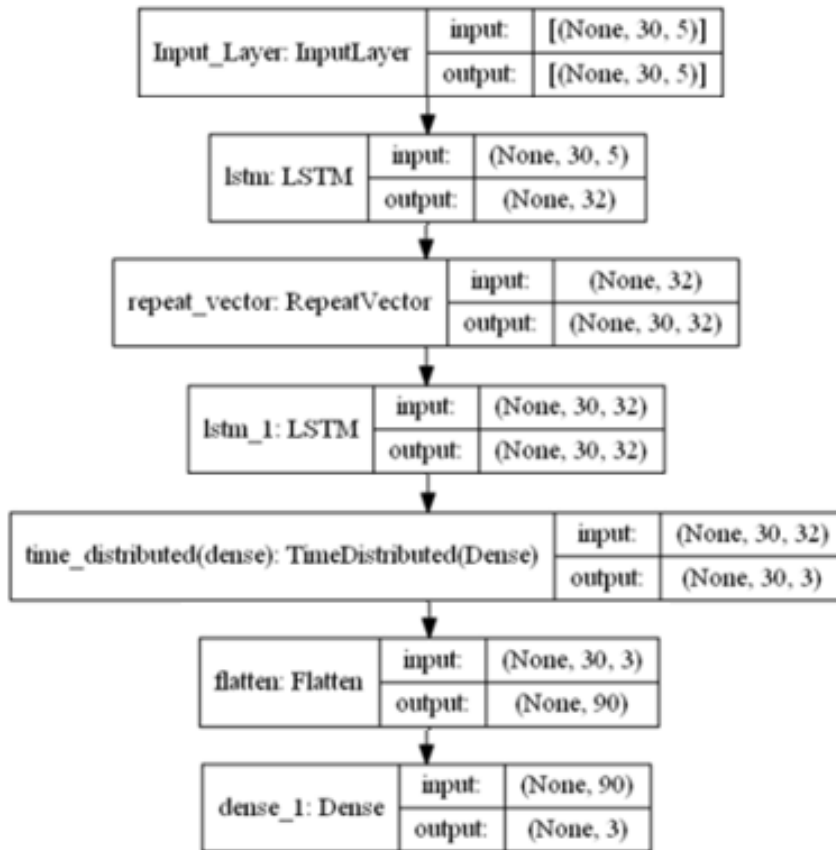


Figure 3.19: AE-LSTM architecture.

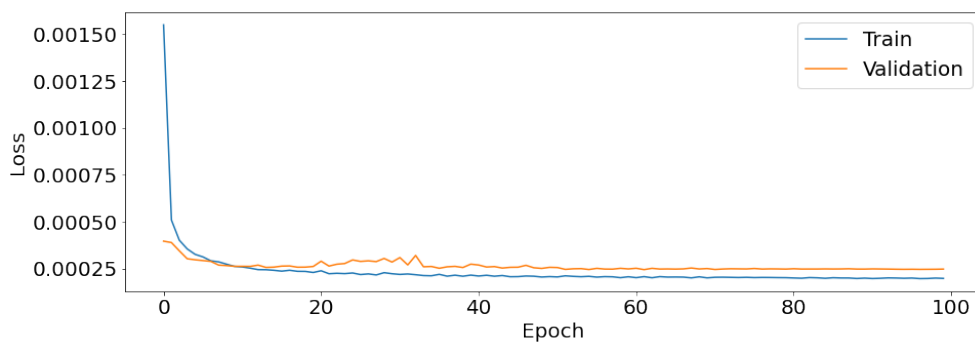


Figure 3.20: Squared error loss, $L_2 = (\mathbf{y} - \hat{\mathbf{y}})^2$, for the training and the validation datasets in the AE-LSTM model.

Table 3.1: Two standard metrics, RMSEs and MAEs, of ML models for each traffic parameter.

RMSE												
Parameter	Baseline		MLP		CNN		LSTM		CNN-LSTM		AE-LSTM	
	Train	Test	Train	Test	Train	Test	Train	Test	Train	Test	Train	Test
Flow rate	11.02	11.75	3.58	3.61	3.10	3.15	3.02	3.08	2.50	2.65	2.89	2.90
Speed	10.25	10.81	5.23	5.35	5.0	5.09	4.89	5.0	4.60	4.63	4.75	4.77
Density	24.15	24.71	7.32	7.55	7.22	7.29	7.02	7.11	6.65	6.70	6.75	6.80

MAE												
Parameter	Baseline		MLP		CNN		LSTM		CNN-LSTM		AE-LSTM	
	Train	Test	Train	Test	Train	Test	Train	Test	Train	Test	Train	Test
Flow rate	6.52	6.98	4.18	4.63	4.0	4.10	3.90	3.98	3.70	3.75	3.75	3.80
Speed	5.49	6.18	2.75	2.80	2.70	2.71	2.58	2.60	2.46	2.50	2.50	2.55
Density	11.14	11.95	5.51	5.48	5.32	5.39	5.12	5.15	4.52	5.0	5.01	5.08

Using all proposed ML models, traffic variables including the flow rate, the speed and the density under non-recurrent events on Link 9 of the Kwinana Freeway are predicted and compared to find the optimal prediction model.

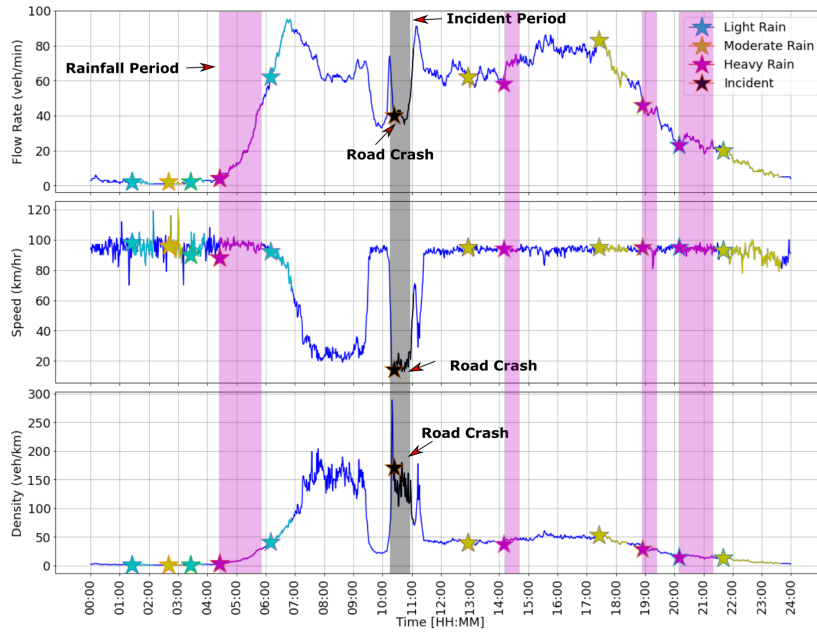


Figure 3.21: Observed traffic flow rate (top), speed (middle) and density (bottom) with road crashes and rainfall during the prediction period (4 September 2018).

Figure 3.22 shows long-term predictions of traffic parameters using the baseline model. As the baseline model gives average values of each traffic parameters, it thus cannot capture traffic patterns during non-recurrent events. Here, we present the performance of various ML models for predicting traffic pattern under the road crash and the rain.

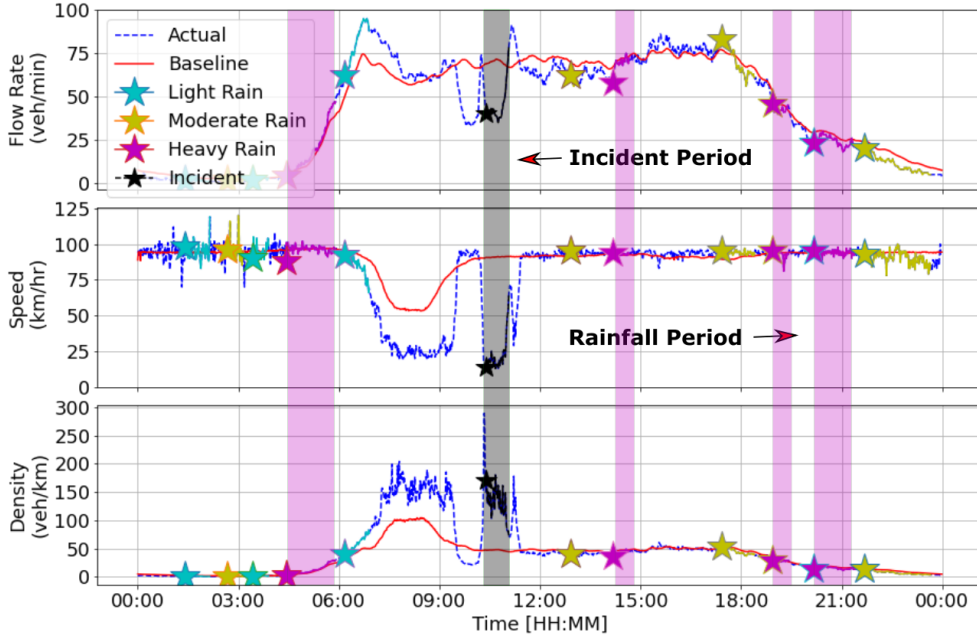


Figure 3.22: Baseline predictions of traffic flow rate (veh/min), speed (km/hr) and density (veh/km) under a road incident (★) and rain.

Figures 3.23, 3.24, 3.25, 3.26 and 3.27 show long-term predictions of traffic parameters using the MLP, CNN, LSTM, 1D CNN-LSTM and AE-LSTM models, respectively. It is found that the best long-term prediction model is based on the 1D CNN-LSTM networks.

For short-term prediction of traffic flow under non-recurrent events, we consider separately the effect of a road crash and the heavy rain on traffic flow within 30 minutes after the occurrence of the incident (solid line).

In this thesis, observed data of traffic flow under a road crash (a dark star) between 10:25 and 10:55, and the heavy rain (a purple star) between 20:10 and 20:40 were compared with the predicted data. Figure 3.28 presents the short-term prediction of traffic flow under a road crash. It illustrates that two ML models based on the LSTM and the 1D CNN-LSTM networks performed better than other ML models as they attained the low values of the RMSEs of 1.75, 2.85 and 2.50, and MAEs of 2.30, 2.18 and 2.75 for the flow rate, speed and density predictions, respectively, as shown in Table 3.2.

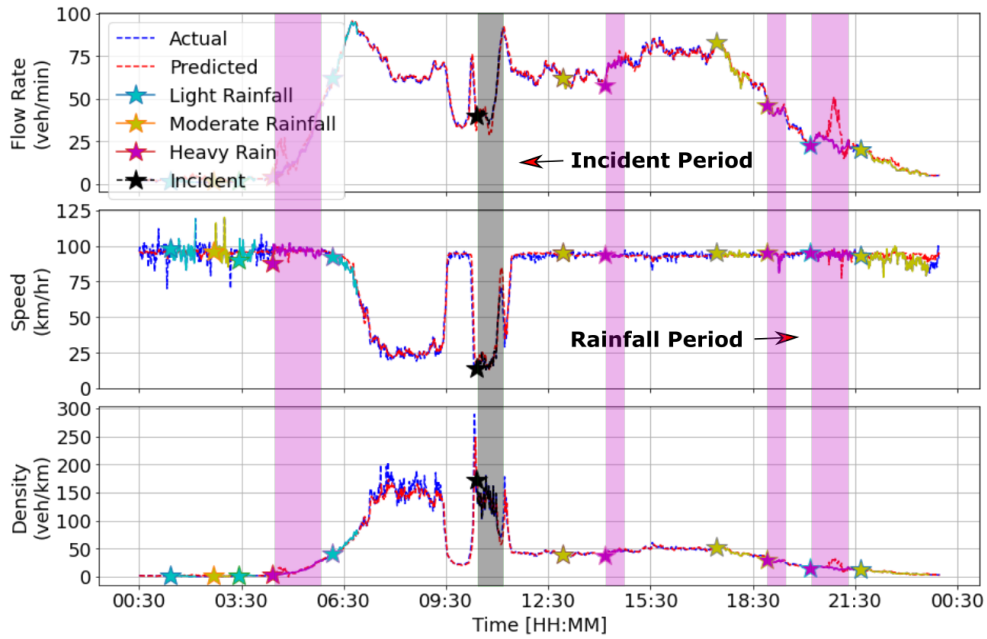


Figure 3.23: Long-term traffic prediction of the flow rate (veh/min), speed (km/hr) and density (veh/km) obtained from the best multivariate ML model based on the MLP network.

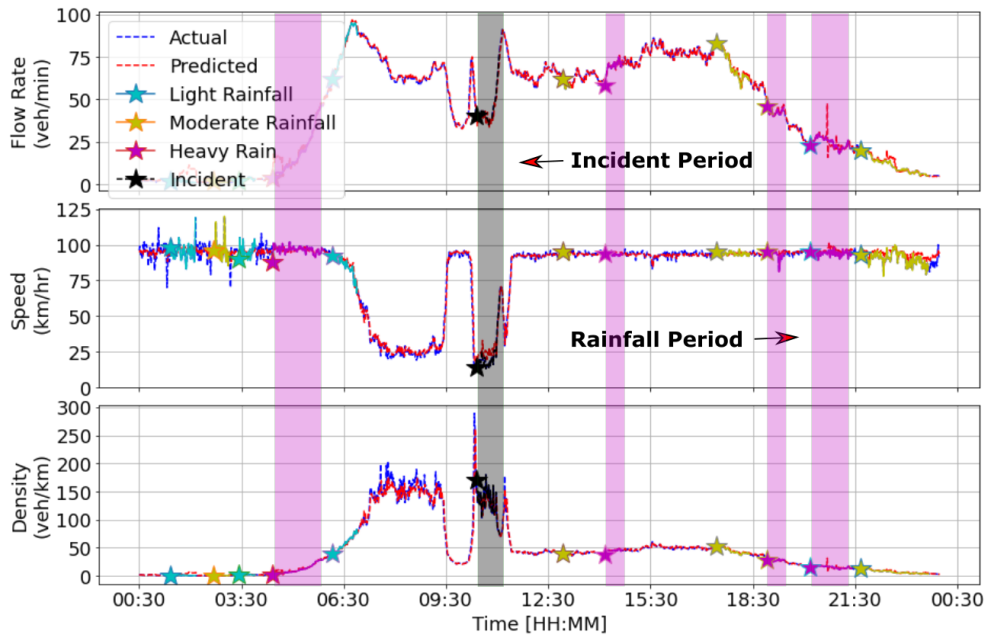


Figure 3.24: Long-term traffic prediction of the flow rate (veh/min), speed (km/hr) and density (veh/km) obtained from the best multivariate ML model based on the CNN network.

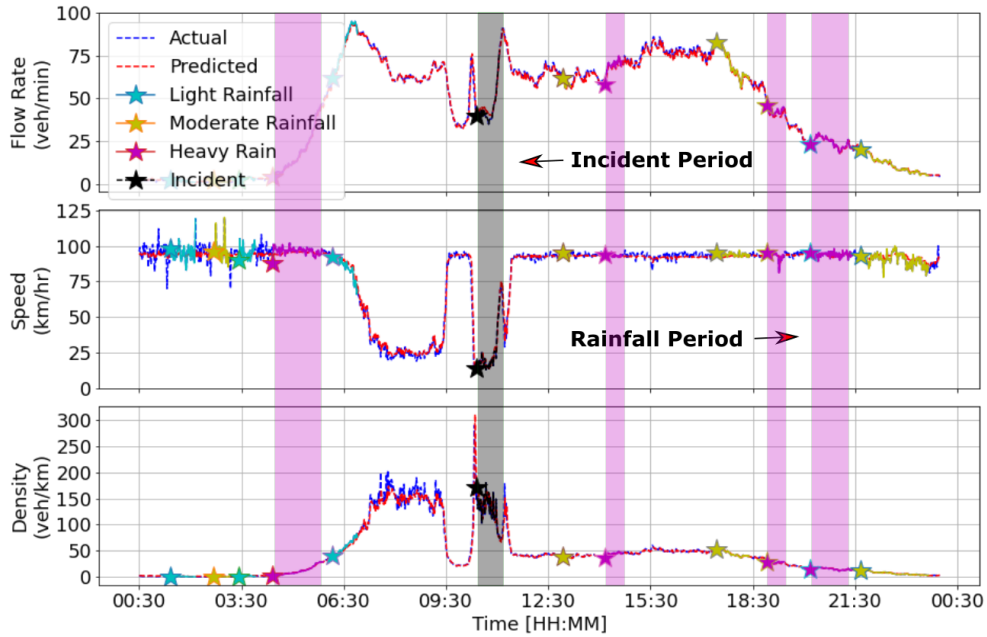


Figure 3.25: Long-term traffic prediction of the flow rate (veh/min), speed (km/hr) and density (veh/km) obtained from the best multivariate ML model based on the LSTM network.

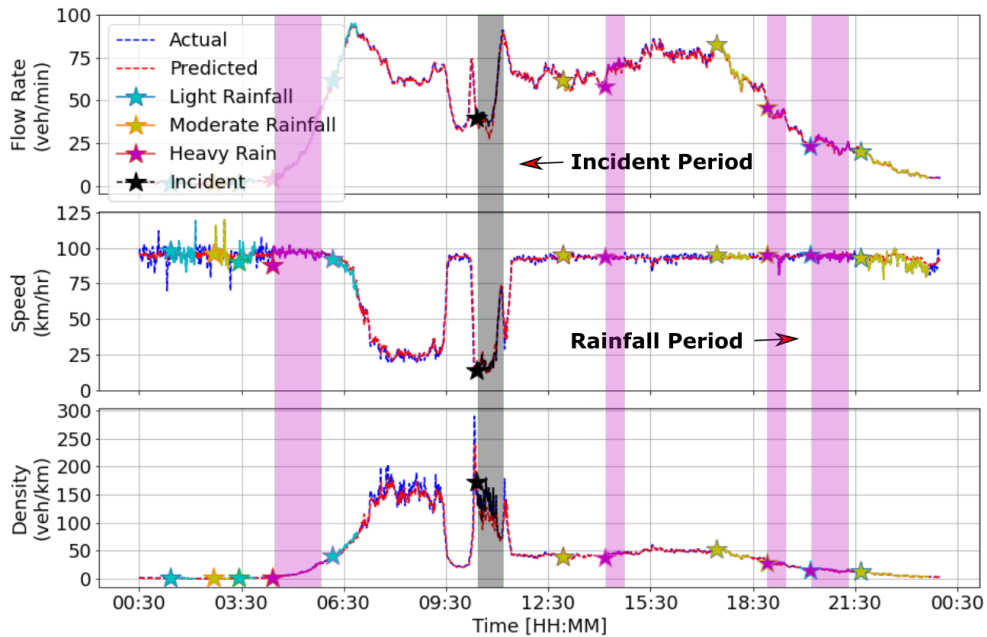


Figure 3.26: Long-term traffic prediction of the flow rate (veh/min), speed (km/hr) and density (veh/km) obtained from the best multivariate ML model based on the CNN-LSTM network.

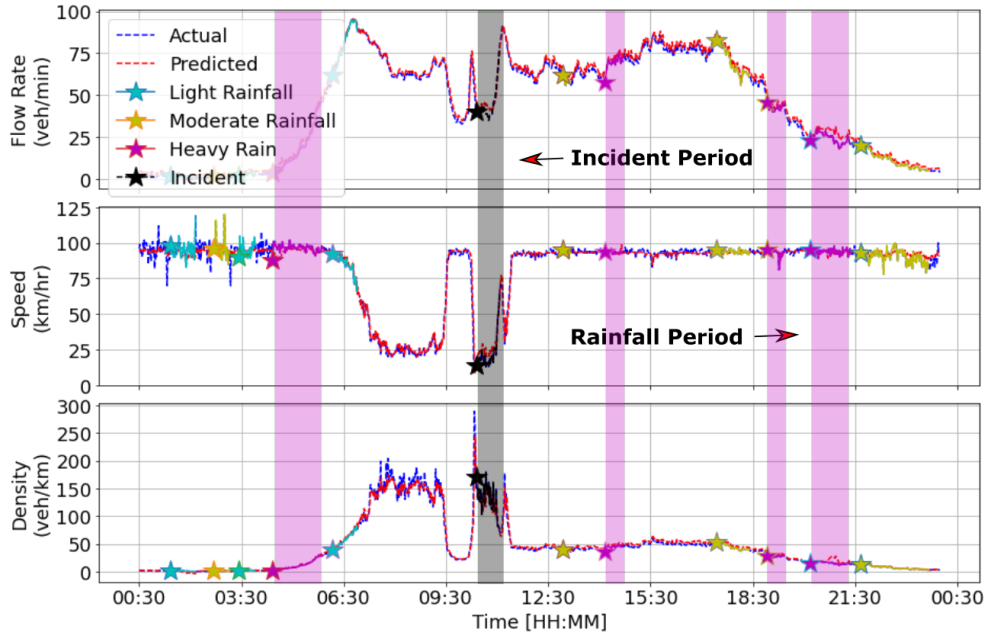


Figure 3.27: Long-term traffic prediction of the flow rate (veh/min), speed (km/hr) and density (veh/km) obtained from the best multivariate ML model based on the AE-LSTM network.

Table 3.2: RSMEs and MAEs of ML models' performance for short-term prediction under a road crash.

RMSE						
Parameter	Baseline	MLP	CNN	LSTM	CNN-LSTM	AE-LSTM
Flow rate	9.65	1.85	1.82	1.80	1.75	1.78
Speed	14.26	3.57	2.98	2.92	2.85	2.89
Density	10.38	3.59	2.65	2.63	2.50	2.55
MAE						
Parameter	Baseline	MLP	CNN	LSTM	CNN-LSTM	AE-LSTM
Flow rate	5.93	2.38	2.38	2.33	2.30	2.35
Speed	7.14	3.15	2.27	2.24	2.18	2.22
Density	5.09	3.65	2.80	2.85	2.75	2.79

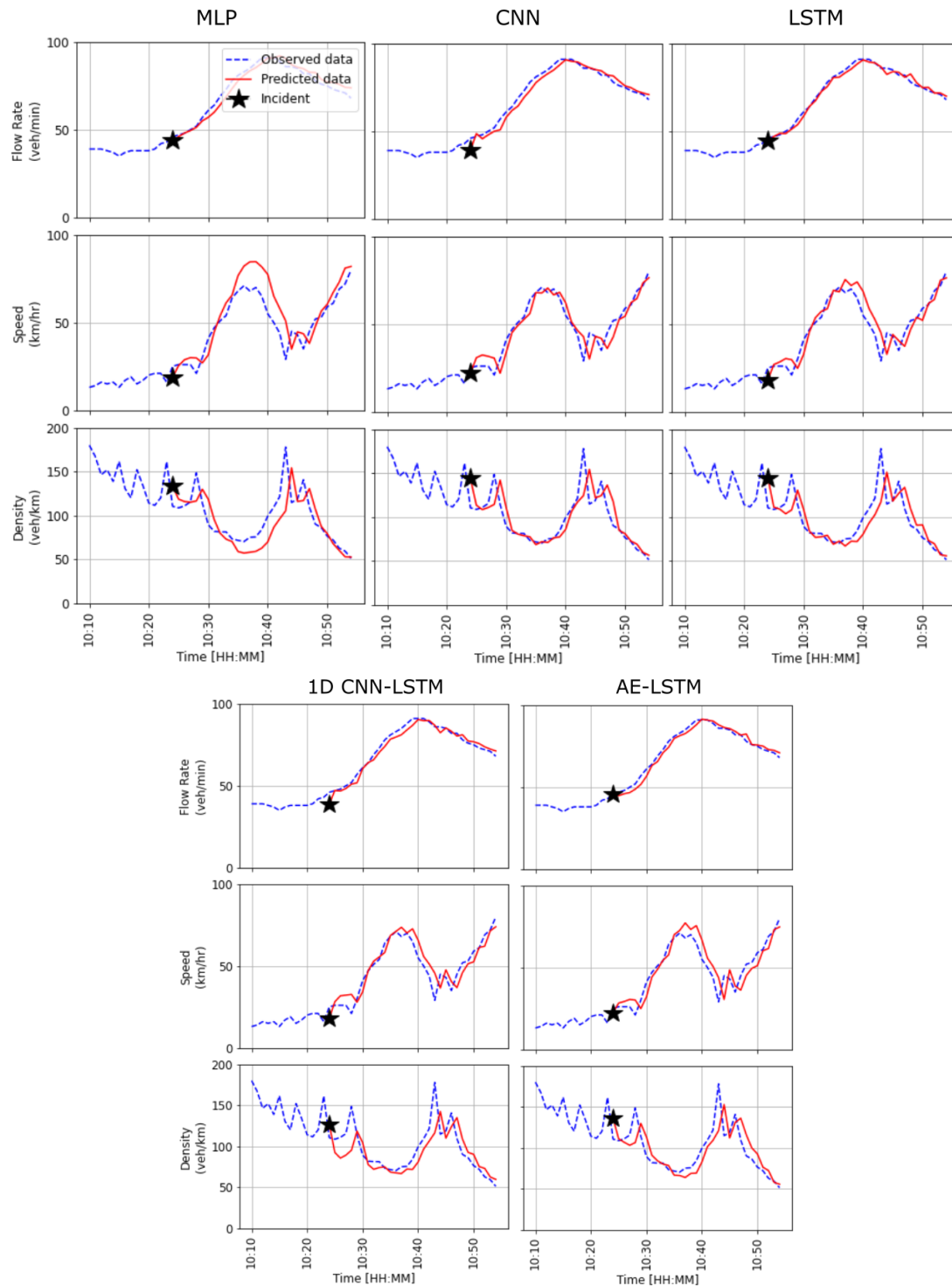


Figure 3.28: Short-term predictions under a road incident on 4 September 2018 between 10:25 and 10:55 obtained from five prediction models based on various ML networks: the MLP, the CNN, the LSTM, the 1D CNN-LSTM and the Autoencoder LSTM networks.

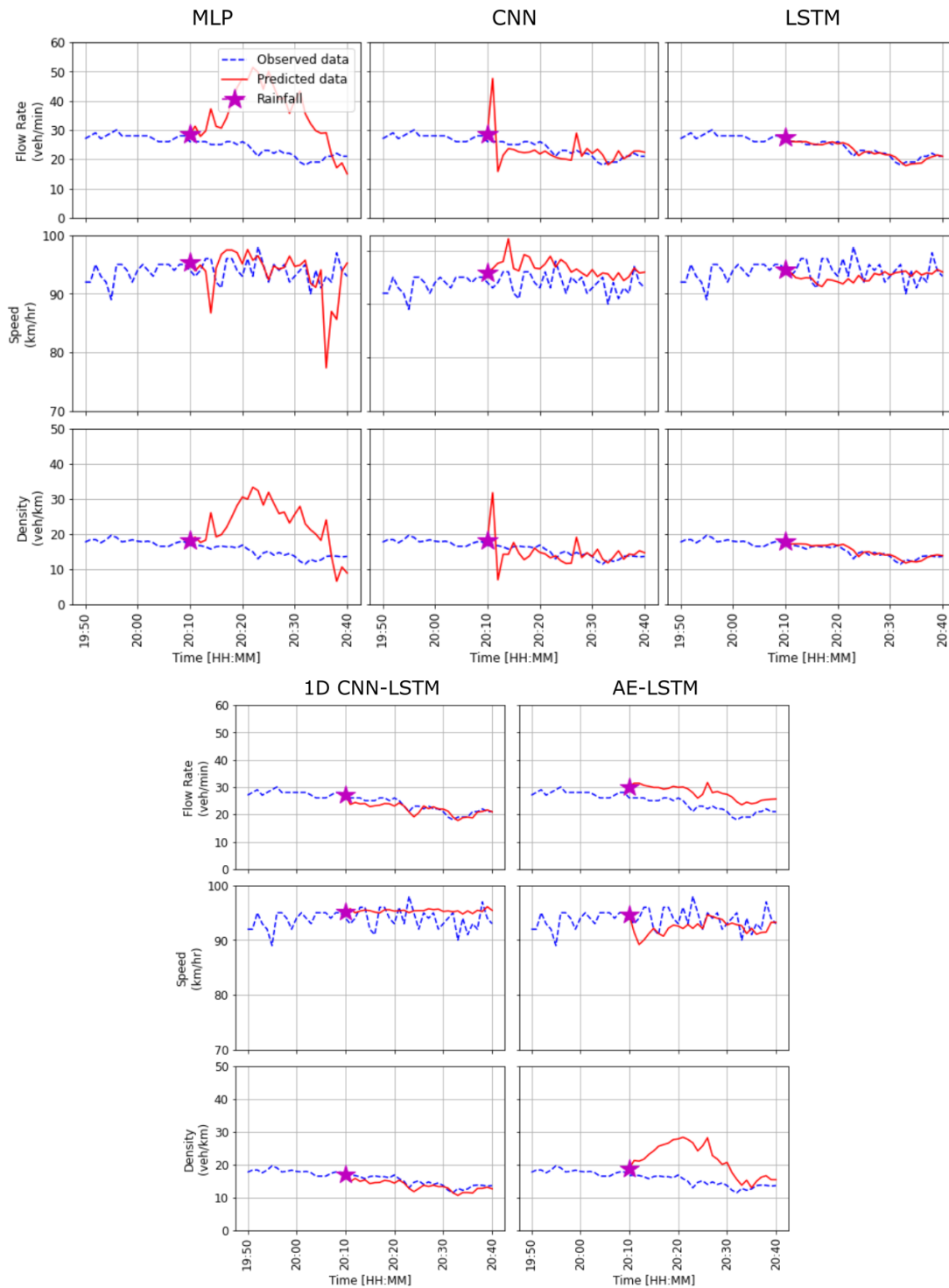


Figure 3.29: Short-term predictions under the rain on 4 September 2018 between 20:10 and 20:40 obtained from five prediction models based on various ML networks: the MLP, the CNN, the LSTM, the 1D CNN-LSTM and the Autoencoder LSTM networks.

Figure 3.29 shows the short-term prediction of traffic flow under the heavy rain. The results indicate that the MLP model gives the worst prediction with RMSEs of 4.03, 5.30 and 7.09 for the flow rate, speed and density predictions, respectively. The 1D-CNN LSTM model performed better than other models as it attained RMSEs of 1.18, 3.45 and 1.15, and MAEs of 1.67, 1.73 and 1.87 for the flow rate, speed and density predictions, respectively, as shown in Table 3.3.

Table 3.3: RSMEs and MAEs of ML models’ performance for short-term prediction under **the rain**.

RMSE						
Parameter	Baseline	MLP	CNN	LSTM	CNN-LSTM	AE-LSTM
Flow rate	9.65	4.03	3.30	1.23	1.18	1.78
Speed	14.26	5.30	4.10	3.80	3.45	3.50
Density	10.38	7.09	4.55	1.26	1.15	3.75
MAE						
Parameter	Baseline	MLP	CNN	LSTM	CNN-LSTM	AE-LSTM
Flow rate	5.93	3.38	2.79	1.78	1.67	1.81
Speed	7.14	3.15	1.89	1.82	1.73	1.79
Density	5.09	3.65	2.80	2.09	1.87	3.23

3.6 Concluding remark

Using an input data with large observations and five features, the multivariate prediction models based on the Multilayer Perceptron (MLP), One-dimensional Convolutional Neural Network (1-D CNN), the Long Short-term Memory (LSTM) network, 1D-CNN LSTM and Autoencoder LSTM networks have been developed to predict freeway traffic under non-recurrent events. The data features include the flow rate, speed, density, the boolean incident and rainfall. From the results obtained from our proposed multivariate prediction models, we can conclude that:

- The proposed models capture traffic pattern under non-recurrent events. Few discrepancies have been observed in the traffic flow rates between the predicted and observed values. The difference is noticeable when there was an incident.

- The 1D-CNN LSTM prediction model for the density, flow rate, and speed gives more accurate results than those obtained from other ML models.

In the off-ramp and on-ramp areas, more delays and disruption occur, further research will look at the congestion that happens due to the lane change and non-recurrent events. For this purpose, the traffic flow characteristics will be predicted by the time-delay deep neural network model. A deep traffic congestion model will be developed to predict the bottleneck in the traffic flow. This will help to predict the congestion propagation for the targeted routes.

Chapter 4

Simulation Models

4.1 General overview

As freeway traffic involves various uncertainties, a stochastic model can describe queue accumulate and collision in a coherent manner with traffic stream principles. This section presents a stochastic LWR model describing the traffic flow evolution under non-recurrent events and a stochastic optimisation model presenting the impact of traffic control strategies on traffic congestion.

4.2 Stochastic Cell Transmission Model

Freeway traffic dynamics with on-ramps and off-ramps are described by the first-order partial differential equation (the LWR model):

$$\frac{\partial}{\partial t}k(x,t) + \frac{\partial}{\partial x}(q(x,t) + r(x,t) - s(x,t)) = f(x,t), \quad (4.1)$$

where $k(x,t)$ is traffic density, $q(x,t)$ denotes flow rate, $f(x,t)$ is a force term due to lane change, $r(x,t)$ and $s(x,t)$ are incoming on-ramp flow and outgoing off-ramp flows, respectively.

For simplicity, any quantity $f(x,t)$ is denoted by f_i^t and the speed $\beta(x,t)v_f$ is represented by \hat{v}_i .

4.2.1 Traffic flow dynamics

In any road segments (cells) of the multi-lane roadway, if the i th cell has l_i lanes and lane capacity of C_i (veh/h/lane), its maximum flow rate, q_i^{max} , and maximum density, k_i^{max} , will be

$$q_i^{max} = l_i C_i \quad \text{and} \quad k_i^{max} = l_i k_{jam}, \quad (4.2)$$

respectively. From equation (4.1), the traffic density of the i th segment, according to the conservation of vehicles, are respectively determined by

$$k_i^t = k_i^{t-1} + \frac{\Delta t}{\Delta x_i} (q_{i-1}^t - q_i^t + r_i^t - s_i^t), \quad (4.3)$$

where q_{i-1}^t and q_i^t denote incoming from the upstream cell and outgoing flows to the downstream cell of the i th cell in different zones.

For merging zone, there are two upstream cells of the merging cell: the source and the ordinary cell, as shown in Figure 4.1.

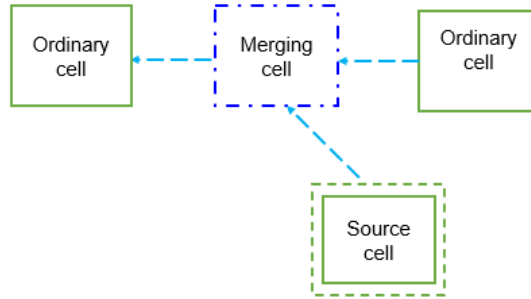


Figure 4.1: Merging zone

Let's define

$$q_{temp} = \min \{ (1 - \beta_i^t) v_f k_{i-1}^t; w_i (k_{jam} - k_i^t); q_i^{max} \}, \quad (4.4)$$

$$r_{temp} = (1 - \alpha_i^t) \left(d_i^t + \frac{N_i^t}{\Delta t} \right), \quad (4.5)$$

where $w_i (k_{jam} - k_i^t)$ is the flow capacity when the density is higher than the critical density, d_i^t is demand and N_i^t is the maximum number of vehicles that

can be present in cell i at time t .

If $q_{\text{temp}} + r_{\text{temp}} < w_i(k_{\text{jam}} - k_i^t)$ then the upstream and on-ramp incoming volumes are

$$q_{i-1}^t = q_{\text{temp}} \quad \text{and} \quad r_i^t = r_{\text{temp}}. \quad (4.6)$$

Otherwise,

$$q_{i-1}^t = \frac{q_{\text{temp}}}{q_{\text{temp}} + r_{\text{temp}}} w_i(k_{\text{jam}} - k_i^t), \quad (4.7)$$

$$r_i^t = \frac{r_{\text{temp}}}{q_{\text{temp}} + r_{\text{temp}}} w_i(k_{\text{jam}} - k_i^t). \quad (4.8)$$

Flow out from the merged cell is given by

$$q_i^t = \min \{ q_{i-1}^t + r_i^t; (1 - \beta)v_f k_i^t; w_{i+1}(k_{\text{jam}} - k_{i+1}^t); q_{i+1}^{\text{max}} \}. \quad (4.9)$$

For the diverging zone, there are two downstream cells of the diverging cell: the sink cell and the ordinary cell, as shown in Figure 4.2.

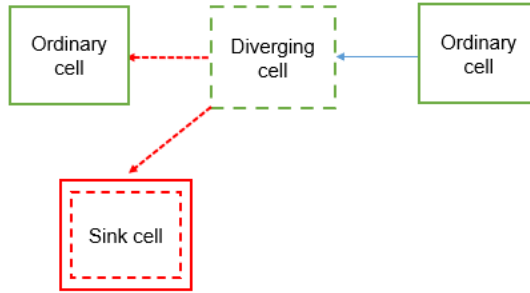


Figure 4.2: Diverging zone

Suppose that discharge rate, s_i^t , is given; traffic volume flowing out to the next cell may be determined by

$$q_i^t = \min \{ q_{i-1}^t - s_i^t; (1 - \beta)v_f k_i^t; w_{i+1}(k_{\text{jam}} - k_{i+1}^t); q_{i+1}^{\text{max}} \}. \quad (4.10)$$

In other zones, particularly the first cell, let d_0^t and N_0^t be the arrival rate and the number of vehicles in the main-road queue, N_0^t . Suppose that d_0^t and N_0^t are

given; traffic volume flowing into the first cell of the road network and flowing out from the cell may be determined by

$$q_{-1}^t = \min \left\{ d_0^t + \frac{N_0^t}{\Delta t}; q_0^m ax; w_0(k_{jam} - k_0^t) \right\}, \quad (4.11)$$

$$q_0^t = \min \{ q_{-1}^t; (1 - \beta)v_f k_0^t; w_1(k_{jam} - k_1^t); q_1^{max} \}, \quad (4.12)$$

For the traffic flowing out from an ordinary cell, it may be given by

$$q_i^t = \begin{cases} \min \{ q_{i-1}^t; (1 - \beta)v_f k_i^t \} & \text{the last cell} \\ \min \{ q_{i-1}^t; (1 - \beta)v_f k_i^t; w_{i+1}(k_{jam} - k_{i+1}^t); q_{i+1}^{max} \} & \text{Otherwise} \end{cases} \quad (4.13)$$

The number of vehicles in each cell is calculated by $n_i^t = k_i^t \Delta x$ in which the density k_i^t depends on traffic flowing in and out of the cell. These cells include the first cell, the ramp cell and the ordinary cell. Therefore, the number of vehicles in each cell can be determined as follows:

- the first cell,

$$n_0^{t+1} = n_0^t + \Delta t (q_{in}^t - q_0^t), \quad (4.14)$$

- a merged cell with two incoming flows,

$$n_i^{t+1} = n_i^t + \Delta t (q_{i-1}^t + r_i^t - q_i^t), \quad (4.15)$$

- a diverging cell with outgoing flow, s_i^t ,

$$n_i^{t+1} = n_i^t + \Delta t (q_{i-1}^t - s_i^t - q_i^t), \quad (4.16)$$

- an ordinary cell, the number of vehicles is

$$n_i^{t+1} = n_i^t + \Delta t (q_{i-1}^t - q_i^t). \quad (4.17)$$

Using the demand/supply of the road network, virtual queues at the start and

three on-ramps at time step $t + 1$ may be calculated by

$$N_0^{t+1} = N_0^t + \Delta t(d_0^t - q_0^t), \quad (4.18)$$

$$N_i^{t+1} = N_i^t + \Delta t(d_i^t - r_i^t), \quad (i = 1, 2, 3), \quad (4.19)$$

where d_0^t and d_i^t are, respectively, the arrival rates at the start and the i th ramp, q_0^t is the outflow rate from the first cell of the road network, and r_i^t represents the outflow from the i th on-ramp.

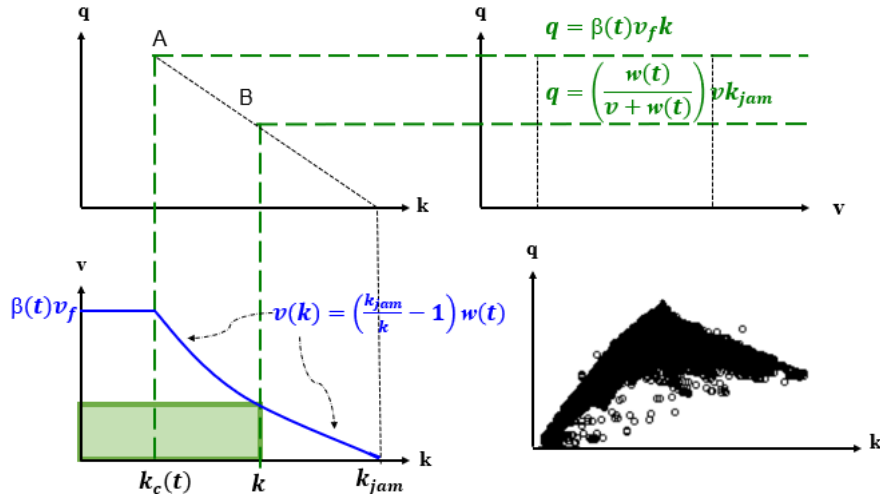


Figure 4.3: Relationship of traffic variables.

The fundamental triangular diagram shown in Figure 4.3 shows the fundamental relationship of traffic variables. From the CTM, the number of vehicles in each cell, n_i^t , The traffic speed in the cell is determined by

$$v_i^t = \begin{cases} \hat{v}_i & \text{for } k_i^t < k_c^t \\ \left(\frac{k_{jam}}{k_i^t} - 1 \right) w_i^t & \text{otherwise.} \end{cases} \quad (4.20)$$

Algorithm 1 CTM-SIM algorithm

```
1: procedure MAIN(start, end)
2:   cells,  $\ell, L$  = roadnetwork()
3:    $d, s$  = DATA(start, end, d0, d1, d2, d3, s0, s1)
4:    $dx \leftarrow 0.1$  ▷ cell length (km)
5:   Global  $TotCell \leftarrow \sum L_i/dx$ 
6:   Global  $v_f \leftarrow v_{max}/3600$  ▷ free speed (km/s)
7:    $dt \leftarrow dx/v_{max}$  ▷ timestep (s)
8:    $TotStep \leftarrow (end - start)/dt$ 
9:   Global  $q \leftarrow [[0.0] * TotCell] * TotStep$  ▷ flowout (veh/s)
10:  Global  $k \leftarrow [[0.0] * TotCell] * TotStep$  ▷ density (veh/km)
11:   $n \leftarrow [[0] * TotCell] * TotStep$  ▷ # vehs (veh/cell)
12:   $N \leftarrow [[0] * 4] * TotStep$  ▷ queue (veh)
13:   $ramp \leftarrow [[0] * 3] * TotStep$  ▷ ramp flow (veh/s)
14:   $q0 \leftarrow [0] * TotStep$  ▷ Inlet flow (veh/s)
15:  Global  $Q \leftarrow \ell * q_{max}/3600$  ▷ Flow capacity (veh/s)
16:  Global  $K \leftarrow \ell * k_{max}$  ▷ Jam density (veh/km)
17:  Global  $w \leftarrow w/3600$  ▷ Shock speed (km/s)
18:   $t \leftarrow 0$ 
19:  while  $t \leq TotStep$  do
20:     $q0, q, ramp = \text{FLOW}(t, dt, dx, n, N, d)$ 
21:     $N = \text{QUEUE}(t, dt, N, d, q0, ramp)$ 
22:     $n = \text{CAR}(t, dt, n, s, q0, ramp)$ 
23:     $t \leftarrow t + 1$ 
24:  end while
25:  return  $q, n, N$ 
26: end procedure
```

Algorithm 2 SCTM-SIM algorithm

```
1: procedure MAIN( $cell_c, \beta_{min}, \beta_{max}, q_{min}, q_{max}, start, end$ )
2:   cells,  $\ell, L = \text{roadnetwork}()$ 
3:    $d, s = \text{DATA}(start, end, d0, d1, d2, d3, s0, s1)$ 
4:    $dx \leftarrow 0.1$  ▷ cell length (km)
5:   Global  $TotCell \leftarrow \sum L_i/dx$ 
6:   Global  $v_f \leftarrow v_{max}/3600$  ▷ free speed (km/s)
7:    $dt \leftarrow dx/v_{max}$  ▷ timestep (s)
8:    $TotStep \leftarrow (end - start)/dt$ 
9:   Global  $q \leftarrow [[0.0] * TotCell] * TotStep$  ▷ flowout (veh/s)
10:  Global  $k \leftarrow [[0.0] * TotCell] * TotStep$  ▷ density (veh/km)
11:   $n \leftarrow [[0] * TotCell] * TotStep$  ▷ # vehs (veh/cell)
12:   $N \leftarrow [[0] * 4] * TotStep$  ▷ queue (veh)
13:   $ramp \leftarrow [[0] * 3] * TotStep$  ▷ ramp flow (veh/s)
14:   $q0 \leftarrow [0] * TotStep$  ▷ Inlet flow (veh/s)
15:  Global  $Q \leftarrow \ell * q_{max}/3600$  ▷ Flow capacity (veh/s)
16:  Global  $K \leftarrow \ell * k_{max}$  ▷ Jam density (veh/km)
17:  Global  $w \leftarrow w/3600$  ▷ Shock speed (km/s)
18:   $\alpha \leftarrow 0$ 
19:   $\beta \leftarrow [[0] * TotCell] * TotStep$  ▷ VSL parameters
20:   $t \leftarrow 0$ 
21:  while  $t \leq TotStep$  do
22:     $\beta, q_{max} = \text{STOCHASTIC}(\beta_{min}, \beta_{max}, q_{min}, q_{max}, cell_c)$ 
23:     $Q \leftarrow \ell * q_{max}/3600$ 
24:     $q0, q, ramp = \text{SFLOW}(t, dt, dx, \alpha, \beta, n, N, d, Q, K, v_f, w)$ 
25:     $N = \text{QUEUE}(t, dt, N, d, q0, ramp)$ 
26:     $n = \text{CAR}(t, dt, n, s, q, q0, ramp)$ 
27:     $t \leftarrow t + 1$ 
28:  end while
29:  return  $q, n, N$ 
30: end procedure
```

Algorithm 3 Tool functions

```
procedure FIN(cell, t, dt, arr, Queue)
  i ← cell
  q1 ← min( $v_f * k[i][t]$ ,  $w[i + 1] * (K[i + 1] - k[i + 1][t])$ ),  $Q[i]$ )
  q2 ← arr + (Queue/dt)
  if  $q1 + q2 \leq w[i + 1] * (K[i + 1] - k[i + 1][t])$  then
    qout, ramp ← q1, q2
  else
    qout ← ( $q1 / (q1 + q2)$ ) *  $w[i + 1] * (K[i + 1] - k[i + 1][t])$ 
    ramp ← ( $q2 / (q1 + q2)$ ) *  $w[i + 1] * (K[i + 1] - k[i + 1][t])$ 
  end if
  return qout, ramp
end procedure
procedure FOUT(cell, t, dt, ramp)
  i ← cell
  q0 ←  $q[i - 1][t] + ramp$ 
  qout ← min(q0,  $v_f * k[i][t]$ ,  $w[i + 1] * (K[i + 1] - k[i + 1][t])$ ),  $Q[i]$ )
  return qout
end procedure
procedure SFIN(cell, t, dt,  $\alpha$ ,  $\beta$ , arr, Queue)
  i ← cell
  q1 ← min( $(1 - \beta) * v_f * k[i][t]$ ,  $w[i + 1] * (K[i + 1] - k[i + 1][t])$ ),  $Q[i]$ )
  q2 ←  $(1 - \alpha) * (arr + (Queue/dt))$ 
  if  $q1 + q2 \leq w[i + 1] * (K[i + 1] - k[i + 1][t])$  then
    qout, ramp ← q1, q2
  else
    qout ← ( $q1 / (q1 + q2)$ ) *  $w[i + 1] * (K[i + 1] - k[i + 1][t])$ 
    ramp ← ( $q2 / (q1 + q2)$ ) *  $w[i + 1] * (K[i + 1] - k[i + 1][t])$ 
  end if
  return qout, ramp
end procedure
procedure SFOUT(cell, t, dt,  $\beta$ , ramp)
  i ← cell
  q0 ←  $q[i - 1][t] + ramp$ 
  qout ← min(q0,  $(1 - \beta) * v_f * k[i][t]$ ,  $w[i + 1] * (K[i + 1] - k[i + 1][t])$ ),  $Q[i]$ )
  return qout
end procedure
```

Algorithm 4 Tool functions (continue)

```
procedure QUEUE( $t, dt, N, d, q0, ramp$ )  
   $N[0][t+1] \leftarrow N[0][t] + dt * (d[0][t] - q0[t])$   $\triangleright$  Queue length  
   $N[1][t+1] \leftarrow N[1][t] + dt * (d[1][t] - ramp[0][t])$   
   $N[2][t+1] \leftarrow N[2][t] + dt * (d[2][t] - ramp[1][t])$   
   $N[3][t+1] \leftarrow N[3][t] + dt * (d[3][t] - ramp[2][t])$   
  return  $N$   $\triangleright$  queue lengths at inlet, all on-ramps  
end procedure  
procedure CAR( $t, dt, \beta, n, s, q, q0, ramp$ )  
   $nmin \leftarrow 0$   
  for  $i$  in cells do  
    switch( $i$ )  
      Case  $i$  is the first cell  
         $n[0][t+1] \leftarrow n[0][t] + dt * (q0[t] - q[0][t])$   
      Case  $i$  is the 1st merge cell  
         $n[i][t+1] \leftarrow n[i][t] + dt * (q[i-1][t] + ramp[0][t] - q[i][t])$   
      Case  $i$  is the 2nd merge cell  
         $n[i][t+1] \leftarrow n[i][t] + dt * (q[i-1][t] + ramp[1][t] - q[i][t])$   
      Case  $i$  the 3rd merge cell  
         $n[i][t+1] \leftarrow n[i][t] + dt * (q[i-1][t] + ramp[2][t] - q[i][t])$   
      Case  $i$  is the 1st diverge cell  
         $n[i][t+1] \leftarrow n[i][t] + dt * (q[i-1][t] - s[0][t] - q[i][t])$   
      Case  $i$  is the 2nd diverge cell  
         $n[i][t+1] \leftarrow n[i][t] + dt * (q[i-1][t] - s[1][t] - q[i][t])$   
      Case Default  
         $n[i][t+1] \leftarrow n[i][t] + dt * (q[i-1][t] - q[i][t])$   
    end switch  
  end for  
  return  $n$   $\triangleright$  number of vehicles  
end procedure
```

Algorithm 5 Tool functions (continue)

```
procedure FLOW( $t, dt, dx, n, N, d$ )
   $ramp \leftarrow [[0] * 3] * TotStep$  ▷ ramp flow (veh/s)
   $q0 \leftarrow [0] * TotStep$  ▷ Inlet flow (veh/s)
  for  $i$  in cells do
     $k[i][t] \leftarrow n[i][t]/dx$ 
    switch( $i$ )
      Case  $i$  is the first cell
         $q0[t] \leftarrow \min((d[0][t] + (N[0][t]/dt), Q[0], w[0] * (K[0] - k[0][t]))$ 
         $q[0][t] \leftarrow \min(q0[t], v_f * k[0][t], w[1] * (K[1] - k[1][t]), Q[0])$ 
      Case  $i$  is the upstream cell of 1st merge cell
         $q[i][t], ramp[0][t] = FIN(i, t, dt, d[1][t], N[1][t])$ 
      Case  $i$  is the 1st merge cell
         $q[i][t] = FOUT(i, t, dt, ramp[0][t])$ 
      Case  $i$  is the upstream of 2nd merge cell
         $q[i][t], ramp[1][t] = FIN(i, t, dt, d[2][t], N[2][t])$ 
      Case  $i$  is the 2nd merge cell
         $q[i][t] = FOUT(i, t, dt, ramp[1][t])$ 
      Case  $i$  is the upstream of 3rd merge cell
         $q[i][t], ramp[2][t] = FIN(i, t, dt, d[3][t], N[3][t])$ 
      Case  $i$  the 3rd merge cell
         $q[i][t] = FOUT(i, t, dt, ramp[2][t])$ 
      Case  $i$  is the last cell
         $q[i][t] \leftarrow \min(q[i-1][t], v_f * k[i][t], Q[i])$ 
      Case Default
         $\psi = \min\{v_f * k[i][t], w[i+1][t] * (K[i+1] - k[i+1][t]), Q[i]\}$ 
         $q[i][t] \leftarrow \min(q[i-1][t], \psi)$ 
    end switch
  end for
  return  $q0, q, ramp$ 
end procedure
procedure STOCHASTIC( $v1_{min}, v1_{max}, v2_{min}, v2_{max}, cell_c$ )
  import random
  for  $i$  in  $cell_c$  do
     $v1[i] \leftarrow \text{random.uniform}(v1_{min}, v1_{max})$ 
     $v2[i] \leftarrow \text{random.uniform}(v2_{min}, v2_{max})$ 
  end for
  return  $v1, v2$ 
end procedure
```

Algorithm 6 Tool functions (continue)

```
procedure SFLOW( $t, dt, dx, \alpha, \beta, n, N, d$ )
   $ramp \leftarrow \llbracket [0] * 3 \rrbracket * TotStep$  ▷ ramp flow (veh/s)
   $q0 \leftarrow [0] * TotStep$  ▷ Inlet flow (veh/s)
  for  $i$  in cells do
     $k[i][t] \leftarrow n[i][t]/dx$ 
    switch( $i$ )
      Case  $i$  is the first cell
         $q0[t] \leftarrow \min((d[0][t] + (N[0][t]/dt), Q[0], w[0] * (K[0] - k[0][t]))$ 
         $\phi \leftarrow \{q0[t], (1 - \beta[0]) * v_f * k[0][t], w[1] * (K[1] - k[1][t]), Q[0]\}$ 
         $q[0][t] \leftarrow \min(\phi)$ 
      Case  $i$  is the upstream cell of 1st merge cell
         $q[i][t], ramp[0][t] = SFIN(i, t, dt, \alpha[i], \beta[i], d[1][t], N[1][t])$ 
      Case  $i$  is the 1st merge cell
         $q[i][t] = SFOUT(i, t, dt, \beta[i], ramp[0][t])$ 
      Case  $i$  is the upstream of 2nd merge cell
         $q[i][t], ramp[1][t] = SFIN(i, t, dt, \alpha[i], \beta[i], d[2][t], N[2][t])$ 
      Case  $i$  is the 2nd merge cell
         $q[i][t] = SFOUT(i, t, dt, \beta[i], ramp[1][t])$ 
      Case  $i$  is the upstream of 3rd merge cell
         $q[i][t], ramp[2][t] = SFIN(i, t, dt, \alpha[i], \beta[i], d[3][t], N[3][t])$ 
      Case  $i$  the 3rd merge cell
         $q[i][t] = SFOUT(i, t, dt, \alpha[i], \beta[i], ramp[2][t])$ 
      Case  $i$  is the last cell
         $q[i][t] \leftarrow \min(q[i-1][t], (1 - \beta[i]) * v_f * k[i][t], Q[i])$ 
      Case Default
         $\psi = \min\{(1 - \beta[i]) * v_f * k[i][t], w[i+1][t] * (K[i+1] - k[i+1][t]), Q[i]\}$ 
         $q[i][t] \leftarrow \min(q[i-1][t], \psi)$ 
    end switch
  end for
  return  $q0, q, ramp$ 
end procedure

procedure DATA( $start, end, d0, d1, d2, d3, s0, s1$ ) ▷ read data
   $dt \leftarrow 0.4$  ▷ time step (s)
  while  $t \leq (end - start)/dt$  do ▷ simulation time
     $d[0][t] \leftarrow d0[t + start]/3600$  ▷ Main demand
     $d[1][t] \leftarrow d1[t + start]/3600$  ▷ H558 demand
     $d[2][t] \leftarrow d2[t + start]/3600$  ▷ H554 demand
     $d[3][t] \leftarrow d3[t + start]/3600$  ▷ H553 demand
     $s[0][t] \leftarrow s0[t + start]/3600$  ▷ H559 demand
     $s[1][t] \leftarrow s1[t + start]/3600$  ▷ H551 demand
  end while
  return  $d, s$  ▷ arrival and discharge rates
end procedure
```

Table 4.1: The road network structure of study region.

Edge	From	To	Length (m)	lanes	Remarks
1	start	J1	100	3	
2	J1	H559	100	3	Off to Leach Hwy
3	H559	J2	100	3	
4	J2	H558	587	3	Leach WB on-ramp
3	H558	J3	230	4	
4	J3	H554	210	3	Leach EB on-ramp
5	H554	J4	125	4	
6	J4	H553	190	3	Cranford on-ramp
7	H553	J5	2000	4	
9	J5	J6	100	3	**lane closure
10	J6	H551	589	3	Off to Canning Hwy
11	H551	end	100	3	

4.2.2 Numerical studies

In this study, the region is the road network from the Off-to-Leach (H559) to Off-to-Canning (H551) of the Kwinana Freeway northbound (see Table 4.1). There are three on-ramps and two off-ramps, as shown in Figure 4.4.

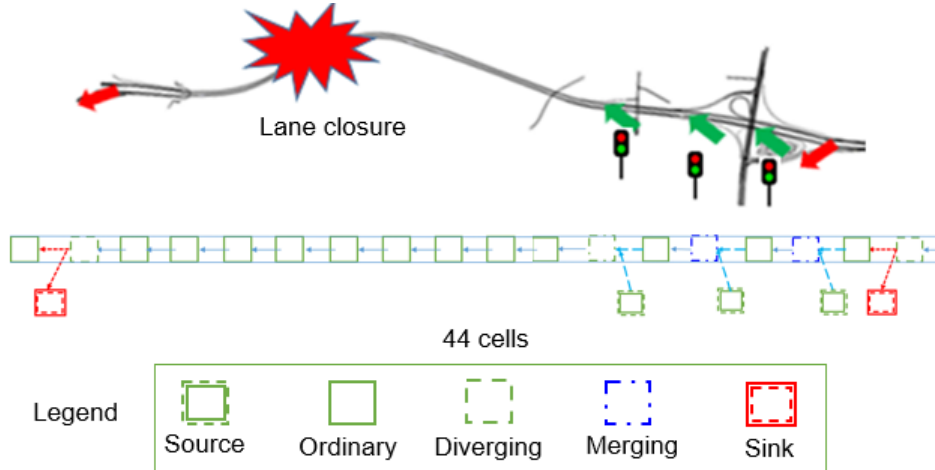


Figure 4.4: CTM road network.

The road network comprises several road links (segments) from the main road, three on-ramps and two off-ramp roads. The main road, as shown in Figure 4.4, has 11 edges with variable lengths ΔL_i . To ensure numerical stability, each edge is discretised into a number of cells with n_c cells with maximum length of Δx ,

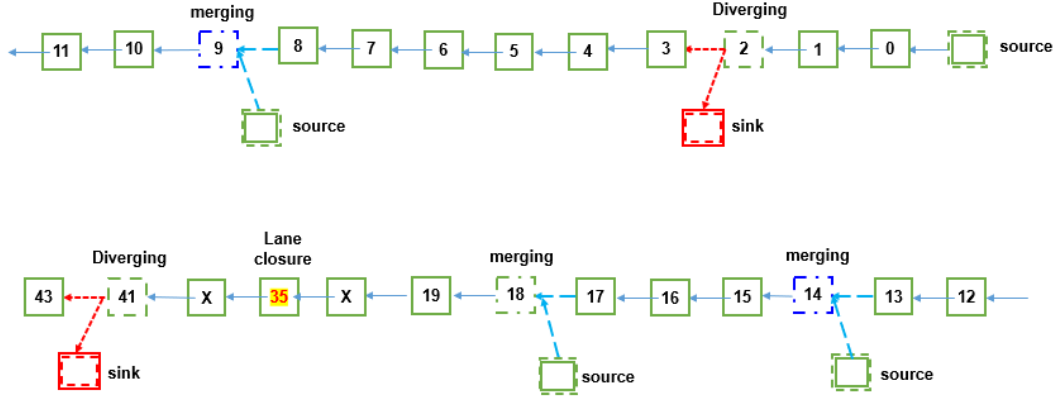


Figure 4.5: Road network with 3 on-ramps and 2 off-ramps.

and

$$L_i = \begin{cases} n_c \Delta x & \text{if } L_i \bmod \Delta x = 0 \\ (n_c - 1) \Delta x + \frac{L_i}{\Delta x} & \text{otherwise.} \end{cases} \quad (4.21)$$

In this study, for the cell length of 100 *m* and a free speed, v_f , of 90 *km/hour* during the daytime between 6 am and 6 pm, the size of time steps is give by

$$\Delta t = \frac{\ell_c}{v_f} = \frac{100 \text{ m.}}{90 \text{ km/hour}} = 4 \text{ seconds.} \quad (4.22)$$

Based on the Godunov scheme for a chain of segments, traffic density is updated every time step based on incoming flow (outgoing flow) to (from) the main road. The simulation starts with the initial solution

$$k_i^{(0)} = \hat{k}_i. \quad (4.23)$$

Using traffic data from the Mainroad Western Australia (MRWA), the on-ramp arrival rate and the off-ramp discharge rate are updated every 15 minutes (at $t_0 + 225 \Delta t$), while for the main road segments, the arrival rate and discharge rate are applied every minute (at $t_0 + 15 \Delta t$) to the first cell and the last cell of the road network.

For SCTM, the following model parameters are defined as random variables:

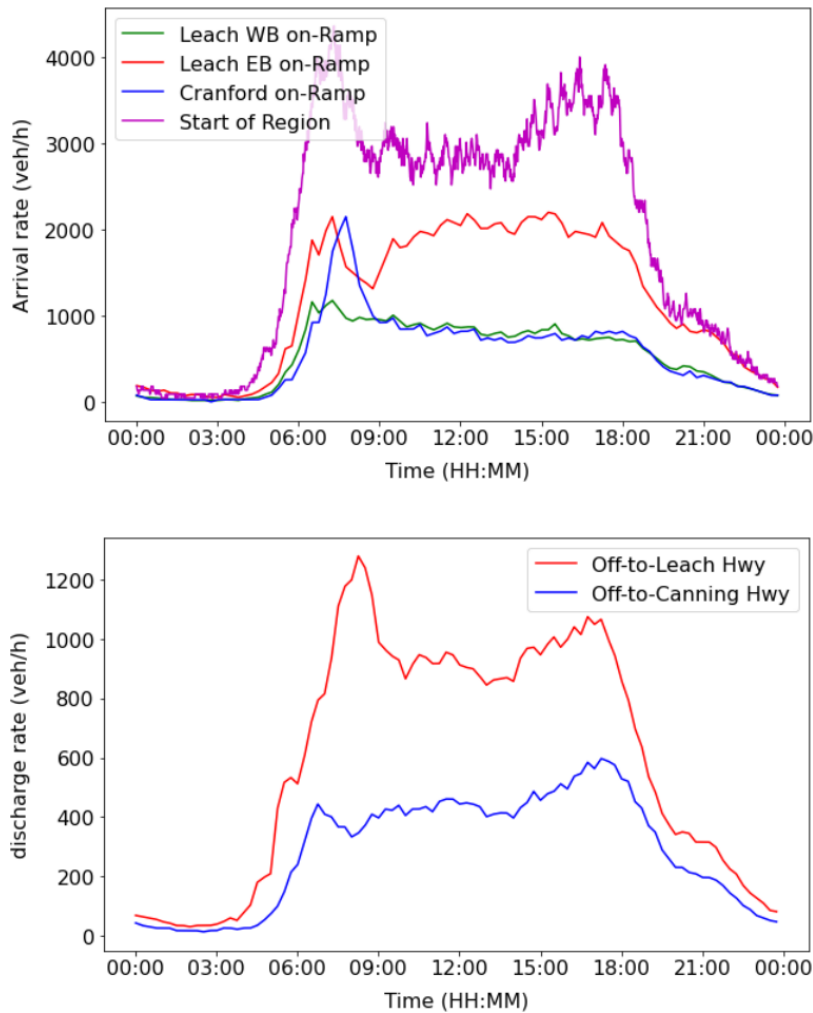


Figure 4.6: Incoming and outgoing flows on 4 September 2018.

- Free speed of an ordinary cell is in the range of 90 to 100 km/h;
- Free speed of an upstream merging cell, the lane-closure cell and its upstream cell is in the range of 40 to 50 km/h;
- Flow capacity per lane is in the range of 2000 and 2200 veh/h;
- Variable speed limit parameter, β , of the diverging cell, the lane-closure cell, and its upstream cell is in the range of 0.35 and 0.45.

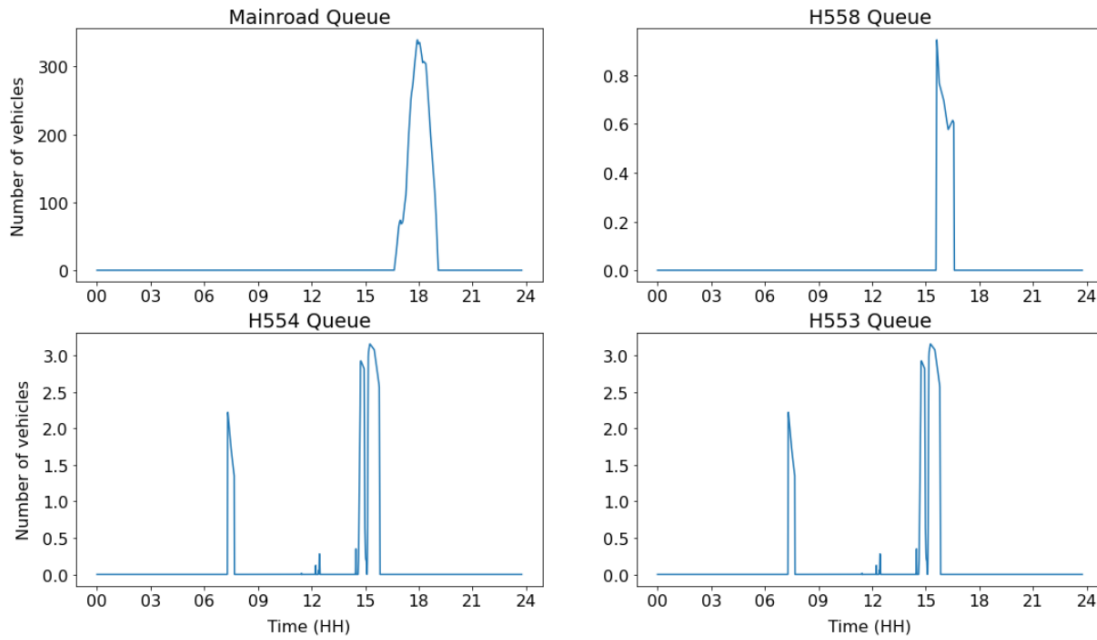
Figure 4.6 represents the incoming and outgoing flows on September 4, 2018. Incoming flow shows demand arrival rates at the main entry and three on-ramp

roads, and outgoing flow shows the supply discharging rates at two off-ramp roads.

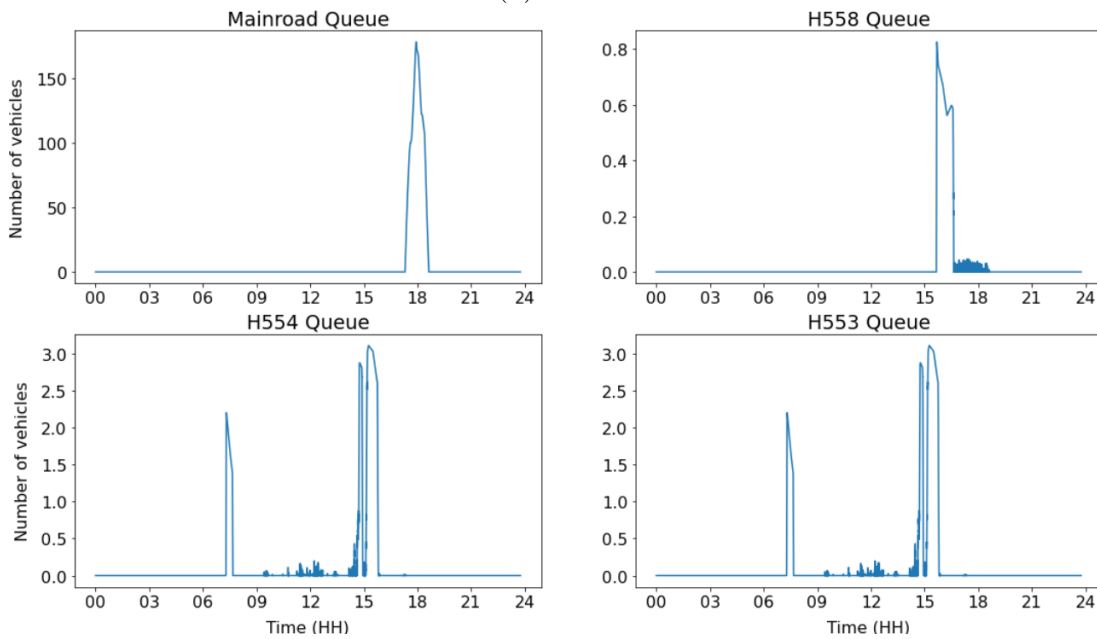
Using Algorithm 1, Algorithm 2 and various tool functions, these following results for the cell transmission model (CTM) and Stochastic cell transmission model (SCTM) are obtained. Figure 4.7 presents the number of vehicles waiting in the queue at the first cell of the main road with no lane closure and three on-ramp cells for the CTM and the SCTM. The On-ramp vehicle queue length is very small compared to the main road queue. The maximum queue lengths occur during peak hours in the morning from 7:00 am to 8 am and in the afternoon from 5 pm to 7 pm. Particularly during evening peak hours on the main road, it may reach over 150 vehicles waiting in the queue of SCTM, with over 300 vehicles waiting in the queue of CTM.

Figures 4.8 and 4.9 show flow rate and density results obtained from the CTM and SCTM with no lane closure. The maximum flow is 6000 of CTM and 6168 of SCTM when the flow increases and the density decreases. The size of mainline density increasing from bottom to top is shown in Figure 4.8.

These graphs 4.10 show the number of vehicles waiting in the queue at the first cell of the main road with lane closure and three on-ramp cells of CTM and SCTM. The maximum queue lengths occur all day. Especially for Figure 4.10 (a) on the main road, it may reach less than 6000 vehicles waiting in the queue of, and on-ramp vehicles waiting in the queue are more than those in the standard simulation with no lane closure. As shown in Figure 4.10 (b) it may reach over 6000 vehicles waiting in the queue on the main road, with on-ramp vehicles waiting in the queue numbering more than those in the standard simulation with no lane closure. Results presented in Figures 4.11 and 4.12 show the flow rates and density obtained from the CTM and SCTM with lane closure at the cell 35 from 3 to 2 lanes from 8:00 am to 10:00 am. The results of this implementation show the congestion at upstream cells caused by lane closure. The lane closure of cell 35 caused the freeway section prior to the incident to



(a) CTM



(b) SCTM

Figure 4.7: Queue size (veh) at the beginning and three on-ramps, including H558 (Leach WB on-ramp), H554 (Leach EB on-ramp) and H553 (Cranford AVE on-ramp) obtained from the CTM and the SCTM.

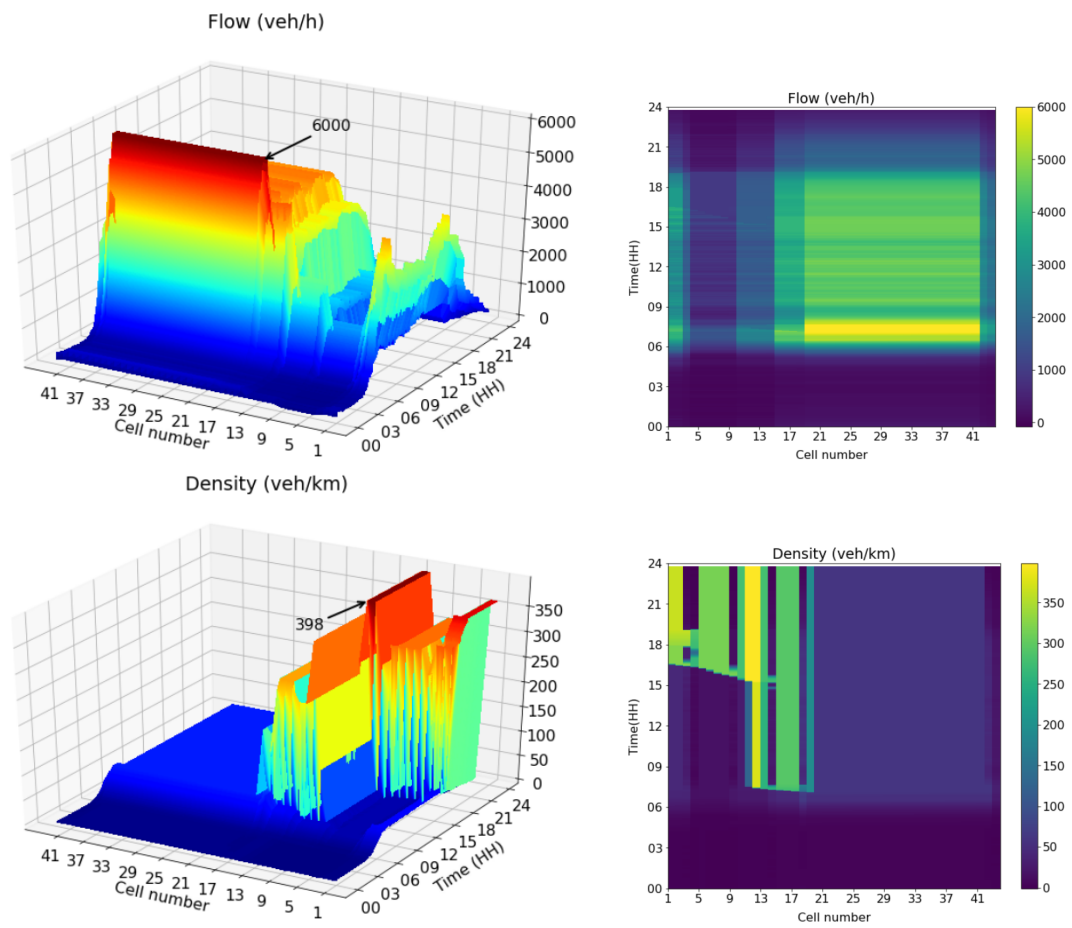


Figure 4.8: Surface and heatmap plots of flow rate (veh/h) and density (veh/km) obtained from the CTM.

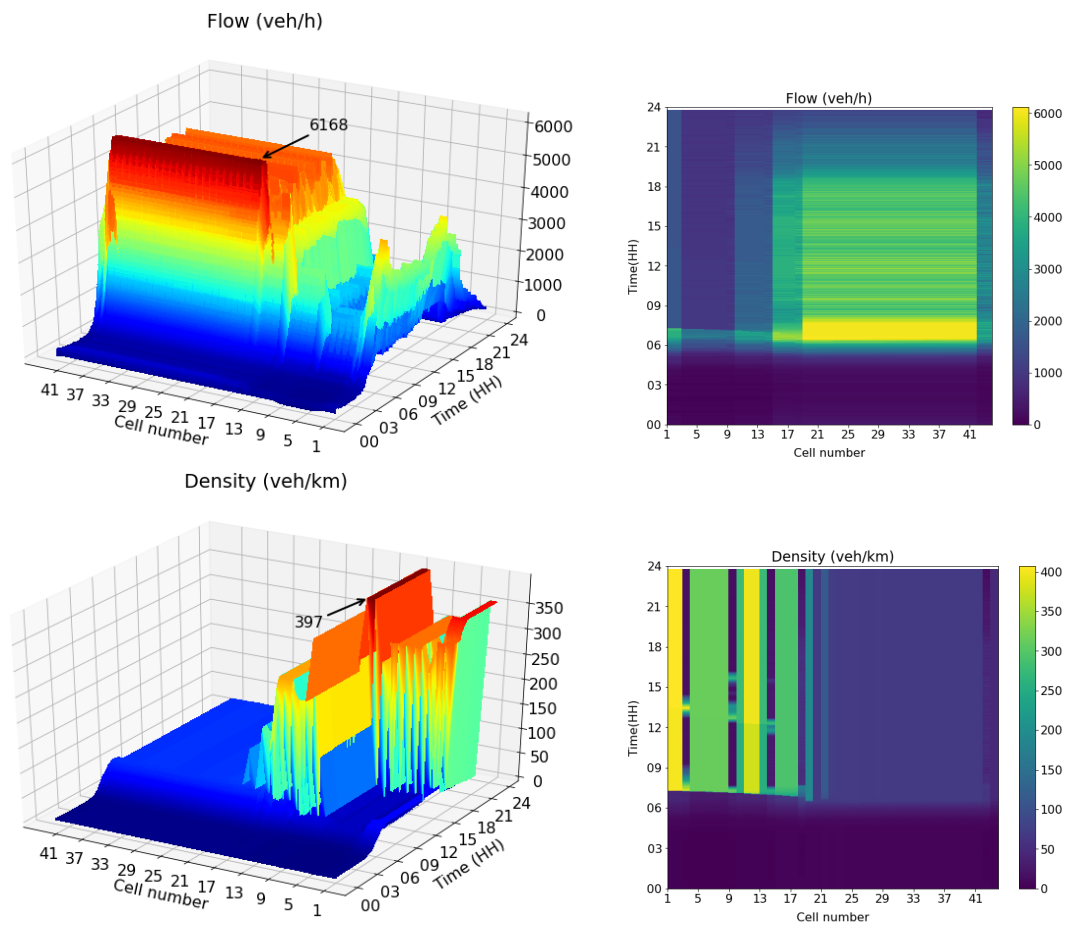
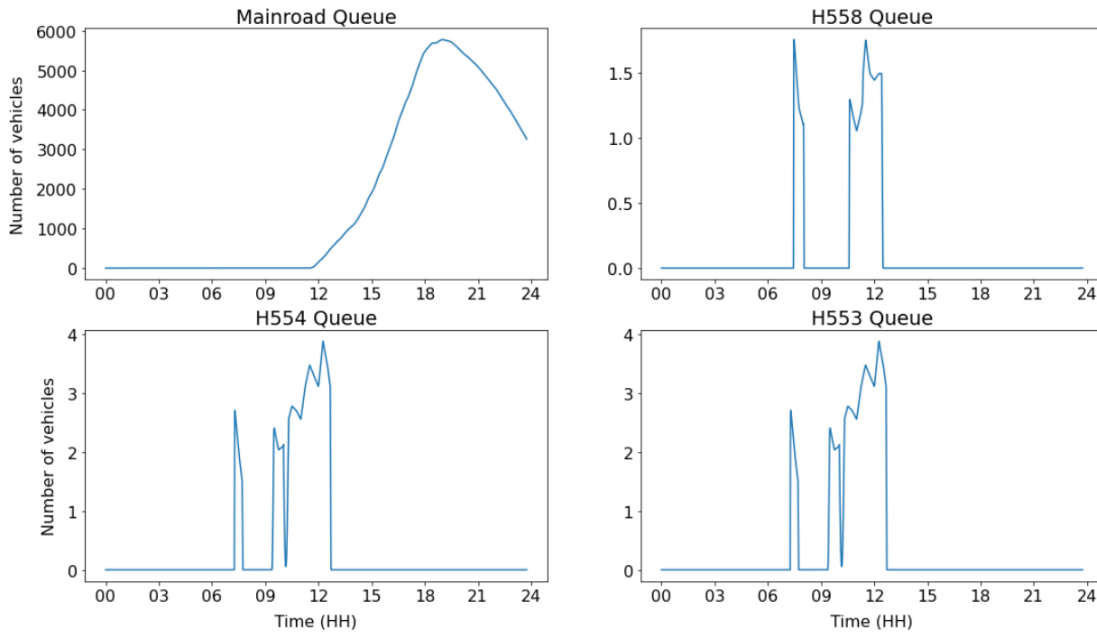
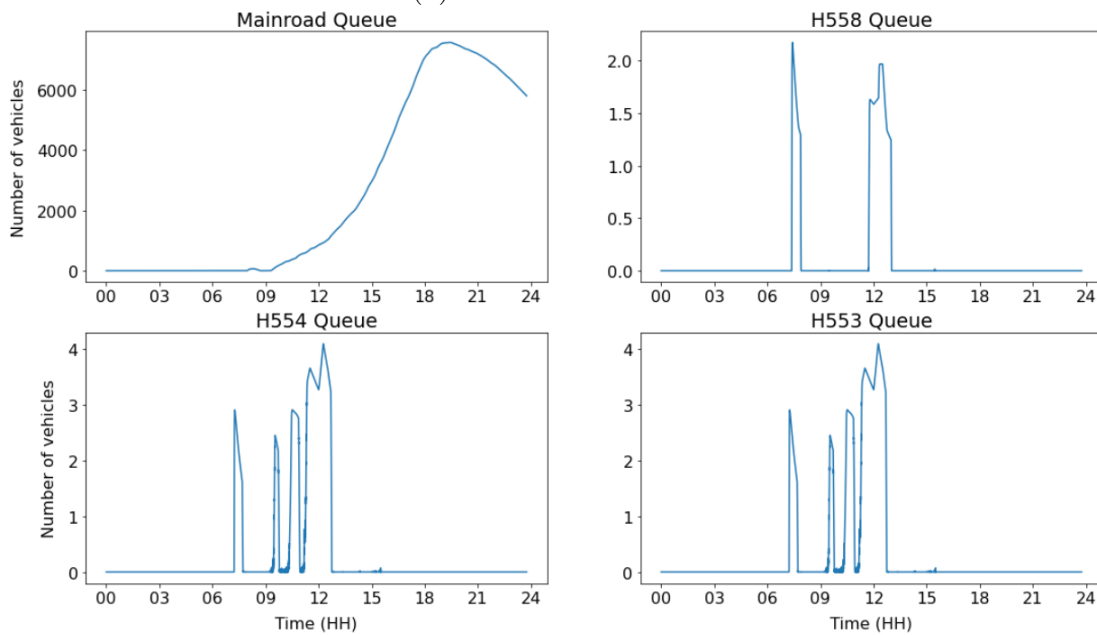


Figure 4.9: Surface and heatmap plots of flow rate (veh/h) and density (veh/km) obtained from the SCTM



(a) lane-closure CTM



(b) lane-closure SCTM

Figure 4.10: Queue size (veh) at the beginning and three on-ramps, including H558 (Leach WB on-ramp), H554 (Leach EB on-ramp) and H553 (Cranford AVE on-ramp) obtained from the CTM and SCTM with lane closure from 6:00 am to 10:00 am.

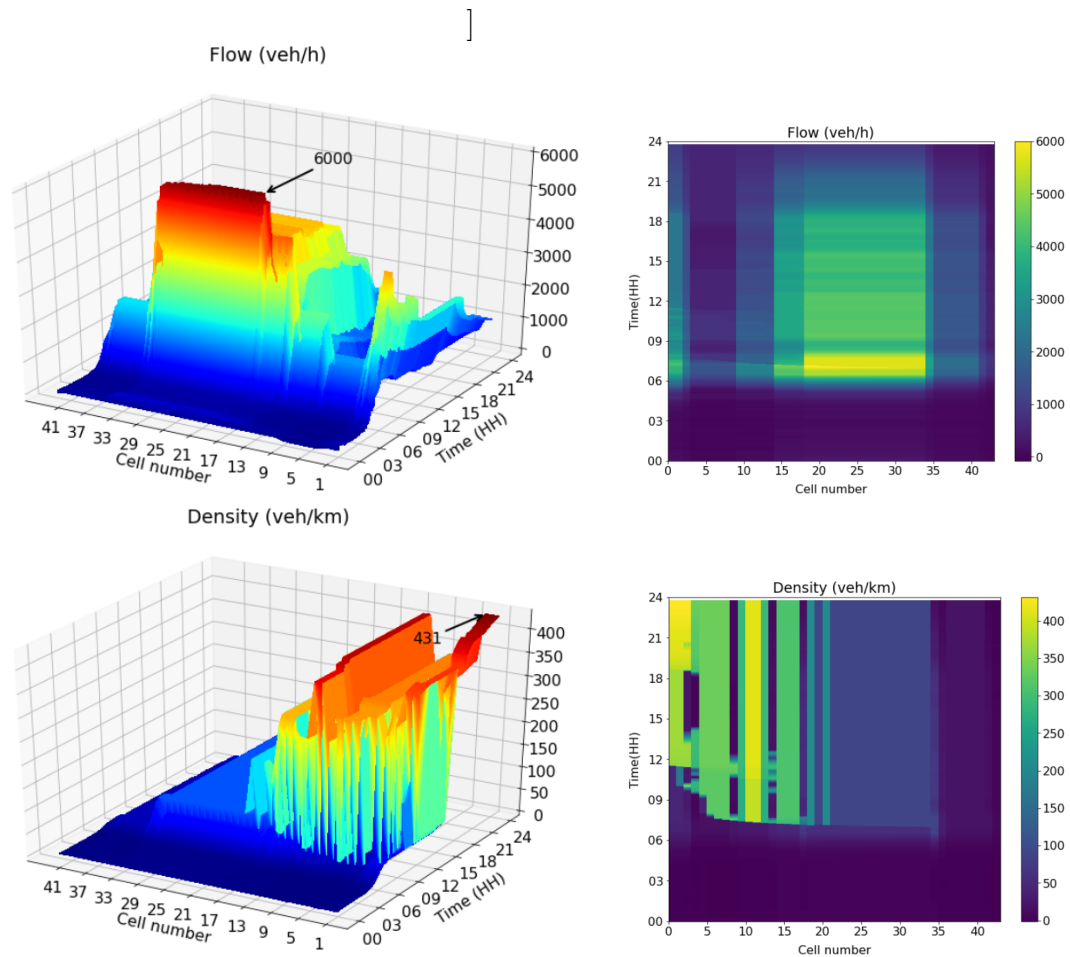


Figure 4.11: Surface and heatmap plots of flow rate (veh/h) and density (veh/km) obtained from the CTM with lane closure from 6:00 am to 10:00 am

become very backed up, with the flow dropping and density rising more than in the standard simulation with no lane closure.

4.3 Stochastic Optimisation Model

The freeway congestion can be avoided with the speed limits, as sometimes the ramp meter is not able to control the traffic flow effectively. This hypothesis was demonstrated by utilising a simple but effective combination of variable speed limits and demand ramp metering by keeping the lane close initially and then without the lane closure.

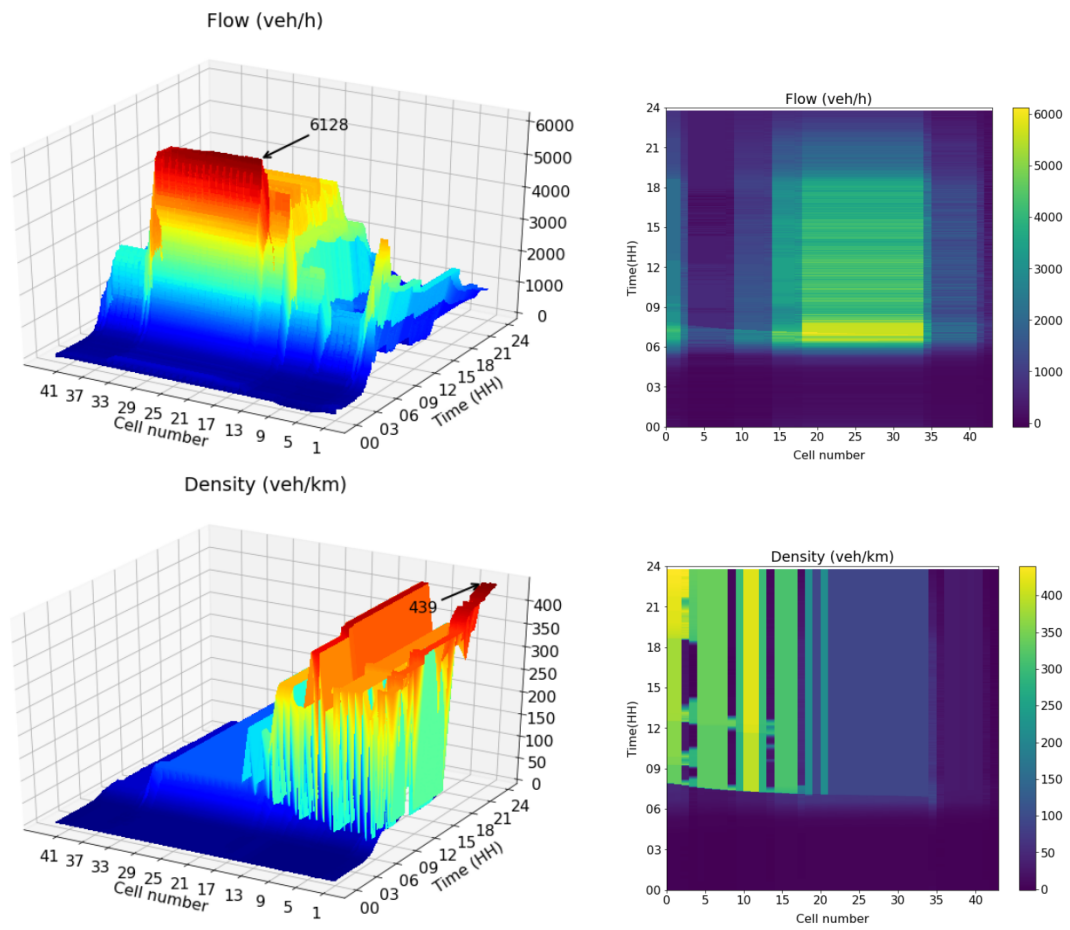


Figure 4.12: Surface and heatmap plots of flow rate (veh/h) and density (veh/km) obtained from the SCTM with lane closure from 6:00 am to 10:00 am.

4.3.1 Objective function and constraints

For optimal traffic flow, minimising total travel time, on the roadway with a lane closure at one segment in the time horizon H_c using the RM & VSL controls, decision variables $\alpha(t) = [\alpha_1^\tau, \dots, \alpha_{RM}^\tau]_{\tau=0}^{H_c-1}$ and $\beta(t) = [\beta_1^\tau, \dots, \beta_{VSL}^\tau]_{\tau=0}^{H_c-1}$ may be obtained by solving the following optimisation model:

$$\min \sum_t \Delta t \left\{ \sum_i \Delta x k_i^t + \sum_r N_r^t \right\} \quad (4.24)$$

subject to the following constraints:

- Transport equation

$$\frac{\partial}{\partial t} k(x, t) + \frac{\partial}{\partial x} q(x, t) = \frac{\partial}{\partial x} f(x, t), \quad (4.25)$$

$$\text{with } f(x, t) = \begin{cases} (1 - \alpha(t)) \left(d(x, t) + \frac{N(x, t)}{\Delta t} \right) & x \in \text{a merging cell} \\ s(x, t) & x \in \text{a diverging cell} \\ 0 & \text{otherwise} \end{cases}$$

which can be expressed in an explicit form as

$$k_i^t = k_i^{t-1} + \frac{\Delta t}{\Delta x} (q_{i-1}^{t-1} - q_i^{t-1} - f_i^{t-1}). \quad (4.26)$$

- Optimal flow rate

- For upstream-merged cells, let

$$\begin{cases} q_{temp} &= \min \{ v_e^t k_{i-1}^t; w_i (k_{jam} - k_i^t); q_i^{max} \} \\ r_{temp} &= (1 - \alpha_i^t) \left(d_i^t + \frac{N_i^t}{\Delta t} \right); \quad \alpha_i^t < 1 \text{ (the RM parameter)} \end{cases}$$

$$* \text{ if } q_{temp} + r_{temp} \leq w_{i+1} (k_{jam} - k_{i+1}^t) \text{ then } \begin{cases} q_i^t = q_{temp} \\ r_e^t = r_{temp} \end{cases}$$

* otherwise,

$$q_i^t = \frac{q_{temp}}{q_{temp} + r_{temp}} w_{i+1} (k_{jam} - k_{i+1}^t),$$

$$r_e^t = \frac{r_{temp}}{q_{temp} + r_{temp}} w_{i+1} (k_{jam} - k_{i+1}^t).$$

- For other cells,

$$q_i^t = \begin{cases} \min \{q_0^t; v_e^t k_0^t; w_1(k_{jam} - k_1^t); q_0^{max}\} & \text{for the first cell} \\ \min \{q_{i-1}^t; v_e^t k_i^t; q_i^{max}\} & \text{for the last cell} \\ \min \{q_{i-1}^t + r_e^t; v_e^t k_i^t; w_{i+1}(k_{jam} - k_{i+1}^t); q_i^{max}\} & \text{for a merged cell} \\ \min \{q_{i-1}^t - s_i^t; v_e^t k_i^t; w_{i+1}(k_{jam} - k_{i+1}^t); q_i^{max}\} & \text{for a diverged cell} \\ \min \{q_{i-1}^t; v_e^t k_i^t; w_{i+1}(k_{jam} - k_{i+1}^t); q_i^{max}\} & \text{Otherwise} \end{cases} \quad (4.27)$$

with $v_e^t = (1 - \beta_i^t)v_f$ and $\beta_i^t < 1$ (the VSL parameter). The term r_e^t represents the incoming flow from the on-ramp upstream-merged cell. The terms $d(x, t)$ and $s(x, t)$ which are observed data represent on-ramp arrival rates and off-ramp discharge rate, respectively. The term N_i^t represent the queue length of the incoming-flow cell.

- For any cell within the incident zone, vehicles allow moving with the speed of v_ℓ and the flow rate

$$q_i^t = \begin{cases} \min \{q_{i-1}^t; v_\ell k_i^t; w_{i+1}(\frac{\ell-1}{\ell} k_{jam} - k_{i+1}^t); \frac{\ell-1}{\ell} q_i^{max}\} & \text{incident period} \\ \min \{q_{i-1}^t; v_e^t k_i^t; w_{i+1}(k_{jam} - k_{i+1}^t); q_i^{max}\} & \text{otherwise.} \end{cases} \quad (4.28)$$

4.3.2 Numerical studies

This section presents the effects of VSL control on freeway traffic flow with and without lane closure. Using Algorithm 7 and various tool functions, these following results are obtained. Figure 4.5 presents the structure of road network in which cell 35 has an accident and one lane is closed. VSLs are applied at various upstream cells, including cells 2, 8, 13, 17, 18, 22, 26, 30 and 34. The track was divided into 44 units, each with the length of 100 m. One of the busiest in Perth is chosen as the road segment, it has three on-ramps and two off-ramps. The

Algorithm 7 Optimisation algorithm

```
1: procedure MAIN(start, end, startc, endc)
2:   cells, cellc, cellVSL, cellX, ℓ, L = roadnetwork()
3:   d, s = DATA(start, end, d0, d1, d2, d3, s0, s1)
4:   dx ← 0.1                                     ▷ cell length (km)
5:   Global TotCell ← ∑ Li/dx
6:   Global vf ← 90/3600                          ▷ free speed (km/s)
7:   dt ← 4                                       ▷ timestep 4 s
8:   T ← 15 * dt                                  ▷ Update VSL every 1 min
9:   Global TotStep ← (end - start)/dt
10:  Global TotC ← (endc - startc)/T
11:  Global q ← [[0.0] * TotCell] * TotStep       ▷ flowout (veh/s)
12:  Global k ← [[0.0] * TotCell] * TotStep       ▷ density (veh/km)
13:  n ← [[0] * TotCell] * TotStep                ▷ vehs (veh/cell)
14:  N ← [[0] * 4] * TotStep                       ▷ queue (veh)
15:  Global Q ← ℓ * qmax/3600                      ▷ Flow capacity (veh/s)
16:  Global K ← ℓ * kmax                            ▷ Jam density (veh/km)
17:  Global w ← w/3600                             ▷ Shock speed (km/s)
18:  X ← [[0] * TotCell] * TotStep                ▷ VSL parameters
19:  X = OPTIMISE(startc, endc, T, dt, cellVSL, cellX, d, s, X)
20:  q, n, N = SCTMSIM(αmin, αmax, qmin, qmax, cellc, t, dt, dx, X, n, N, d)
21: end procedure
```

Algorithm 8 Tool functions

```
procedure OPTIMISE( $start_c, end_c, T, cdt, cell_{VSL}, cell_X, d, s, \beta$ )
   $control = []$ 
   $M \leftarrow len(cell_{VSL})$ 
   $tc \leftarrow 0$ 
   $X = OPDE(start_c, end_c, T, dt, cell_{VSL}, cell_X, d, s, \beta)$ 
  for  $i$  in range( $TotC$ ) do
     $vsl = []$ 
    for  $j$  in range( $M$ ) do
       $vsl.append(X[M * tc + j])$ 
      if not  $i \bmod T$  then
         $tc \leftarrow tc + 1$ 
      end if
       $control.append(vsl)$ 
    end for
  end for
  # update  $\beta$ 
   $tc \leftarrow 0$ 
  for  $i$  in range( $TotC$ ) do
    for  $j$  in range( $TotCell$ ) do
      if  $j$  in  $cell_{VSL}$  then
         $\beta[j][start_c + i] \leftarrow X[tc]$ 
         $tc \leftarrow tc + 1$ 
      end if
    end for
  end for
  return  $\beta$ 
end procedure
```

Algorithm 9 Tool functions

```
procedure OPDE(startc, endc, T, dt, cellVSL, cellX, d, s,  $\beta$ )
  procedure OBJ(X) ▷ Objective function
    VHT  $\leftarrow$  0.0
    tc  $\leftarrow$  0
    for i in range(TotC) do
      for j in cellVSL do
         $\beta[j][start_c + i] = X[tc]$ 
        tc  $\leftarrow$  tc + 1
      end for
    end for
    q, n, N = SCTMSIM( $\alpha_{min}$ ,  $\alpha_{max}$ ,  $q_{min}$ ,  $q_{max}$ , cellc, t, dt, dx, X, n, N, d)
    func = (n.sum().sum() + N.sum().sum()) * (T/3600)
    return func
  end procedure
  bounds = []
  vslmin, vslmax = 0.4, 0.6
  for i in range(len(cellVSL)) do
    bounds.append((vslmin, vslmax))
  end for
  bounds = bounds * TotC
  res = de(OBJ, bounds) ▷ call DE algorithm
   $\beta = res[0]$ 
  return  $\beta$ 
end procedure
procedure SCTMSIM( $\alpha_{min}$ ,  $\alpha_{max}$ ,  $q_{min}$ ,  $q_{max}$ , cellc, t, dt, dx,  $\beta$ , n, N, d)
  ramp  $\leftarrow$  [[0] * 3] * TotStep ▷ ramp flow (veh/s)
  q0  $\leftarrow$  [0] * TotStep ▷ Inlet flow (veh/s)
  t  $\leftarrow$  0
  while t  $\leq$  TotStep do
     $\alpha$ ,  $q_{max}$  = STOCHASTIC( $\alpha_{min}$ ,  $\alpha_{max}$ ,  $q_{min}$ ,  $q_{max}$ , cellc)
    Q  $\leftarrow$   $\ell$  *  $q_{max}$ /3600
    q0, q, ramp = SFLOW(t, dt, dx,  $\alpha$ ,  $\beta$ , n, N, d, Q)
    N = QUEUE(t, dt, N, d, q0, ramp)
    n = CAR(t, dt, n, s, q, q0, ramp)
    t  $\leftarrow$  t + 1
  end while
  return q, n, N
end procedure
```

peak hours, from 8:00 am to 10:00 am, are the ones are chosen. Cells 9, 14, and 18 serve as on-ramps, whereas cells 2 and 41 serve as off-ramps.

Optimal traffic performance on a normal roadway here is obtained by controlling the speed limit, $(1 - \beta)v_f$ with $\beta \in [0.1, 0.4]$, at 5 cells of the roadway including two diverging cells (cell 2 and cell 41) and three upstream cells of merging cells (cell 8, cell 13 and cell 17).

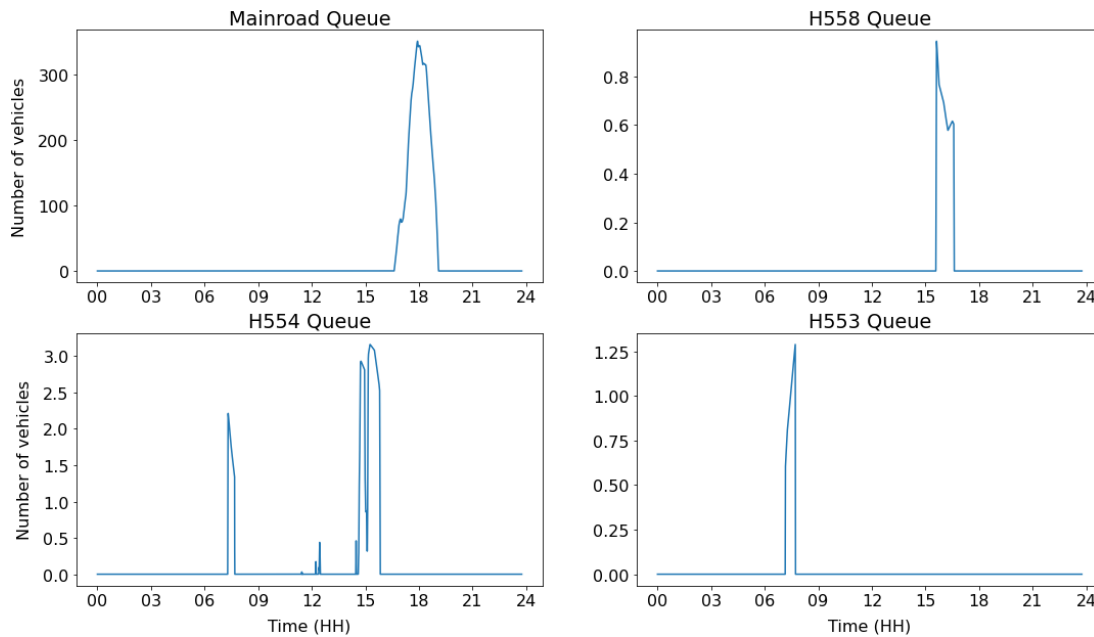


Figure 4.13: Queue size (veh) at the beginning and three on-ramps, including H558 (Leach WB on-ramp), H554 (Leach EB on-ramp) and H553 (Cranford AVE on-ramp) obtained from the optimisation model.

Figures 4.13 show the number of vehicles waiting in the queue at the first cell of the main-road without lane closure and three on-ramp cells of an optimisation model. The On-ramp vehicle queue length is minimal compared to the main-road queue. The maximum queue lengths occur during peak hours in the morning from 7:00 am to 8:00 am on (Leach EB and Cranford AVE) and the afternoon from 13:00 pm to 19:00 pm on (Leach WB and Leach EB). Particularly on the main-road during evening peak hours, vehicles waiting in the queue may reach over 300, which is similar to results in Figure 4.7 (a). However, the optimisation model shows a reduction of queue lengths on the main-road and three on-ramps.

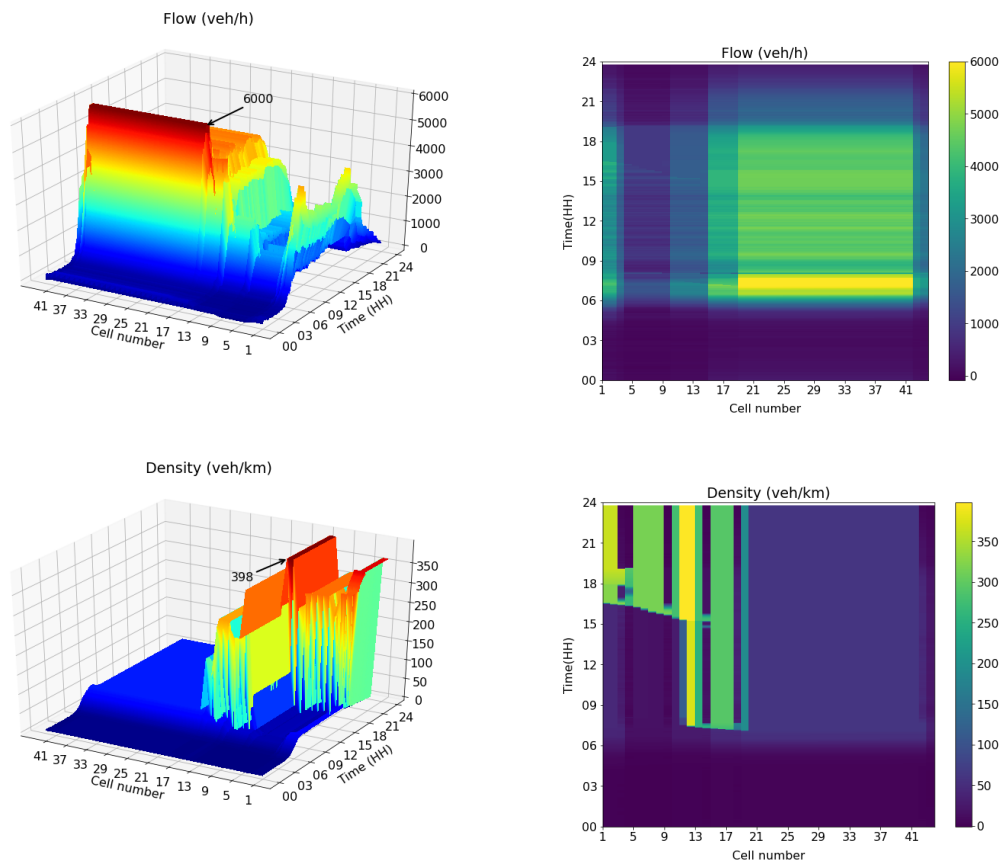


Figure 4.14: Surface and heatmap plots of flow rate (veh/h) and density (veh/km) obtained from the optimisation Model.

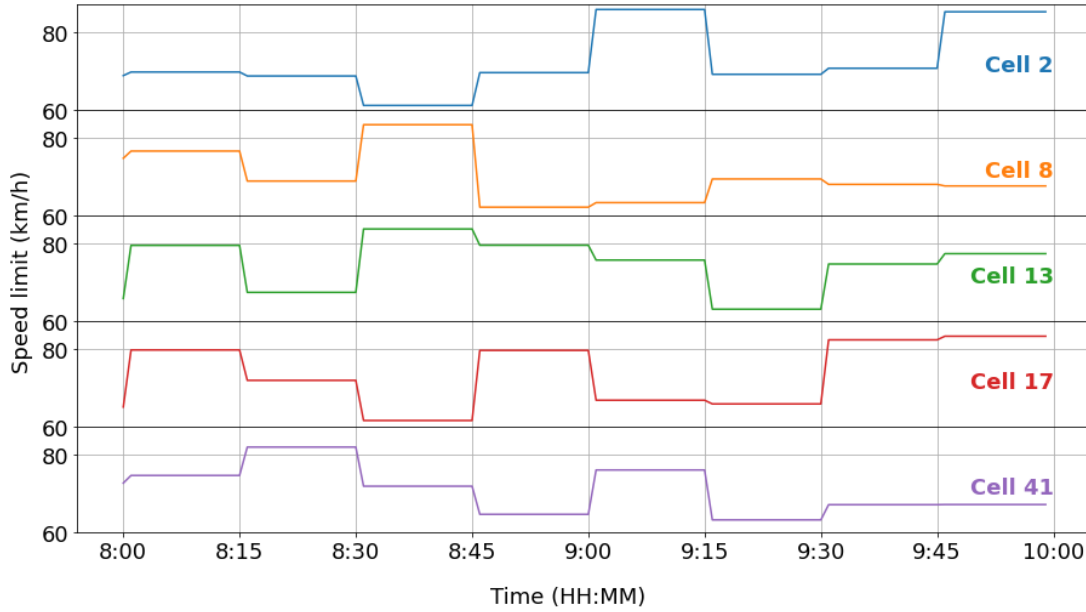


Figure 4.15: Variable speed limit (km/h) obtained from the optimisation model.

Figure 4.15 shows the variable speed limit obtained from the optimisation model. Here, the VSL range is between 60 and 95 km per hour at the control cells.

For the lane-closure Roadway, optimal traffic performance on a lane-closure roadway here is obtained by controlling the speed limit, $(1 - \beta)v_f$ with $\beta \in [0.4, 0.6]$, at 10 cells of the roadway including two diverging cells (cell 2 and cell 41), upstream cells of merging cells (cell 8, cell 13 and cell 17), and five upstream cells of the lane-closure cell (cell 18, cell 22, cell 26, cell 30 and cell 34).

Figures 4.16 show the number of vehicles waiting in the queue at the first cell of the main-road with lane closure and three on-ramp cells of an optimisation model. The On-ramp vehicle queue length is minimal compared to the main-road queue. The maximum queue lengths occur during peak hours in the morning from 7:00 am to 8:00 am on (Leach EB and Cranford AVE) and the afternoon from 13:00 pm to 19:00 pm on (Leach WB and Leach EB). Particularly on the main-road during evening peak hours, vehicles waiting in the queue may reach over 300, which is similar to results in Figure 4.7 (a). However, the optimisation model

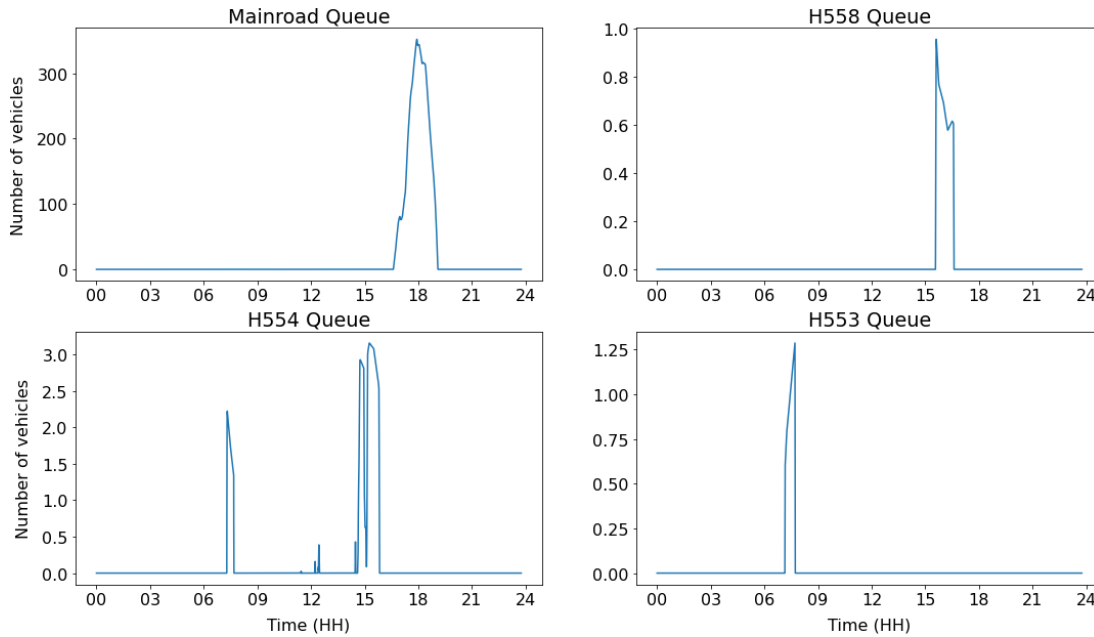


Figure 4.16: Queue size (veh) at the beginning and three on-ramps, including H558 (Leach WB on-ramp), H554 (Leach EB on-ramp) and H553 (Cranford AVE on-ramp) obtained from the optimisation model with lane closure.

shows a reduction of queue lengths on the Main-road and three on-ramps.

Figures 4.14 and 4.17 show the results of flow rate and density obtained from the optimisation model. The results here show the flow rate and density. Here, the congestion at upstream cells caused by lane closure is improved with VSL control on the freeway, with and without lane closure.

Figure 4.18 shows the variable speed limit (km/h) obtained from the optimisation model with lane closure. The VSL range is between 35 and 55 km per hour at these control cells. These results show that the proposed data-driven traffic optimisation model is helpful for traffic control and management.

The control was optimised in both scenarios so that total time spent in the network was minimal, with coordinated case results in both networks showing higher outflows and reduction in total time. These results indicate that decisions made between variable speed limits and ramp metering need to be made according to random demand arrivals on both the on-ramp and freeway.

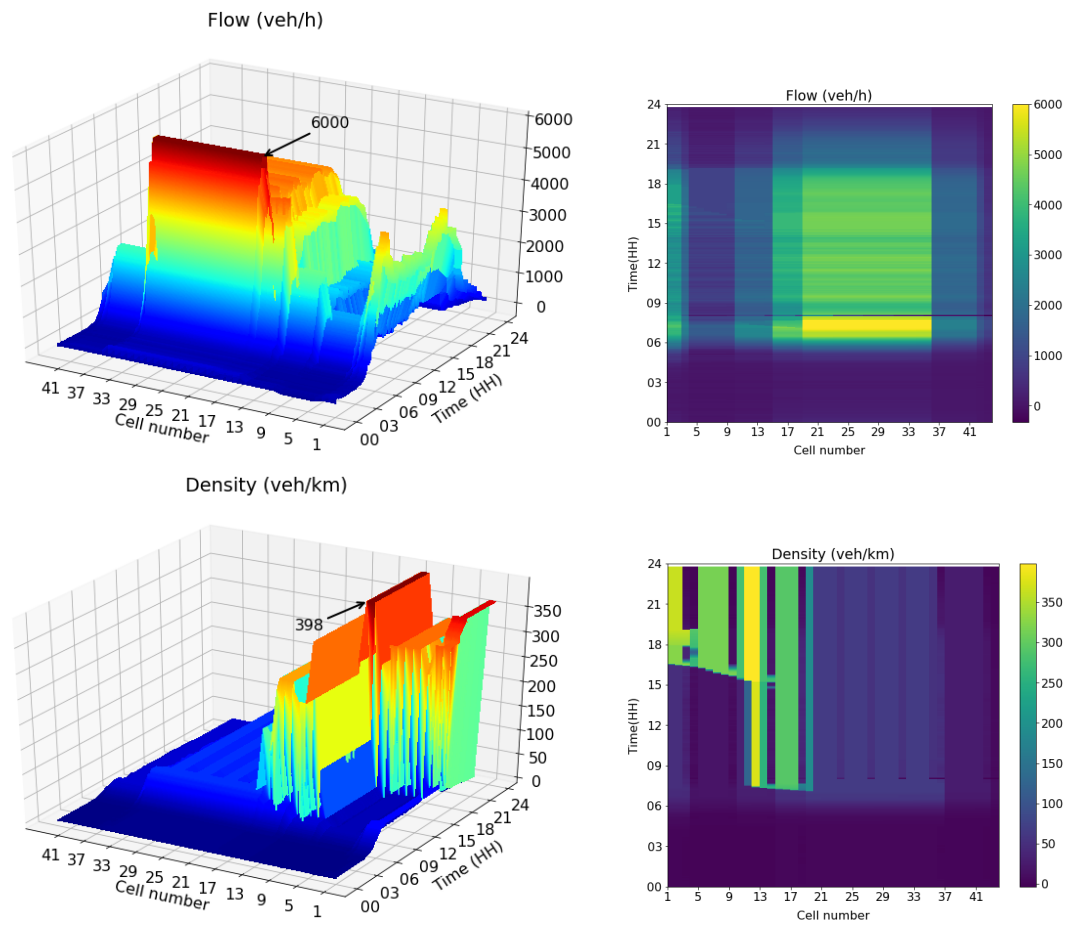


Figure 4.17: Surface and heatmap plots of flow rate (veh/h) and density (veh/km) obtained from the optimisation Model with lane closure

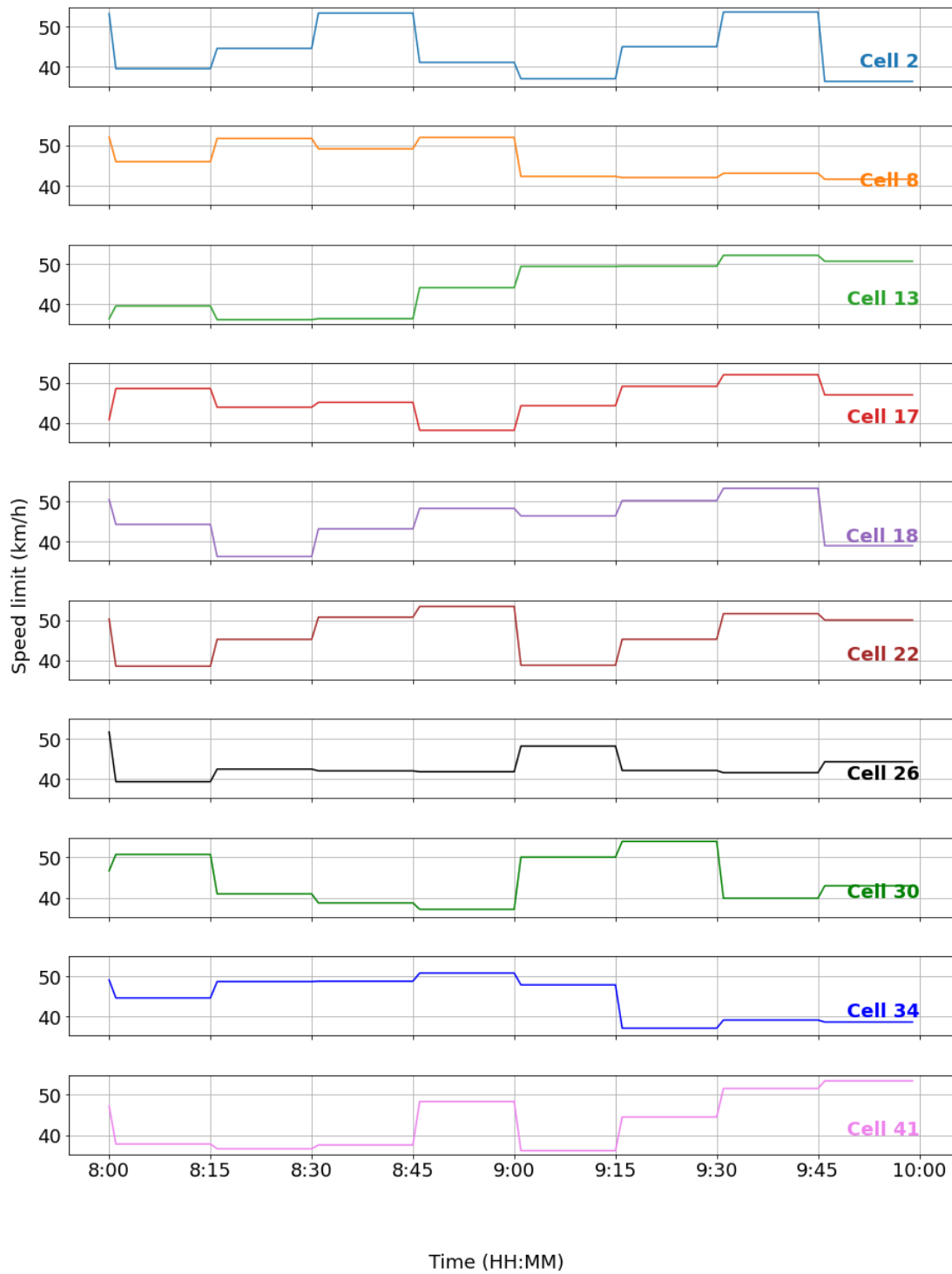


Figure 4.18: Variable speed limit (km/h) obtained from the optimisation model with lane closure.

4.4 Concluding Remarks

In summary, findings of the SCTM reveal that lane closure in upstream cells results in congestion, with lane closure in cell 35 prior to the incident causing a traffic backup in the freeway section. As a result, the traffic flow drops, with density rising to higher than the standard simulation in which there has been no lane closure.

Based on the above findings, this study recommends the utilisation of a stochastic cell transmission model (SCTM) set in a Kwinana freeway section to simulate both the density and flow rate of traffic under measuring rates of arrival at the main entrance and three on-ramp roads and discharging rates at two off-ramp roads. In the SCTM, random parameters of the fundamental flow-density diagrams (i.e. capacities, variable speed limits, ramp metering & free-flow speeds) govern the stochastic ties of both sending and receiving functions. Data-driven Traffic simulation based on the SCTM method can describe traffic flow on the freeway with lane closure.

The optimisation model presenting the problem of ramp metering and variable speed limits with non-recurrent traffic demand flows reveals that robust optimisation can effectively control total delays and mitigate traffic congestion when there is uncertainty in the system in a range of scenarios. Results also show it also offers a more effective way to manage the problem of total system delay.

Although many traffic control measures (e.g. variable speed limit controls and ramp-metering & route guidance) have been used to optimise traffic distribution on road networks, traffic optimisation using system engineering under the guidance of system science is clearly a better way to optimise current transportation facilities. This method can more effectively be used better to adjust the relationships between traffic demand and supply to improve the use of road resources. Further studies could also employ this approach to create models under set-valued fundamental diagrams to determine the route choice behaviours of drivers.

Chapter 5

Conclusions and Further Work

It is well known that many mathematical techniques have been employed to depict the same process when studying traffic flow modelling from various angles. It also has trouble deciding on a suitable technique for generating the physical appearance on the freeway under non-recurrent events. Although over the last decade non-recurrent traffic congestion has been examined in various aspects and provides a basic understanding of the traffic problem, traffic congestion is still discussed and researched in several areas. This dissertation focuses on two aspects, traffic prediction and traffic control under non-recurrent events. The research efforts of this dissertation are described in Section 5.1. The potential future study directions in specific areas are given in Section 5.2.

5.1 Contributions

The main contribution of this dissertation is the development of mathematical tools for traffic control on the freeway under non-recurrent events. The tools consist of the multivariate prediction models of traffic parameters, the traffic simulation model and the optimisation model of traffic flow control via variable speed limit and ramp metering.

1. As short-term traffic prediction is critical to the freeway traffic operating system, the proposed forecasting model aims to predict the next 30 minutes of traffic parameters including the flow rate (volume), density and speed.
2. For transportation management and control systems, traffic information during peak hours or road incidents is essential. Macroscopic traffic flow models have been proposed to capture traffic flow dynamics including the creation and dissipation of lines of traffic, shock waves, etc. The proposed traffic simulation model is implemented from the original LWR model by taking into account the effect of uncertainty on the demand and supply of the road network. Numerical experiments were performed and evaluate the model efficiency. In conclusion, we may state that
 - The models are simple for the real-time modelling of traffic dynamics on road networks and sufficient for analysing characteristics of the flow-Density dynamic under non-recurrent events.
 - The models require less processing power. Additionally, the computational demand is independent of the number of vehicles in the network and does not rise with rising traffic volumes.
 - The models can predict traffic parameters with less input sensitivity and estimate the total kilometre travel, total hour travel and total delay, numerically.
 - The proposed model with real-time traffic demand and uncertainty free speed and flow capacity can capture traffic phenomena under non-recurrent events.
3. For the on-ramp and mainline traffic control, two control strategies, Ramp Metering (RM) and Variable Speed Limit (VSL), are extensively studied to improve the overall traffic condition. As the traffic

parameters are uncertain, a stochastic optimisation model with the list of RM and VSL parameters during horizontal times as the decision variables is proposed. The optimisation model is subject to two constraints, including the explicit SCTM traffic flow and the cell capacity of each road segment. The results show that the proposed optimisation model with random on-ramp flow rates gives and the optimum VSL parameters by minimising total travel time.

5.2 Future Research

As traffic theories are a crucial element of traffic model and analysis, the development of traffic engineering theories and their applications are important for better description of the interactions among vehicles, drivers, and the highway system with control devices, signage, and markings.

A suggestion for future research is the development of traffic engineering models of multicommodity flow problem with a supply-demand uncertainty and the optimal total throughput by maximising the sum of all demands. Moreover, further applications are in the development of traffic simulation models with various control strategies including ramp metering, variable speed limit, additional lanes and signage, etc.

Moreover, traffic congestion modelling with a particular emphasis on the ability to predict unexpected events in traffic flow is essential as there are many random aspects in both driver behaviour and traffic conditions. In addition, cross-comparisons of the enhanced models with other exist models in terms of the accuracy and computational effort are also necessary.

Appendix

Statement of Attribution

The research presented in Chapter 3 was published (two papers) in IEEE conference proceeding, “8th International Conference on Control, Decision and Information Technologies (CoDIT)” on May 17th 2022 and Alexandria engineering journal on October 2022:

- 1) Aljuaydi, Fahad, Benchawan Wiwatanapataphee, and Yong Hong Wu. "Deep learning-based prediction models for freeway traffic flow under non-recurrent events." *2022 8th International Conference on Control, Decision and Information Technologies (CoDIT)*. Vol. 1. IEEE, 2022.
- 2) Aljuaydi, Fahad, Benchawan Wiwatanapataphee, and Yong Hong Wu. "Multivariate machine learning-based prediction models of freeway traffic flow under non-recurrent events." *Alexandria engineering journal* (2022).

All authors provided the concept and designed methodology; I developed the model, simulated and wrote the manuscript; Professor. Benchawan supervised the research; all authors discussed the results, commented on the manuscript and approved the final version.

Student name: Fahad Aljuaydi

Signature:



Date: 06/12/2022

Co-authors:

Name: A/Professor Benchawan Wiwatanapataphee

Signature:



Date: 09/12/2022

Name: Professor Yong Hong Wu

Signature:



Date: 09/12/2022

Copyright Information



- Home
- Help ▾
- Email Support
- Sign in
- Create Account



Deep Learning-Based Prediction Models for Freeway Traffic Flow under Non-Recurrent Events

Conference Proceedings:
2022 8th International Conference on Control, Decision and Information Technologies (CoDIT)

Author: Fahad Aljuaydi
Publisher: IEEE
Date: 17 May 2022

Copyright © 2022, IEEE

Thesis / Dissertation Reuse

The IEEE does not require individuals working on a thesis to obtain a formal reuse license, however, you may print out this statement to be used as a permission grant:

Requirements to be followed when using any portion (e.g., figure, graph, table, or textual material) of an IEEE copyrighted paper in a thesis:

- 1) In the case of textual material (e.g., using short quotes or referring to the work within these papers) users must give full credit to the original source (author, paper, publication) followed by the IEEE copyright line © 2011 IEEE.
- 2) In the case of illustrations or tabular material, we require that the copyright line © [Year of original publication] IEEE appear prominently with each reprinted figure and/or table.
- 3) If a substantial portion of the original paper is to be used, and if you are not the senior author, also obtain the senior author's approval.




Requirements to be followed when using an entire IEEE copyrighted paper in a thesis:

- 1) The following IEEE copyright/ credit notice should be placed prominently in the references: © [year of original publication] IEEE. Reprinted, with permission, from [author names, paper title, IEEE publication title, and month/year of publication]
- 2) Only the accepted version of an IEEE copyrighted paper can be used when posting the paper or your thesis on-line.
- 3) In placing the thesis on the author's university website, please display the following message in a prominent place on the website: In reference to IEEE copyrighted material which is used with permission in this thesis, the IEEE does not endorse any of [university/educational entity's name goes here]'s products or services. Internal or personal use of this material is permitted. If interested in reprinting/republishing IEEE copyrighted material for advertising or promotional purposes or for creating new collective works for resale or redistribution, please go to http://www.ieee.org/publications_standards/publications/rights/rights_link.html to learn how to obtain a License from RightsLink.

If applicable, University Microfilms and/or ProQuest Library, or the Archives of Canada may supply single copies of the dissertation.

[BACK](#)
[CLOSE WINDOW](#)

Permission [221123-000012]  



Lee, Natalia (ELS-SEO) <C.Natalia@elsevier.com>

To: ayman abdel-khalik <ayman.abdel-khalik@alexu.edu.eg>; Fahad Aljuaydi

Fri 25/11/2022 10:12 AM

Dear Ayman,

Thank you for sharing this with me.

As the request has been now recorded in the system, there is no further process required from us.

Best Regards,

Natalia Lee

Senior Publisher




ELSEVIER | Global STM Journals

+82 2 6714 3137 office

+82 2 725 4388 fax

c.natalia@elsevier.com

Permission [221123-000012]  



ayman abdel-khalik <ayman.abdel-khalik@alexu.edu.eg> 

To: Fahad Aljuaydi; Lee, Natalia (ELS-SEO) <C.Natalia@elsevier.com>

Thu 24/11/2022 11:58 AM

Dear Fahad ,

Based in feedback provided below, I have no problem to give you a permission to use the paper text/figures in your thesis.

Dear Natalia: please advise if the is any extra step needed.

Regards

Ayman

Ayman S. Abdel-Khalik, Ph.D., SMIEEE

Professor of Electric Machines and Drives

Editor-in-Chief, Alexandria Engineering Journal (AEJ)

Associate Editor, IEEE Transactions on Industrial Electronics

Associate Editor, IET Electric Power Applications

Department of Electrical Engineering

Alexandria University

[002 01156719900](tel:00201156719900)

Dear professor Ayman,

Hope this email finds you well.

Please see in the below email .

Please I would like to seeking your permission to use the text of my paper titled: **Multivariate Machine Learning-Based Prediction Models of Freeway Traffic Flow under Non-Recurrent Events** in my thesis either directly (100%) or as a reference for my original writing on the subject. I ask you to consider my request for my necessary need for it in presenting and discussing my doctoral dissertation.

Thank you so much for help

Sincerely,

Fahad Aljuaydi

Our reference: AEJ 3442

Article reference: AEJ_AEJ-D-22-03483

Article title: Multivariate Machine Learning-Based Prediction Models of Freeway Traffic Flow under Non-Recurrent Events

published in: Alexandria Engineering Journal

ISSN : [1110-0168](#)

Volume: N/A

Dear Fahad Aljuaydi

Thank you for contacting us.

Please note that, permissions for the journal Alexandria Engineering Journal are managed by the society.

Kindly contact the Faculty of Engineering, Alexandria University - Dr. Mohmed mteamah@yahoo.com to obtain this permission.

Kind regards,

Roopa Lingayath

Senior Copyrights Coordinator

ELSEVIER | HCM - Health Content Management

Visit [Elsevier Permissions](#)

From: Administrator

Date: Tuesday, November 22, 2022 07:39 PM GMT

Dear Customer

Thank you for contacting Elsevier's Permissions Helpdesk.

This is an automated acknowledgement to confirm we have received your query. Ticket number 221123-000012 has been opened on your behalf and we aim to respond within two business days.

Regards,

Permissions Helpdesk

Bibliography

- A. F. Abidin, et al. (2015). ‘Integrating Twitter traffic information with Kalman filter models for public transportation vehicle arrival time prediction’. In *big-data analytics and cloud computing*, pp. 67–82. Springer.
- A. Al-Kaisy, et al. (2005). ‘Developing passenger car equivalency factors for heavy vehicles during congestion’. *Journal of transportation engineering* **131**(7):514–523.
- A. Alhariqi, et al. (2022). ‘Calibration of the intelligent driver model (IDM) with adaptive parameters for mixed autonomy traffic using experimental trajectory data’. *Transportmetrica B: transport dynamics* **10**(1):421–440.
- F. Aljuaydi, et al. (2022). ‘Deep Learning-Based Prediction Models for Freeway Traffic Flow under Non-Recurrent Events’. In *2022 8th International Conference on Control, Decision and Information Technologies (CoDIT)*, vol. 1, pp. 815–820. IEEE.
- J. An, et al. (2019). ‘A novel fuzzy-based convolutional neural network method to traffic flow prediction with uncertain traffic accident information’. *Ieee Access* **7**:20708–20722.
- B. Anbaroglu, et al. (2014). ‘Spatio-temporal clustering for non-recurrent traffic congestion detection on urban road networks’. *Transportation Research Part C: Emerging Technologies* **48**:47–65.

- E. Arnold (1998). ‘Ramp metering: A review of the literature. Technical report, December 1997–December 1998’. Tech. rep., Virginia Transportation Research Council, Charlottesville, VA (United States
- R. Arnott & K. Small (1994). ‘The economics of traffic congestion’. *American scientist* **82**(5):446–455.
- A. Aw & M. Rascle (2000). ‘Resurrection of” second order” models of traffic flow’. *SIAM journal on applied mathematics* **60**(3):916–938.
- M. Bando, et al. (1998). ‘Analysis of optimal velocity model with explicit delay’. *Physical Review E* **58**(5):5429.
- M. Bando, et al. (1995). ‘Dynamical model of traffic congestion and numerical simulation’. *Physical review E* **51**(2):1035.
- M. Beckmann, et al. (1956). ‘Studies in the Economics of Transportation’. Tech. rep.
- M. Ben-Akiva, et al. (2002). ‘Network state estimation and prediction for real-time transportation management applications’. In *Transportation Research Board 81st Annual Meeting*.
- Y. Bengio (2009). *Learning deep architectures for AI*. Now Publishers Inc.
- D. Branston (1976). ‘Models of single lane time headway distributions’. *Transportation Science* **10**(2):125–148.
- F. J. Braz, et al. (2022). ‘Road traffic forecast based on meteorological information through deep learning methods’. *Sensors* **22**(12):4485.
- D. Buckley (1968). ‘A semi-poisson model of traffic flow’. *Transportation Science* **2**(2):107–133.

- V. X. Can, et al. (2020). ‘An analysis of urban traffic incident under mixed traffic conditions based on SUMO: A case study of Hanoi’. *Int. J. Adv. Res. Eng. Technol.* **11**(11):573–581.
- M. Castro-Neto, et al. (2009). ‘Online-SVR for short-term traffic flow prediction under typical and atypical traffic conditions’. *Expert systems with applications* **36**(3):6164–6173.
- R. E. Chandler, et al. (1958). ‘Traffic dynamics: studies in car following’. *Operations research* **6**(2):165–184.
- H. Chang, et al. (2012). ‘Dynamic near-term traffic flow prediction: system-oriented approach based on past experiences’. *IET intelligent transport systems* **6**(3):292–305.
- T. Chang-Fu, et al. (2007). ‘Extended speed gradient model for traffic flow on two-lane freeways’. *Chinese Physics* **16**(6):1570.
- S. Chanut & C. Buisson (2003). ‘Macroscopic model and its numerical solution for two-flow mixed traffic with different speeds and lengths’. *Transportation research record* **1852**(1):209–219.
- C. P. Chen & C.-Y. Zhang (2014). ‘Data-intensive applications, challenges, techniques and technologies: A survey on Big Data’. *Information sciences* **275**:314–347.
- J. Chen & Y. Fang (2015). ‘Macroscopic modeling for traffic flow on three-lane highways’. *International Journal of Modern Physics C* **26**(11):1550127.
- J. Chen, et al. (2013). ‘An extended macroscopic model for traffic flow on a highway with slopes’. *International Journal of Modern Physics C* **24**(09):1350061.
- R. L. Cheu, et al. (2003). ‘Support vector machine models for freeway incident detection’. In *Proceedings of the 2003 IEEE International Conference on Intelligent Transportation Systems*, vol. 1, pp. 238–243. IEEE.

- M. Chikaraishi, et al. (2020). ‘On the possibility of short-term traffic prediction during disaster with machine learning approaches: An exploratory analysis’. *Transport Policy* **98**:91–104.
- T. Chuan & S. Di-Hua (2010). ‘Continuum modeling for two-lane traffic flow with consideration of the traffic interruption probability’. *Chinese Physics B* **19**(12):120501.
- R. Collobert & J. Weston (2008). ‘A unified architecture for natural language processing: Deep neural networks with multitask learning’. In *Proceedings of the 25th international conference on Machine learning*, pp. 160–167.
- A. Dabiri & B. Kulcsár (2015). ‘Freeway traffic incident reconstruction—A bi-parameter approach’. *Transportation Research Part C: Emerging Technologies* **58**:585–597.
- C. F. Daganzo (1994). ‘The cell transmission model: A dynamic representation of highway traffic consistent with the hydrodynamic theory’. *Transportation Research Part B: Methodological* **28**(4):269–287.
- C. F. Daganzo (1995). ‘Requiem for second-order fluid approximations of traffic flow’. *Transportation Research Part B: Methodological* **29**(4):277–286.
- C. F. Daganzo, et al. (1999). ‘Possible explanations of phase transitions in highway traffic’. *Transportation Research Part A: Policy and Practice* **33**(5):365–379.
- L. Davis (2002). ‘Comment on “Analysis of optimal velocity model with explicit delay”’. *Physical Review E* **66**(3):038101.
- A. I. Delis, et al. (2018). ‘A macroscopic multi-lane traffic flow model for ACC/-CACC traffic dynamics’. *Transportation Research Record* **2672**(20):178–192.

- O. Derbel, et al. (2012). ‘Extended safety descriptor measurements for relative safety assessment in mixed road traffic’. In *2012 15th International IEEE Conference on Intelligent Transportation Systems*, pp. 752–757. IEEE.
- O. Derbel, et al. (2013). ‘Modified intelligent driver model for driver safety and traffic stability improvement’. *IFAC Proceedings Volumes* **46**(21):744–749.
- Q. H. Do, et al. (2020). ‘Prediction of Data Traffic in Telecom Networks based on Deep Neural Networks’. *Journal of Computer Science* **16**(9):1268–1277.
- N. Dogru & A. Subasi (2018). ‘Traffic accident detection using random forest classifier’. In *2018 15th learning and technology conference (L&T)*, pp. 40–45. IEEE.
- J. Drake & J. L. Schofer (1966). ‘A statistical analysis of speed-density hypotheses’. *Highway Research Record* *154* pp. 53–87.
- S. Du, et al. (2018). ‘A hybrid method for traffic flow forecasting using multimodal deep learning’. *arXiv preprint arXiv:1803.02099* .
- L. C. Edie (1961). ‘Car-following and steady-state theory for noncongested traffic’. *Operations research* **9**(1):66–76.
- A. Essien, et al. (2019a). ‘Improving urban traffic speed prediction using data source fusion and deep learning’. In *2019 IEEE International Conference on Big Data and Smart Computing (BigComp)*, pp. 1–8. IEEE.
- A. E. Essien, et al. (2019b). ‘A scalable deep convolutional LSTM neural network for large-scale urban traffic flow prediction using recurrence plots’. In *2019 IEEE AFRICON*, pp. 1–7. IEEE.
- F. B. Fitch (1944). ‘McCulloch Warren S. and Pitts Walter. A logical calculus of the ideas immanent in nervous activity. Bulletin of mathematical biophysics, vol. 5, pp. 115–133’. *Journal of Symbolic Logic* **9**(2).

- J. R. D. Frejo & E. F. Camacho (2011). ‘Feasible cooperation based model predictive control for freeway traffic systems’. In *2011 50th IEEE Conference on Decision and Control and European Control Conference*, pp. 5965–5970. IEEE.
- J. R. D. Frejo & B. De Schutter (2018). ‘Feed-Forward ALINEA: A ramp metering control algorithm for nearby and distant bottlenecks’. *IEEE Transactions on Intelligent Transportation Systems* **20**(7):2448–2458.
- D. C. Gazis, et al. (1959). ‘Car-following theory of steady-state traffic flow’. *Operations research* **7**(4):499–505.
- D. C. Gazis, et al. (1961). ‘Nonlinear follow-the-leader models of traffic flow’. *Operations research* **9**(4):545–567.
- I. Goodfellow, et al. (2016). *Deep learning*. MIT press.
- I. J. Goodfellow, et al. (2013). ‘Multi-digit number recognition from street view imagery using deep convolutional neural networks’. *arXiv preprint arXiv:1312.6082* .
- B. Greenshields, et al. (1935a). ‘A study of traffic capacity’. In *Highway research board proceedings*, vol. 1935. National Research Council (USA), Highway Research Board.
- B. Greenshields, et al. (1935b). ‘A study of traffic capacity’. In *Highway research board proceedings*, vol. 1935. National Research Council (USA), Highway Research Board.
- B. D. Greenshields, et al. (1934). ‘The photographic method of studying traffic behavior’. In *Highway Research Board Proceedings*, vol. 13.
- C. Gu, et al. (2022). ‘Distributionally robust ramp metering under traffic demand uncertainty’. *Transportmetrica B: Transport Dynamics* pp. 1–15.

- A. K. Gupta & V. Katiyar (2005). ‘Analyses of shock waves and jams in traffic flow’. *Journal of Physics A: Mathematical and General* **38**(19):4069.
- A. K. Gupta & V. Katiyar (2006). ‘A new anisotropic continuum model for traffic flow’. *Physica A: Statistical Mechanics and its Applications* **368**(2):551–559.
- F. A. Haight, et al. (1963). *Some mathematical aspects of the problem of merging*. Institute of Transportation and Traffic Engineering, University of California.
- M. Hajiahmadi, et al. (2015). ‘Integrated predictive control of freeway networks using the extended link transmission model’. *IEEE Transactions on Intelligent Transportation Systems* **17**(1):65–78.
- M. E. Hallenbeck, et al. (2003). ‘Measurement of recurring versus non-recurring congestion’. Tech. rep., Washington (State). Dept. of Transportation.
- M. M. Hamed, et al. (1995). ‘Short-term prediction of traffic volume in urban arterials’. *Journal of Transportation Engineering* **121**(3):249–254.
- Y. Han (2017). *A stochastic modeling of traffic breakdown for freeway merge bottlenecks and variable speed limit control strategies using connected automated vehicles*. The University of Wisconsin-Madison.
- Y. Han, et al. (2020). ‘Hierarchical ramp metering in freeways: an aggregated modeling and control approach’. *Transportation research part C: emerging technologies* **110**:1–19.
- Z. He, et al. (2019). ‘Network-wide identification of turn-level intersection congestion using only low-frequency probe vehicle data’. *Transportation Research Part C: Emerging Technologies* **108**:320–339.
- A. Hegyi, et al. (2005). ‘Optimal coordination of variable speed limits to suppress shock waves’. *IEEE Transactions on intelligent transportation systems* **6**(1):102–112.

- G. E. Hinton & R. R. Salakhutdinov (2006). ‘Reducing the dimensionality of data with neural networks’. *science* **313**(5786):504–507.
- S. Hochreiter & J. Schmidhuber (1997). ‘Long short-term memory’. *Neural computation* **9**(8):1735–1780.
- S. P. Hoogendoorn & P. H. Bovy (2001). ‘State-of-the-art of vehicular traffic flow modelling’. *Proceedings of the Institution of Mechanical Engineers, Part I: Journal of Systems and Control Engineering* **215**(4):283–303.
- M. A. Hossain & J. Tanimoto (2022). ‘A microscopic traffic flow model for sharing information from a vehicle to vehicle by considering system time delay effect’. *Physica A: Statistical Mechanics and its Applications* **585**:126437.
- Z. Hou, et al. (2008). ‘An iterative learning approach for density control of freeway traffic flow via ramp metering’. *Transportation Research Part C: Emerging Technologies* **16**(1):71–97.
- T.-Y. Hu, et al. (2005). ‘A new simulation-assignment model DynaTAIWAN for mixed traffic flows’. In *Proceedings of the 12th World Congress on ITS*.
- W. Hu, et al. (2010). ‘The short-term traffic flow prediction based on neural network’. In *2010 2nd International Conference on Future Computer and Communication*, vol. 1, pp. V1–293. IEEE.
- Y. Hu, et al. (2018). ‘A new lattice model of three-lane traffic flow’. *International Journal of Modern Physics C* **29**(12):1850118.
- H. Huang, et al. (2006). ‘Continuum modeling for two-lane traffic flow’. *Acta Mechanica Sinica* **22**(2):131–137.
- B. Huval, et al. (2013). ‘Deep learning for class-generic object detection’. *arXiv preprint arXiv:1312.6885*.
- S. Ishak, et al. (2003). ‘Optimization of dynamic neural network performance for short-term traffic prediction’. *Transportation Research Record* **1836**(1):45–56.

- R. J. Javid & R. J. Javid (2018). ‘A framework for travel time variability analysis using urban traffic incident data’. *IATSS research* **42**(1):30–38.
- Y. Jia, et al. (2017). ‘Traffic flow prediction with rainfall impact using a deep learning method’. *Journal of advanced transportation* **2017**.
- R. Jiang, et al. (2018). ‘Experimental and empirical investigations of traffic flow instability’. *Transportation research part C: emerging technologies* **94**:83–98.
- R. Jiang, et al. (2002). ‘A new continuum model for traffic flow and numerical tests’. *Transportation Research Part B: Methodological* **36**(5):405–419.
- W. Jiang (2022). ‘Internet traffic prediction with deep neural networks’. *Internet Technology Letters* **5**(2):e314.
- C.-J. Jin, et al. (2019). ‘The similarities and differences between the empirical and experimental data: investigation on the single-lane traffic’. *Transportmetrica B: transport dynamics* **7**(1):1323–1337.
- W.-L. Jin (2010a). ‘A kinematic wave theory of lane-changing traffic flow’. *Transportation research part B: methodological* **44**(8-9):1001–1021.
- W.-L. Jin (2010b). ‘Macroscopic characteristics of lane-changing traffic’. *Transportation research record* **2188**(1):55–63.
- W.-L. Jin (2013). ‘A multi-commodity Lighthill-Whitham-Richards model of lane-changing traffic flow’. *Procedia-Social and Behavioral Sciences* **80**:658–677.
- Z. Kan, et al. (2022). ‘Assessing individual activity-related exposures to traffic congestion using GPS trajectory data’. *Journal of Transport Geography* **98**:103240.
- B. S. Kerner & H. Rehborn (1997). ‘Experimental properties of phase transitions in traffic flow’. *Physical Review Letters* **79**(20):4030.

- F. Kessels (2019). *Mesoscopic Models*, pp. 99–106. Springer International Publishing, Cham.
- A. Kesting (2008). *Microscopic modeling of human and automated driving: towards traffic adaptive cruise control*. Ph.D. thesis, Dresden, Techn. Univ., Diss., 2008.
- Z. H. Khan & T. A. Gulliver (2018). ‘A macroscopic traffic model for traffic flow harmonization’. *European Transport Research Review* **10**(2):30.
- Z. H. Khan, et al. (2018). ‘A macroscopic traffic model based on weather conditions’. *Chinese Physics B* **27**(7):070202.
- D. P. Kingma & J. Ba (2014). ‘Adam: A method for stochastic optimization’. *arXiv preprint arXiv:1412.6980* .
- A. Koesdwiady, et al. (2016). ‘Improving traffic flow prediction with weather information in connected cars: A deep learning approach’. *IEEE Transactions on Vehicular Technology* **65**(12):9508–9517.
- E. Kolla, et al. (2022). ‘Simulation-based reconstruction of traffic incidents from moving vehicle mono-camera’. *Science & Justice* **62**(1):94–109.
- D. Krajzewicz (2010). ‘Traffic simulation with SUMO—simulation of urban mobility’. In *Fundamentals of traffic simulation*, pp. 269–293. Springer.
- C. Krupitzer, et al. (2019). ‘Beyond position-awareness—Extending a self-adaptive fall detection system’. *Pervasive and Mobile Computing* **58**:101026.
- M. Kumar & K. Kumar (2022). ‘Traffic Congestion Prediction Using Categorized Vehicular Speed Data’. In *Conference of Transportation Research Group of India*, pp. 367–384. Springer.
- W. H. Lam, et al. (2005). ‘Short-term travel time forecasts for transport information system in hong kong’. *Journal of Advanced Transportation* **39**(3):289–306.

- J. A. Laval & C. F. Daganzo (2004). ‘Multi-lane hybrid traffic flow model: Quantifying the impacts of lane-changing maneuvers on traffic flow’. . .
- J. A. Laval & C. F. Daganzo (2006). ‘Lane-changing in traffic streams’. *Transportation Research Part B: Methodological* **40**(3):251–264.
- L. Li & X. M. Chen (2017). ‘Vehicle headway modeling and its inferences in macroscopic/microscopic traffic flow theory: A survey’. *Transportation Research Part C: Emerging Technologies* **76**:170–188.
- L. Li, et al. (2015a). ‘Trend modeling for traffic time series analysis: An integrated study’. *IEEE Transactions on Intelligent Transportation Systems* **16**(6):3430–3439.
- S.-b. Li, et al. (2015b). ‘Dynamic variable speed limit strategies based on traffic flow model for urban expressway’. In *2015 International Conference on Transportation Information and Safety (ICTIS)*, pp. 55–63. IEEE.
- W. Li, et al. (2020). ‘Real-time movement-based traffic volume prediction at signalized intersections’. *Journal of Transportation Engineering, Part A: Systems* **146**(8):04020081.
- Y. Li, et al. (2017). ‘An extended microscopic traffic flow model based on the spring-mass system theory’. *Modern Physics Letters B* **31**(09):1750090.
- Y. Li, et al. (2018). ‘Analysis balance parameter of optimal ramp metering’. In *IOP Conference Series: Materials Science and Engineering*, vol. 359, 1, p. 012007. IOP Publishing.
- M. J. Lighthill & G. B. Whitham (1955a). ‘On kinematic waves II. A theory of traffic flow on long crowded roads’. *Proceedings of the Royal Society of London. Series A. Mathematical and Physical Sciences* **229**(1178):317–345.

- M. J. Lighthill & G. B. Whitham (1955b). ‘On kinematic waves II. A theory of traffic flow on long crowded roads’. *Proceedings of the Royal Society of London. Series A. Mathematical and Physical Sciences* **229**(1178):317–345.
- L. Lin, et al. (2013). ‘A k nearest neighbor based local linear wavelet neural network model for on-line short-term traffic volume prediction’. *Procedia-Social and Behavioral Sciences* **96**:2066–2077.
- Q. Liu, et al. (2018). ‘Short-term traffic speed forecasting based on attention convolutional neural network for arterials’. *Computer-Aided Civil and Infrastructure Engineering* **33**(11):999–1016.
- J. Long, et al. (2011). ‘Urban traffic jam simulation based on the cell transmission model’. *Networks and Spatial Economics* **11**(1):43–64.
- B. P. Loo & Z. Huang (2022). ‘Spatio-temporal variations of traffic congestion under work from home (WFH) arrangements: Lessons learned from COVID-19’. *Cities* p. 103610.
- X. Ma, et al. (2017). ‘Learning traffic as images: a deep convolutional neural network for large-scale transportation network speed prediction’. *Sensors* **17**(4):818.
- X. Ma, et al. (2015). ‘Long short-term memory neural network for traffic speed prediction using remote microwave sensor data’. *Transportation Research Part C: Emerging Technologies* **54**:187–197.
- J. M. Maciejowski (2002). *Predictive control: with constraints*. Pearson education.
- S. Maerivoet & B. De Moor (2005). ‘Traffic flow theory’. *arXiv preprint physics/0507126* .
- H. S. Mahmassani (2001). ‘Dynamic network traffic assignment and simulation methodology for advanced system management applications’. *Networks and spatial economics* **1**(3):267–292.

- R. Mahnke, et al. (2005). ‘Probabilistic description of traffic flow’. *Physics Reports* **408**(1-2):1–130.
- T. V. Mathew (2014). ‘Lane changing models’. *Transportation systems engineering anonymous* pp. 15–1.
- J. McGroarty (2010). ‘Neihoff Urban Studio–W10 January 29, 2010’ .
- A. Miglani & N. Kumar (2019). ‘Deep learning models for traffic flow prediction in autonomous vehicles: A review, solutions, and challenges’. *Vehicular Communications* **20**:100184.
- S. Mollier, et al. (2019). ‘Two-dimensional macroscopic model for large scale traffic networks’. *Transportation Research Part B: Methodological* **122**:309–326.
- E. Montroll & R. Potts (1964). ‘Car following and acceleration noise’. *Highway Research Board Special Report* (79).
- S. Moridpour, et al. (2010). ‘Lane changing models: a critical review’. *Transportation letters* **2**(3):157–173.
- K. Moskowitz & M. Raff (1954). ‘Waiting for a gap in a traffic stream’. In *Highway Research Board Proceedings*, vol. 33.
- A. Muralidharan & R. Horowitz (2015). ‘Computationally efficient model predictive control of freeway networks’. *Transportation Research Part C: Emerging Technologies* **58**:532–553.
- K. Nagel & M. Schreckenberg (1992). ‘A cellular automaton model for freeway traffic’. *Journal de physique I* **2**(12):2221–2229.
- G. F. Newell (1993). ‘A simplified theory of kinematic waves in highway traffic, part I: General theory’. *Transportation Research Part B: Methodological* **27**(4):281–287.

- D. Ni (2020). ‘Limitations of current traffic models and strategies to address them’. *Simulation Modelling Practice and Theory* **104**:102137.
- M. Ni, et al. (2014). ‘Using social media to predict traffic flow under special event conditions’. In *The 93rd annual meeting of transportation research board*.
- A. Nigam & S. Srivastava (2023). ‘Hybrid deep learning models for traffic stream variables prediction during rainfall’. *Multimodal Transportation* **2**(1):100052.
- M. Papageorgiou & A. Kotsialos (2002). ‘Freeway ramp metering: An overview’. *IEEE transactions on intelligent transportation systems* **3**(4):271–281.
- H. J. Payne (1971). ‘Model of freeway traffic and control’. *Mathematical Model of Public System* pp. 51–61.
- H. Peng, et al. (2018). ‘Forecasting traffic flow: Short term, long term, and when it rains’. In *International Conference on Big Data*, pp. 57–71. Springer.
- H. Peng, et al. (2020). ‘Spatial temporal incidence dynamic graph neural networks for traffic flow forecasting’. *Information Sciences* **521**:277–290.
- L. A. Pipes (1953). ‘An operational analysis of traffic dynamics’. *Journal of applied physics* **24**(3):274–281.
- I. G. Ploss & I. P. Vortisch (2006). ‘Estimating real-time urban traffic states in VISUM online’. In *International Seminar on Intelligent Transport Systems (ITS) in Road Network Operations*.
- J. Pu, et al. (2019). ‘STLP-OD: Spatial and temporal label propagation for traffic outlier detection’. *IEEE Access* **7**:63036–63044.
- H.-s. Qi, et al. (2013). ‘Formation and propagation of local traffic jam’. *Discrete Dynamics in Nature and Society* **2013**.

- L. Qi, et al. (2018). ‘A dynamic road incident information delivery strategy to reduce urban traffic congestion’. *IEEE/CAA Journal of Automatica Sinica* **5**(5):934–945.
- M. Rahman, et al. (2013). ‘Review of microscopic lane-changing models and future research opportunities’. *IEEE transactions on intelligent transportation systems* **14**(4):1942–1956.
- V. Ramanujam (2007). *Lane changing models for arterial traffic*. Ph.D. thesis, Massachusetts Institute of Technology.
- N. Ranjan, et al. (2020). ‘City-wide traffic congestion prediction based on CNN, LSTM and transpose CNN’. *IEEE Access* **8**:81606–81620.
- P. Reina & S. Ahn (2019). ‘Lane flow distribution of congested traffic on three-lane freeways’. *International Journal of Transportation Science and Technology* .
- Y. Ren, et al. (2022). ‘TBSM: A traffic burst-sensitive model for short-term prediction under special events’. *Knowledge-Based Systems* **240**:108120.
- P. I. Richards (1956a). ‘Shock waves on the highway’. *Operations research* **4**(1):42–51.
- P. I. Richards (1956b). ‘Shock waves on the highway’. *Operations research* **4**(1):42–51.
- F. Rosenblatt (1962). *Perceptions and the theory of brain mechanisms*. Spartan books.
- D. E. Rumelhart, et al. (1985). ‘Learning internal representations by error propagation’. Tech. rep., California Univ San Diego La Jolla Inst for Cognitive Science.
- S. S. Sajjadi (2013). *Investigating Impact of Sources of Non-recurrent Congestion on Freeway Facilities*. North Carolina State University.

- M. I. Sameen & B. Pradhan (2017). ‘Severity prediction of traffic accidents with recurrent neural networks’. *Applied Sciences* **7**(6):476.
- A. Sasoh & T. Ohara (2002). ‘Shock wave relation containing lane change source term for two-lane traffic flow’. *Journal of the Physical Society of Japan* **71**(9):2339–2347.
- K. Shaaban, et al. (2016). ‘Literature review of advancements in adaptive ramp metering’. *Procedia Computer Science* **83**:203–211.
- W. Shen & K. Shikh-Khalil (2017). ‘Traveling waves for a microscopic model of traffic flow’. *arXiv preprint arXiv:1709.08892* .
- H.-C. Shin, et al. (2012). ‘Stacked autoencoders for unsupervised feature learning and multiple organ detection in a pilot study using 4D patient data’. *IEEE transactions on pattern analysis and machine intelligence* **35**(8):1930–1943.
- V. Shvetsov & D. Helbing (1999). ‘Macroscopic dynamics of multilane traffic’. *Physical review E* **59**(6):6328.
- D. Singh & C. K. Mohan (2018). ‘Deep spatio-temporal representation for detection of road accidents using stacked autoencoder’. *IEEE Transactions on Intelligent Transportation Systems* **20**(3):879–887.
- A. Skabardonis, et al. (2003). ‘Measuring recurrent and nonrecurrent traffic congestion’. *Transportation Research Record* **1856**(1):118–124.
- A. R. Soheili, et al. (2013). ‘Adaptive numerical simulation of traffic flow density’. *Computers & Mathematics with Applications* **66**(3):227–237.
- P. R. Stopher (2004). ‘Reducing road congestion: a reality check’. *Transport Policy* **11**(2):117–131.
- Y. Sugiyama, et al. (2008). ‘Traffic jams without bottlenecks—experimental evidence for the physical mechanism of the formation of a jam’. *New journal of physics* **10**(3):033001.

- F. Tajdari, et al. (2019). ‘Integrated ramp metering and lane-changing feedback control at motorway bottlenecks’. In *2019 18th European Control Conference (ECC)*, pp. 3179–3184. IEEE.
- T. Tang & H. Huang (2004). ‘Continuum models for freeways with two lanes and numerical tests’. *Chinese Science Bulletin* **49**(19):2097.
- T. Tang, et al. (2008a). ‘A car-following model with the anticipation effect of potential lane changing’. *Acta Mechanica Sinica* **24**(4):399.
- T. Tang, et al. (2008b). ‘A new macro model with consideration of the traffic interruption probability’. *Physica A: Statistical Mechanics and its Applications* **387**(27):6845–6856.
- T.-Q. Tang, et al. (2014). ‘A macro model for traffic flow on road networks with varying road conditions’. *Journal of Advanced Transportation* **48**(4):304–317.
- T.-Q. Tang, et al. (2015). ‘A macro traffic flow model accounting for real-time traffic state’. *Physica A: Statistical Mechanics and its Applications* **437**:55–67.
- T.-Q. Tang, et al. (2009). ‘Macroscopic modeling of lane-changing for two-lane traffic flow’. *Journal of Advanced Transportation* **43**(3):245–273.
- R. Tao, et al. (2016). ‘Simulation analysis on urban traffic congestion propagation based on complex network’. In *2016 IEEE International Conference on Service Operations and Logistics, and Informatics (SOLI)*, pp. 217–222. IEEE.
- D. Tian, et al. (2019). ‘An automatic car accident detection method based on cooperative vehicle infrastructure systems’. *IEEE Access* **7**:127453–127463.
- Y. Tian, et al. (2018). ‘LSTM-based traffic flow prediction with missing data’. *Neurocomputing* **318**:297–305.
- T. Toledo (2007). ‘Driving behaviour: models and challenges’. *Transport Reviews* **27**(1):65–84.

- M. Treiber & D. Helbing (2002). ‘Realistische Mikrosimulation von Strassenverkehr mit einem einfachen Modell’. In *16th Symposium Simulationstechnik ASIM*, vol. 2002, p. 80.
- M. Treiber, et al. (2000). ‘Microscopic simulation of congested traffic’. In *Traffic and granular flow’99*, pp. 365–376. Springer.
- M. Treiber & A. Kesting (2011). ‘Evidence of convective instability in congested traffic flow: A systematic empirical and theoretical investigation’. *Procedia-Social and Behavioral Sciences* **17**:683–701.
- M. Treiber, et al. (2006). ‘Delays, inaccuracies and anticipation in microscopic traffic models’. *Physica A: Statistical Mechanics and its Applications* **360**(1):71–88.
- M. Treiber, et al. (2010). ‘Three-phase traffic theory and two-phase models with a fundamental diagram in the light of empirical stylized facts’. *Transportation Research Part B: Methodological* **44**(8-9):983–1000.
- J. Treiterer & J. Myers (1974). ‘The hysteresis phenomenon in traffic flow’. *Transportation and traffic theory* **6**:13–38.
- I. Tsapakis, et al. (2013). ‘Impact of weather conditions on macroscopic urban travel times’. *Journal of Transport Geography* **28**:204–211.
- R. T. Underwood (2008). ‘Speed, volume, and density relationship: Quality and theory of traffic flow, yale bureau of highway traffic (1961) 141–188’. *New Haven, Connecticut* .
- S. C. Vishnoi & C. G. Claudel (2021). ‘Variable Speed Limit and Ramp Metering Control of Highway Networks Using Lax-Hopf Method: A Mixed Integer Linear Programming Approach’. *IEEE Transactions on Intelligent Transportation Systems* .

- J. Von Neumann (1951). ‘The general and logical theory of automata, Cerebral Mechanisms in Behavior. The Hixon Symposium’. *New York: John Wiley & Sons* .
- F. Vrbanić, et al. (2021). ‘Variable speed limit and ramp metering for mixed traffic flows: A review and open questions’. *Applied Sciences* **11**(6):2574.
- G. Wall & N. Hounsell (2020). ‘Microscopic modelling of motorway diverges’. *European Journal of Transport and Infrastructure Research* **5**(3).
- K. Wang, et al. (2021). ‘A hybrid deep learning model with 1DCNN-LSTM-Attention networks for short-term traffic flow prediction’. *Physica A: Statistical Mechanics and its Applications* **583**:126293.
- R. Wang, et al. (2016). ‘Multiple model particle filter for traffic estimation and incident detection’. *IEEE Transactions on Intelligent Transportation Systems* **17**(12):3461–3470.
- Y.-Q. Wang, et al. (2019). ‘Evolution laws and stability analyses of traffic network constituted by changing ramps and main road’. *International Journal of Modern Physics B* **33**(20):1950228.
- Z. Wang, et al. (2018). ‘Estimating the spatiotemporal impact of traffic incidents: An integer programming approach consistent with the propagation of shockwaves’. *Transportation Research Part B: Methodological* **111**:356–369.
- Z. Wang, et al. (2020). ‘Hybrid time-aligned and context attention for time series prediction’. *Knowledge-Based Systems* **198**:105937.
- J. G. Wardrop & J. I. Whitehead (1952). ‘Correspondence. some theoretical aspects of road traffic research.’. *Proceedings of the institution of civil engineers* **1**(5):767–768.
- W. Wei, et al. (2019). ‘An autoencoder and LSTM-based traffic flow prediction method’. *Sensors* **19**(13):2946.

- Y. Xue & S.-Q. Dai (2003). ‘Continuum traffic model with the consideration of two delay time scales’. *Physical Review E* **68**(6):066123.
- A. Zarindast, et al. (2022). ‘A Data-Driven Method for Congestion Identification and Classification’. *Journal of Transportation Engineering, Part A: Systems* **148**(4):04022012.
- S. K. Zegeye, et al. (2009). ‘Reduction of travel times and traffic emissions using model predictive control’. In *2009 American Control Conference*, pp. 5392–5397. IEEE.
- A. Zhang & Z. Gao (2012). ‘CTM-based Propagation of Non-recurrent Congestion and Location of Variable Message Sign’. In *2012 Fifth International Joint Conference on Computational Sciences and Optimization*, pp. 462–465. IEEE.
- D. Zhang & M. R. Kabuka (2018). ‘Combining weather condition data to predict traffic flow: a GRU-based deep learning approach’. *IET Intelligent Transport Systems* **12**(7):578–585.
- J. Zhang, et al. (2011a). ‘Data-Driven Intelligent Transportation Systems: A Survey’. *IEEE Transactions on Intelligent Transportation Systems* **12**(4):1624–1639.
- J. Zhang, et al. (2011b). ‘Data-driven intelligent transportation systems: A survey’. *IEEE Transactions on Intelligent Transportation Systems* **12**(4):1624–1639.
- L. Zhang, et al. (2018). ‘Modeling lane-changing behavior in freeway off-ramp areas from the shanghai naturalistic driving study’. *Journal of Advanced Transportation* **2018**.
- N. Zhang, et al. (2008). ‘DynaCAS: Computational experiments and decision support for ITS’. *IEEE Intelligent Systems* **23**(6):19–23.

- W. Zhang, et al. (2019). ‘Short-term traffic flow prediction based on spatio-temporal analysis and CNN deep learning’. *Transportmetrica A: Transport Science* **15**(2):1688–1711.
- Z. Zhang, et al. (2016). ‘Spatial-temporal traffic flow pattern identification and anomaly detection with dictionary-based compression theory in a large-scale urban network’. *Transportation Research Part C: Emerging Technologies* **71**:284–302.
- B. Zhao, et al. (2017a). ‘A data-driven congestion diffusion model for characterizing traffic in metrocity scales’. In *2017 IEEE International Conference on Big Data (Big Data)*, pp. 1243–1252. IEEE.
- J. Zhao, et al. (2019). ‘Traffic speed prediction under non-recurrent congestion: Based on LSTM method and BeiDou navigation satellite system data’. *IEEE Intelligent Transportation Systems Magazine* **11**(2):70–81.
- Z. Zhao, et al. (2017b). ‘LSTM network: a deep learning approach for short-term traffic forecast’. *IET Intelligent Transport Systems* **11**(2):68–75.
- W. Zheng, et al. (2006). ‘Short-term freeway traffic flow prediction: Bayesian combined neural network approach’. *Journal of transportation engineering* **132**(2):114–121.
- Z. Zheng (2014). ‘Recent developments and research needs in modeling lane changing’. *Transportation research part B: methodological* **60**:16–32.
- Z. Zhou, et al. (2021). ‘Deep Spatio-Temporal Convolutional Neural Network for City Traffic Flow Prediction’. In *2021 2nd International Conference on Computing and Data Science (CDS)*, pp. 171–175. IEEE.